Understanding the Potential of Recombinant PTEN in Cancer Therapeutics

A Thesis

Submitted in Partial Fulfillment of the

Requirements for the award of the degree of

DOCTOR OF PHILOSOPHY

By

Neha Arora

Department of Biosciences and Bioengineering

Indian Institute of Technology Guwahati

Guwahati-781039, Assam, India

October 2018

Dedicated to

My Grandparents *Asha Arora*

Madan Lal Arora

Vijay Arora

Tirath Arora

My Parents *Archana Arora*

Vivek Kumar Arora

My Siblings *Arisha Arora*

Vaibhav Arora

and

My Guide *Prof. Siddhartha Sankar Ghosh*

INDIAN INSTITUTE OF TECHNOLOGY

DEPARTMENT OF BIOSCIENCES AND BIOENGINEERING

DECLARATION

I, hereby, declare that the research embodied in this thesis entitled **'Understanding the Potential of Recombinant PTEN in Cancer Therapeutics'** is the outcome of research work carried out by me under the supervision of Prof. Siddhartha Sankar Ghosh, Department of Biosciences and Bioengineering, Indian Institute of Technology Guwahati, for the award of the degree of Doctor of Philosophy. To the best of my knowledge and belief, the present thesis has not been submitted for any degree, diploma, associateship etc. of any Institute or University elsewhere.

Date

Neha Arora

Department of Biosciences and Bioengineering

Indian Institute of Technology Guwahati

INDIAN INSTITUTE OF TECHNOLOGY

DEPARTMENT OF BIOSCIENCES AND BIOENGINEERING

CERTIFICATE

This is to certify that the thesis entitled **'Understanding the Potential of Recombinant PTEN in Cancer Therapeutics'** being submitted to the **Indian Institute of Technology Guwahati** by **Neha Arora (Roll No 136106013)** for the award of the **Doctor of Philosophy** is a bonafide record of research work carried by her. The information and data reported are solely the results of her original findings. She has meticulously carried out the investigations and followed the guideline of the laboratory. This work has not been submitted elsewhere for any degree or diploma.

Prof. Siddhartha Sankar Ghosh

Date (Thesis Supervisor)

Acknowledgement

'It's the people we meet along life's road who help us appreciate the journey'

I consider myself blessed to have a wonderful journey of Ph.D. at Indian Institute of Technology Guwahati. This was all made possible by the guidance, motivation and love of a lot of people who hold immense value in my life.

On this note, I would like to begin with expressing my deepest gratitude to my guide Prof. Siddhartha Sankar Ghosh. First of all, I would like to thank sir for giving me with this golden opportunity to work in his lab and taking care of all the facilities to carry out my research. It was his constant support and guidance that helped me to stay motivated throughout the tenure of Ph.D and helped me to nurture not only as a researcher but also as a human being. I whole heartedly thank sir for being the inspiration I will always look forward to in my life.

I would like to express my utmost gratitude to my doctoral committee members, Prof Pranab Goswami, Dr. Biplab Bose and Dr. Prithwijit Guha for evaluating my work and for giving critical suggestions from time to time to help me improve and understand my research work better. I acknowledge all our former and present Heads of the Department, faculty members and the staff members of the Department of Biosciences and Bioengineering, IIT Guwahati for providing me with the necessary facilities and ambience to conduct my research work. I would also like to thank Centre for Nanotechnology, for providing the state-of-art facilities to carry out experimental work.

I sincerely thank Prof Ashis K. Mukherjee and Prof Abu T. Khan for providing me the opportunity to work in collaboration and explore the possibility of application of my work in multidisciplinary fields.

My first experience with research began under the guidance of Dr. Nandan Kumar Jana (Heritage Institute of Technology Kolkata) and Dr. Piyali Basak (Jadavpur University Kolkata). I am very much thankful to them for teaching me the basics of science and research. They gave me the confidence to understand and pursue further research. I would also extend my acknowledgment to the faculty members and staff members of Heritage Institute of Technology Kolkata and Jadavpur University Kolkata. I would also like to acknowledge all my respected school teachers, especially Mrs Runa Pyne, for their support and guidance in my academic life and instilling the basic human values.

I would like to thank Department of Biotechnology (DBT), Government of India for providing full travel grant support to attend the Nano Today conference in Hawaii, USA. I would also like to thank Department of Biosciences and Bioengineering, IIT Guwahati for providing the funding support to attend ICSCC Conference in Goa, India. These conferences provided me the platform to interact with eminent scientists and research scholars and gain deeper insight in the multidisciplinary field of research.

I sincerely appreciate the help, guidance and love of all my labmates, Dr. Subhamoy, Dr. Chockalingam, Dr. Nidhi, Dr. Kohila, Dr. Pallab, Dr. Aditi, Dr. Amit, Dr. Amaresh, Dr. Archita, Dr. Sharmila, Dr. Asif, Dr. Bandhan, Dr. Deepanjali, Dr. Upashi, Anil, Srirupa, Rajib, Anitha, Mukta, Debashree, Plaboni, Vanitha, Gargi, Gavya and Hirak. I thank them all for being there for me always and for providing an amicable work environment. I would also like to thank Dr Mohitosh and all the lab members under the DBT program support facility.

I would like to thank to all my batchmates, Dr. Rakesh, Dr. Ashish, Reshmi, Karukriti, Ankit, Amrendra, Vartika, Poulami, Debika, Gaurav and Debakar with whom I have spend a wonderful time here at IIT Guwahati. From academic conversations to fun outings we have been there for each other always.

'The greatest gift of life is friendship, and I have received it'. I have been very fortunate to find some great friends who are more like family now. I would love to thank Rahul, Sharmistha, Deva, Ruchi, Dr. Ananya, Dr. Rupali, Mitali, Babina, Anuma, Thyahoo, Vimal, Sukhjovan, Aman, Harsh, Nek, Nayaab, Ranbir, Aditya, Kuldeep, Ashna, Pushpendra and Himashree for their support, care and love.

No words are enough to thank the love, affection, care and encouragement that I have received from my family. They have always supported me in all my decisions and loved me at all times. Whatever I am today, I owe to them. I will always remain indebted to the Almighty God for being the guiding light at all times.

It was indeed an experience of a lifetime, a lovely and pleasant stay at IIT Guwahati***, 'and to sum it up, it was all worth it'***.

TABLE OF CONTENTS

ABSTRACT

The most dynamic and diverse class of macromolecules, proteins come armed with an array of opportunities in the field of therapeutics. Their delicate and complex structure is essential to perform multifaceted functions. However, their structure is prone to degradation, which posses a major challenge in harnessing their therapeutic remuneration. Amid numerous formulations, maneuvering nanomaterials provide ample scope for judicious designing of application based nanostructures.

Given the importance of a curative protein in the field of healthcare, the current thesis work focuses on characterizing and evaluating the anti-proliferative efficacy of the two isoforms, PTEN and PTEN-Long, alone and in combination with anti-cancer drugs. The **introduction** section describes in details the role of aberrant signaling in cancer and the panorama of recombinant protein therapy, which is consolidated by presenting literature reports on the subject in the **literature review** section. The **material and methods** section describes in details the materials required and the methodologies of the experimental procedures. The **results and discussion** section begins with the cloning and purification of PTEN and its transcriptional variant PTEN-Long. The cell based studies establishes the anti-proliferative and anti-invasive role of the membrane-permeable recombinant PTEN-Long protein in primary glioblastoma cell line. To investigate the therapeutic benefit of PTEN, silica nanoparticles were successfully employed to mediate stabilization of the GST tagged PTEN protein. Silica nanoparticles mediated cellular delivery resulted in reduced proliferation of drug resistant glioblastoma. Further, amalgamation of delivery and tracking of therapeutically relevant recombinant PTEN on a single platform was made possible by utilizing luminescent silver nanoclusters. The PTEN-nanocluster ensemble was then coated with PEG to formulate spherical nanocomposites. Evaluation of the PTEN-nanocomposite on monolayer culture and spheroid model of U-87 MG and MCF7 demonstrated modulation of cellular signaling culminating into reduced proliferation, opening up promising avenues for PTEN based therapy. Additionally, successful combination therapy of recombinant proteins with small molecule drugs strengthens the foundation for commercial application of the co-therapy strategies in future. The **conclusion and future prospects** section summarizes the findings of the work with potential biomedical application of the recombinant proteins.

Abbreviations

Abs	Absorbance
AgNCs	Silver nanoclusters
Ag	Silver
ANOVA	Analysis of variance
Akt/ PKB	Protein Kinase B
Au	Gold
A549	Adenocarcinomic human alveolar cell
BAX	BCL2 associated X
BSA	Bovine serum albumin
Calcein-AM	Calcein-acetoxymethyl
CD	Circular dichroism
CHCA	α cyano-4-hydroxycinnamic acid
CO_2	Carbon dioxide
DLS	Dynamic light scattering
DMEM	Dulbecco's Modified Eagle's Medium
DMSO	Dimethyl Sulphoxide
DNA	Deoxyribonucleic acid
DTT	Dithiothreitol
EDTA	Ethylenediaminetetraacetic acid
EGFR	Epidermal growth factor receptor
ELISA	Enzyme Linked Immunosorbent Assay
EtBr	Ethidium bromide
EtOH	Ethanol
FACS	Fluorescence activated cell sorting
FAK	Focal adhesion kinase
FBS	Fetal bovine serum
FDA	US food and drug administration
FESEM	Field emission scanning electron microscope
FOXO3a	Forkhead box protein O3
FTIR	Fourier Transform Infrared Spectroscopy
GAPDH	Glyceraldehyde 3-phosphate dehydrogenase
GST	Glutathione S transferase
HeLa	Human cervical cancer cell line
HEPES	N-2-Hydroxyethyl Piperazine N-2 Ethane Sulphonic acid
HRP	Horse radish peroxidase
IPTG	Isopropyl-1-thio-P-D galactopyranoside
k_{cat}	Turnover number

K_m	Michaelis-Menten Kinetics
MALDI-TOF	Matrix assisted laser desorption ionization-time of flight
MCF-7	Human breast cancer cell line
MTCC	Microbial Type Culture Collection
MTT	3-(4, 5-dimethylthiazol-2-yl)-2, 5-diphenyltetrazolium bromide
NaCl	Sodium chloride
NaOH	Sodium hydroxide
NCs	Nanoclusters
NH_4OH	Ammonium hydroxide
NPs	Nanoparticles
OD	Optical density
OPD	o-phenylenediaminedihydrochloride
PBS	Phosphate buffer saline
PEG	Polyethylene glycol
PCR	Polymerase chain reaction
PI	Propidium iodide
PIP_3 diC8	Dioctanoyl Phosphatidylinositol 3,4,5-triphosphate
PNPP	para-Nitrophenylphosphate
PNP	para-Nitrophenol
PTEN	Phosphatase and tensin homolog on chromosome 10
Pt	Platinum
rcf	Relative centrifugal force
RNA	Ribonucleic acid
rpm	Rotation per minute
SDS	Sodium dodecyl sulphate
SDS-PAGE	Sodium dodecyl sulphate-polyacrylamide gel electrophoresis
SNP	Silica nanoparticles
TAE	Tris acetate EDTA
TBS	Tris buffer saline
TBST	Tris buffer saline with tween
TEM	Transmission electron microscope
TEOS	Tetraethyl orthosilicate
TMX	Tamoxifen
TMZ	Temozolomide
U-87 MG	Uppsala 87 malignant glioma (Primary glioblastoma cell line)

X gal	5-bromo-4-chloro-3-indolyl-β-D-galactopyranoside
µg	Microgram
µL	Microlitre
µM	Micromolar
h	Hour
kDa	Kilodalton
mg	Milligram
min	Minute
mL	Millilitre
mm	Millimeter
mM	Millimolar
nm	Nanometer
nM	Nanomolar

LIST OF SCHEMES

LIST OF FIGURES

LIST OF TABLES

Introduction

Section 1

The ever expanding knowledge of genomics has facilitated to identify an array of proteins involved in diverse cellular functions. In our body proteins play the most diverse and dynamic role contributing extensively to the metabolic fitness of the cell. Proteins portray multitude roles such as surface receptors, hormones, signaling molecules; thereby maintaining a delicate equilibrium between cellular functions. Disruption of this equilibrium pushes the cell towards diseased state. This provides tremendous opportunity to capitalize on proteins as an important class of drugs to alleviate disease conditions. The fundamental advantages of using proteins as drugs can be summed to high specificity, which reduces their interference with routine biological processes and thus increasing their acceptance by the body. Protein therapeutics encompasses a major subset of pharmaceutical products applied for the treatment of plethora of diseases. Monoclonal antibodies, growth hormones, cytokines are a few examples of proteins successfully launched for treatment of pathological conditions.

However, the application of proteins as mainstream drugs is limited due to their complex structural architecture. Proteins secondary structural elements folds to form the intricate tertiary structure that endows functionality to the protein. This structure has a half-life and is prone to environment triggered disintegration leading to loss of protein function. Additional restraint of intracellular proteins is poor membrane permeation which makes it even more challenging to achieve the desired therapeutic benefit. Thus the focus rests on maneuvering formulations to attain stability and intracellular delivery of the protein.

Amongst numerous options under trial, nanomaterials based delivery systems are gaining considerable interest. Feasibility of synthesis and size-dependent tunable optical properties makes them advantageous for theranostic applications. Cellular penetration along with sustained release of bioactive agent makes nanomaterials an attractive vehicle for intracellular payload delivery, which further culminates to modulation of intracellular environment. Intracellular environment comprises of a number of cellular signaling pathways working in tandem to regulate cellular survival. The signaling pathways are precisely monitored by cell regulators to sustain balance between growth and apoptosis. Loss of function of the cell signaling regulators is the cardinal reason for disease initiation and

progression. Therefore, a prospective strategy is modulation of the cellular signaling by exogenous supply of the signaling regulators.

In this context, signaling-targeting recombinant proteins such as PTEN-Long and PTEN hold great impetus. Since the discovery of PTEN in 1997, there has been substantial amount of research highlighting its importance in suppressing the AKT signaling pathway. The canonical task of the AKT pathway is cell survival and growth via transcriptional regulation. However, down-regulation of signaling regulator PTEN and recently discovered PTEN-Long is the underlying cause for perturbation of the AKT signaling pathway. Uncontrolled manifestation of the AKT protein causes physiologic disturbances in the cell leading to cancer initiation and progression.

Small molecule drugs have been applied for treatment of different cancers targeting the AKT signaling pathway. However, like any other chemical compounds, these drugs also give rise to serious side effects. Therefore harnessing the potential of recombinant PTEN and PTEN-Long proteins or achieving a combinatorial strategy with small molecule drugs may render the treatment beneficial with reduced drug-associated side effects.

Given the importance of a stable and functional curative protein in field of health care, the current investigation establishes the characterization and therapeutic potential of PTEN-Long in glioblastoma (U-87 MG) alone and in combination with anti-cancer drug temozolomide. The current work also demonstrates fabrication of a novel system comprising of PTEN protein and nanomaterials (nanobioconjugate) to target the aberrant AKT/FAK signaling pathway in glioblastoma (U-87 MG) and breast cancer (MCF7) cell lines. The efficacy of the chemotherapy was augmented in combinatorial approach with anti-cancer drug erlotinib for glioblastoma (U-87 MG) cells. Further, the results on cell lines (monolayer culture) was successfully translated to three dimensional culture (spheroid culture) of glioblastoma (U-87 MG) and breast cancer (MCF7), which boosts the biological relevance and prospective implication of recombinant PTEN in biomedical applications.

Literature Review

Section 2

Indian Institute of Technology Guwahati

2.1 Recombinant Protein Based Therapy

Ever since the engineering of recombinant insulin nearly three decades ago, there has been an appreciable increase in available protein based biopharmaceutical drugs including peptides, hormones, recombinant proteins and monoclonal antibodies (Mitragotri *et al.,* 2014). Recombinant protein comes armed with an array of advantages such as, high yield and specificity (Leader *et al.,* 2008), low immunogenicity and well tolerance. Over small molecule drugs the major advantage of proteins is their high specificity which is difficult to be mimicked by chemical compounds. Consequently target specific action reduces their interference with routine biological processes, thereby reducing possible side effects (Leader, Baca et al. 2008). A variety of molecular types of therapeutic proteins are available for disease treatment, which are generally classified as antibody-based drugs, Fc fusion proteins, anticoagulants, blood factors, bone morphogenetic proteins, engineered protein scaffolds, enzymes, growth factors, hormones, interferons, interleukins and thrombolytics (Dimitrov 2012). The pharmaceutical industry is undergoing a paradigm shift towards proteins as therapeutic moieties. A list of commercially available protein based drugs presented in **Table 2.1**, shows enormous commercial aspects of the protein drugs applied for treatment of a number of diseases.

A number of recombinant protein drugs, a major subset of biologics, are available and many more are in pipeline to target major diseases areas, such as cancer, viral diseases, cardiovascular diseases and endocrine diseases (Russell and Clarke 1999, Liras 2008), as illustrated in **Scheme 2.1 and Table 2.2,** which represent the market distribution of different therapeutic proteins. In many cases, the recombinant protein is effective and plays an irreplaceable role in the treatment of the pathological condition. Such as hemophilia, except blood coagulation factor, which has an extremely limited source, the treatment mostly relies on the recombinant coagulation factor (Swiech *et al.*, 2017). Many recombinant proteins are in clinical practice for more than two decades with an optimal safety and absence of side effects. As in case of growth hormone therapy, where administration of the growth hormone for short as well as long-term adult GH replacement in patients with severe GH deficiency and hypopituitarism was found to be safe (Gibney and Johannsson 2004, Stochholm and Johannsson 2015).

Drug	Sponsor/ Source	Treatment	Sale (2016)
Humira (adalimumab)	AbbVie	Rheumatoid arthritis	$16.078 billion
Harvoni (ledipasvir 90 mg/sofosbuvir 400 mg)	Gilead Sciences	Chronic hepatitis C virus (HCV)	$9.081 billion
Enbrel (etanercept)	Amgen and Pfizer	Rheumatoid arthritis, psoriatic arthritis	$8.874 billion
Rituxan (rituximab, MabThera)	Roche (Genentech) and Biogen	Non-Hodgkin's lymphoma	$8.583 billion
Remicade (infliximab)	Johnson & Johnson and Merck	Crohn's disease	$7.829 billion
Revlimid (lenalidomide)	Celgene	Multiple myeloma	$6.974 billion
Avastin (bevacizumab)	Roche (Genentech)	Metastatic colorectal cancer	$6.752 billion
Herceptin (trastuzumab)	Roche (Genentech)	HER2 overexpressing breast cancer	$6.751 billion
Lantus (insulin glargine)	Sanofi	Type 1 diabetes (pediatric) and in adults with type 2 diabetes	$6.054 billion
Prevnar 13	Pfizer	pneumococcal pneumonia	$5.718 billion
Xarelto (rivaroxaban)	Bayer and Johnson & Johnson	Deep vein thrombosis (DVT) and pulmonary embolism (PE)	$5.390 billion

Drug	Sponsor/ Source	Treatment	Sale (2016)
Eylea (aflibercept)	Bayer and Regeneron Pharmaceuticals	nonvascular (wet) age-related macular degeneration	$5.045 billion
Eylea (aflibercept)	Bayer and Regeneron Pharmaceuticals	nonvascular (wet) age-related macular degeneration	$5.045 billion
Lyrica (pregabalin)	Pfizer	peuropathic pain associated with diabetic peripheral neuropathy	$4.966 billion
Neulasta / Peglasta (pegfilgrastim) and Neupogen / Gran (filgrastim)	Amgen and Kyowa Hakko Kirin	febrile neutropenia	$4.701 billion
Advair /Seretide (fluticasone and salmeterol)	GlaxoSmithKline	Asthma	$4.325 billion

Table 2.1 List of protein based drugs for treatment of different diseases. Data is curated by genetic engineering and biotechnology new (GEN), March 06, 2017 **(**https://www.genengnews.com/the-lists/the-top-15-best-selling-drugs-of-2016/77900868)

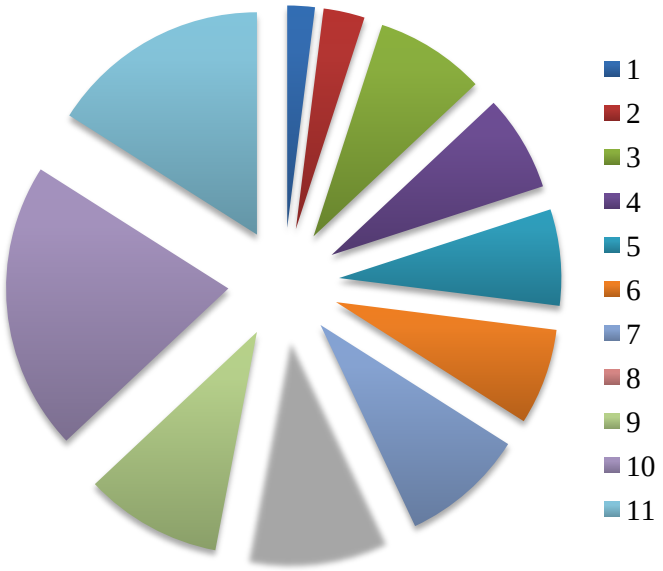

Scheme 2.1 The market distribution of different protein therapeutics. Data is curated by Creative BioMart (https://www.creativebiomart.net/blog/market-and-rd-analysis-of-recombinant-protein-drugs/)

Serial Number	Treatment Type	Market Share (%)
1	Growth Hormones	2%
2	Blood Coagulation	3%
3	Erythropoietin	8%
4	Pure Vaccines	7%
5	Interferons	7%
6	Immunostimulating Agents	7%
7	Autoimmune	9%
8	Immunosuppressive Agents	10%
9	Insulins	10%
10	Oncology	21%
11	Others	16%

Table 2.2 The market share of different protein therapeutics. Data is curated by Creative BioMart (https://www.creativebiomart.net/blog/market-and-rd-analysis-of-recombinant-protein-drugs/)

2.2 Recombinant Protein Therapy in Cancer Treatment

In terms of protein therapeutics, currently only monoclonal antibodies, targeting over-expressed receptors, are prominently available for treatment of different tumors, **Table 2.3**. The development of hybridoma technology for monoclonal antibody production revolutionized the treatment regime for solid tumors. Following approval of the first monoclonal antibody, rituximab, for clinical treatment of non- hodgkin's lymphoma, a number of monoclonal antibodies have been generated and are at present in clinical use for treatment of solid tumors**.** However, the clinical success and the long term benefits of recombinant protein therapy for treatment of different diseases have fostered enormous interest in their application for treatment of cancer. Li and colleagues reported anti-tumor effect of novaferon, a novel recombinant protein produced by DNA shuffling of interferon-α (Li *et al.*, 2014). Evaluation of novaferon bioactivity on tumor cell displayed reduction in proliferation of HepG2 cells *in vitro* and *in vivo*. This promising pre-clinical study has provided strong lead for clinical trial verification. Likewise Zhang and colleagues demonstrated HER-2 receptor targeted activity of another recombinant protein e23sFv-Fdt-casp6 (immune-caspasse-6) *in vitro* and *in vivo* (Zhang *et al.*, 2016).

Brand	Generic	Company	Treatment
Rituxan	Rituximab	Genentech	Non-Hodgkin's Lymphoma
Herceptin	Trastuzumab	Genentech	Breast Cancer
Campath	Alemtuzumab	Schering AG	Non-Hodgkin's Lymphoma
Erbituz	Cetuzimab	Imclone Systems	Colon cancer
Avastin	Bevacizumab	Genentech	Colon cancer

Table 2.3 List of monoclonal antibodies available for treatment of cancer. Data is curated by Laborant (http://laborant.pl/index.php/recombinant-protein-therapeutics-the-future-is-here)

The recombinant protein e23sFv-Fdt-casp6 displayed inhibition of proliferation of HER-2 over-expressing A172 and U251MG *in vitro*, but not U-87 MG cells with undetectable HER-

2 expression. Thus, the ability to produce targeted cytotoxicity makes the recombinant e23sFv-Fdt-casp6 a promising therapeutic alternative for GBM treatment.

From the viewpoint of therapeutics, choosing the potential drug target is extremely crucial. In pathological condition such as cancer, the major focus lies on taming the signaling pathways that have lost their inherent regulation or control, as aberrant signaling is the hallmark of this disease (Hanahan and Weinberg 2000). One such frequently de-regulated signaling pathway associated with pathogenesis is the Akt signaling pathway (Robertson 2005, Tokunaga *et al.*, 2008). The over-expression of pro-proliferation protein Akt and the dependency of the tumor for its proliferation make the Akt signaling pathway an emerging therapeutic target (Robertson 2005, Tokunaga, Oki et al. 2008).

2.3 Cellular Role of the Akt Signaling Pathway

Cellular communication or cellular signaling networks regulate the membrane, cellular organellar and cyto-skeletal activities. A plethora of signaling networks work in tandem to decide the fate of the cell. With the knowledge accumulated over three decades, the Akt cellular signaling pathway has become a central figure in the cellular signaling. The serine/threonine protein kinase Akt defines multitude cellular functions by promoting cell growth, survivial, migration and angiogenesis among others via both protein and transcriptional regulation (Song *et al.,* 2005). The Akt/PKB kinase family encompasses three isoforms, Akt1 (PKBα), Akt2 (PKBβ) and Akt3 (PKBγ). Knockout studies have revealed specific responsibilities of the three isoforms. Akt1 plays a critical role is cell survival (Chen *et al.,* 2001), Akt 2 is essential for the maintenance of glucose homeostasis (Gonzalez and McGraw 2009) and Akt3 is involved in brain growth and development (Tschopp *et al.,* 2005). The PI3K/ Akt pathway is initiated by activation of growth factor receptor tyrosine kinase that leads to allosteric activation of PI3Kinase. The activated PI3Kinase mediates phosphorylation of the lipid phosphatidylinositol 4, 5 diphosphate (PIP_2) to phosphatidylinositol 3, 4, 5 triphosphate (PIP_3). The protein lipid interaction is mediated by two binding domain FYVE and pleckstrin homology (PH) domain (Pawson and Nash 2000, Fresno Vara *et al.,* 2004). Akt was identified as the human homologue of viral oncogene v-akt, which caused leukemia in mice (Staal *et al.,* 1977, Bellacosa *et al.,* 1991, Jones *et al.,*

1991). The activation of Akt is mediated by phosphorylation at two regulatory sites, threonine308 (T308) and serine473 (S473). PIP_3 phopholipid mediates conformational change in Akt, thereby exposing the regulatory phosphorylation sites. The PH domain present in both Akt and protein serine/threonine kinase 3'-phosphoinositide-dependent kinase1 (PDK1) may allow hetero-dimerization of the two proteins resulting in phosphorylation of threonie at T308. Several studies suggest involvement of integrin-linked kinase (ILK) or mTOR2 complex in phosphorylation of the hydrophobic motif S473.

Therefore the molecules upstream of Akt pathway are involved in regulating the activation of Akt. Protein kinase Akt catalyzes de-phosphorylation of a number of cellular substrates. The signature recognition motif includes R-X-R-X-X-S/T-B, where X represents any amino acid and B represents bulky hydrophobic residue (Alessi and Cohen 1998). The cellular implications of de-phosphorylation of the substrates can be broadly defined as

- **Regulation of Cell Cycle Progression**

Akt amend the cell cycle via multiple substrates. Akt positively influences the activity of Skp2 by phosphorylation at Serine72 site (Gao *et al.,* 2009). This permits cytoplasmic localization and enhanced stability of Skp2, which results in cyclinE-Cdk2 dependent degradation of p27 (Liang and Slingerland 2003). The cellular role of p27 involves maintenance of cell in quiescent stage (Lee and Kim 2009). It is well established that Akt phosphorylates GSK3 at serine9 and serine21 residues. GSK3 plays a central role in WNT signaling pathway, by stabilizing the β-catenin destruction complex (Wu and Pan 2010). Phosphorylation of GSK3 by Akt causes its inactivation, thereby impeding the destruction of β-catenin. This allows β-catenin to localize in the nucleus and mediate TCF dependent transcription of genes involved in cell growth and survival.

- **Regulation of Cell Death**

Akt catalyzes the phosphorylation and thereby inactivation of pro-apoptotic protein BAD at serine136 (Hayakawa *et al.,* 2000). Another important group of transcription factors include the forkhead box transcription factors (FoxO). The FoxO transcription factors regulate a plethora of cellular processes ranging from cell proliferation to apoptosis (Zhang *et al.,*

2011). Akt phosphorylates Mdm2, which then translocates to the nucleus to bind and inactivate p53 (Mayo and Donner 2001). Subsequently p53 is translocated to the cytoplasm to mediate its degradation by ubiquitin-proteosome system. Thus, Akt supports cell cycle progression and inhibits apoptosis via multiple regulatory proteins. The substrates of Akt are represented in **scheme 2.2**.

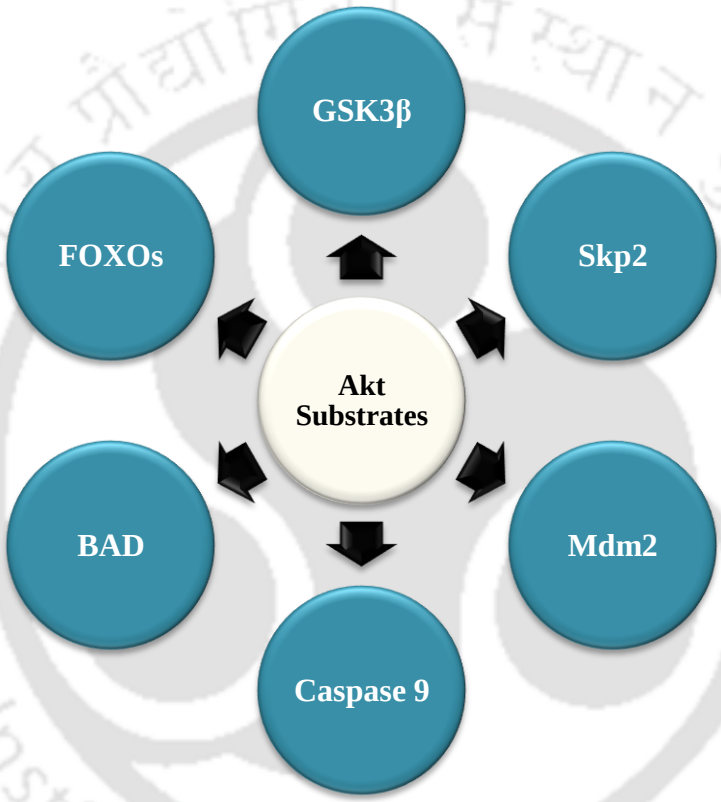

Scheme 2.2 Illustration of substrates phosphorylated by Akt to regulate cellular environment

2.4 Regulation of Akt Pathway by PTEN

The function of Akt is tightly regulated under homeostasis. De-phosphorylation and inactivation of Akt by protein phosphatase 2A (PP2A) at threonine308, decrease the kinase activity. Another protein phosphatase PH domain and leucine rich repeat protein phosphatase (PHLPP) is known to de-phosphorylate Akt at serine473 regulatory site. However, PP2A activity is not specific to Akt, and it is known to de-phosphorylate other substrates as well.

The upstream regulation of Akt is dependent on action of a phosphoinositide lipid. The enzyme phosphoinositide 3-kinase (PI3 Kinase) catalyses the phosphorylation of the lipid PIP_2 to PIP_3. One of the foremost functions of the protein PTEN (phosphatase and tensin homolog deleted on chromosome ten) is antagonizing the function of PI3Kinase (Stambolic *et al.*, 1998). PTEN gene located on chromosome 10, encodes a 403 amino acid dual specificity phosphatase, which belongs to the protein tyrosine phosphatase (PTPs) family. Like the PTPs family, PTEN possess the signature catalytic motif HCXXGXXR (Lee *et al.*, 1999). The N-terminal domain includes the phosphatase domain, which shares structural resemblance to the dual specificity phosphatase VHR. However, the active site pocket or the P-loop is comparatively larger and deeper with basic residues to fit the negatively charged lipid or polypeptide substrates (Myers *et al.*, 1997). Thus, cellular role of PTEN makes it a crucial negative regulator of the Akt transduction pathway, as represented in **Scheme 2.3**.

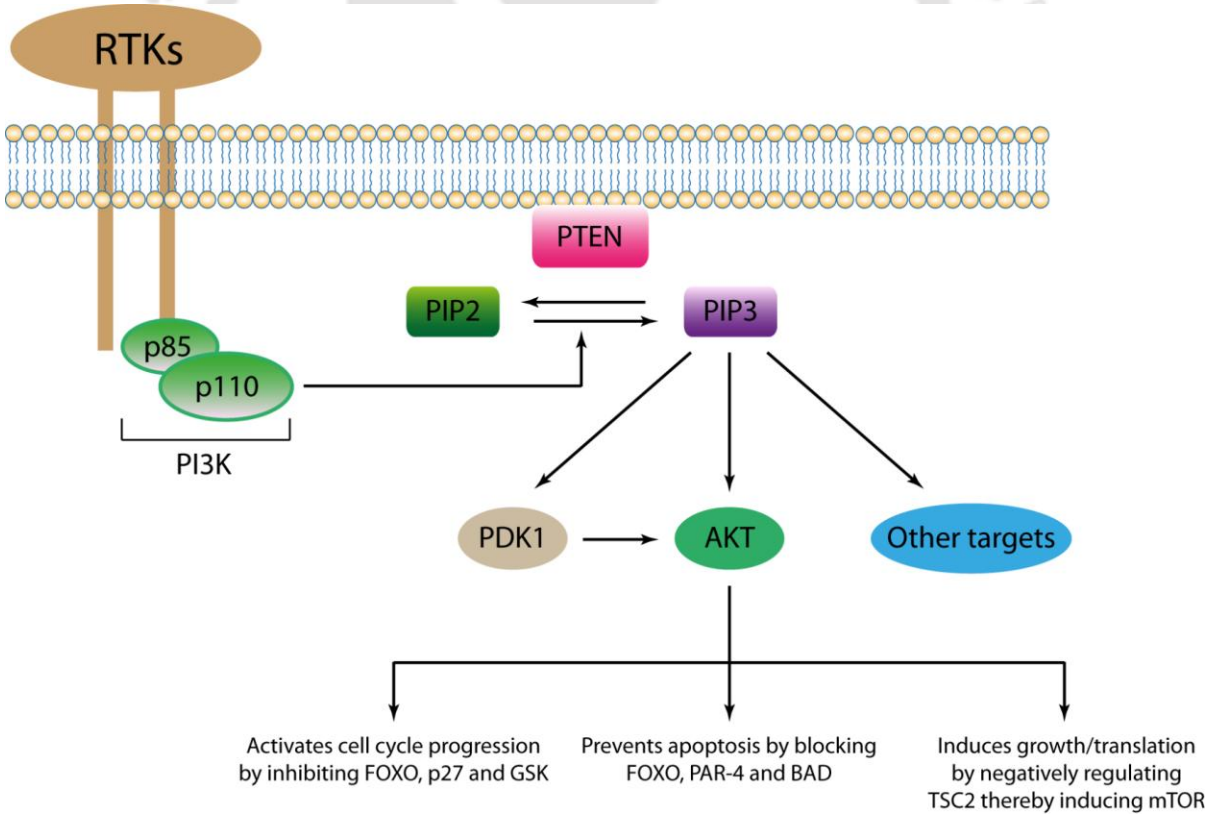

Scheme 2.3 Overview of the PTEN/Akt/PI3K signaling pathway. Adopted and redrawn from the article, 'The role of PTEN signaling perturbations in cancer and in targeted therapy (Keniry and Parsons 2008)'.

Under homeostasis the cellular signaling and the regulatory signals work in a well regulated loop to balance cell survival and apoptosis. Disruption of this loop shifts the cellular behavior to unregulated territory, which is the hallmark of any pathogenic condition. Since PTEN is a critical regulator of the Akt signaling pathway loss of PTEN protein function due to mutations or down-regulation has been correlated with including tumor initiation (particularly glioma, breast and kidney), progression and poor prognosis. Many of the missense mutations fall within the phosphatase domain, including several within the highly conserved signature motif (HCXXGXXR). Within this catalytic domain, the cysteine residue is essential for catalysis, and the arginine residue plays a crucial role in binding of the phosphoryl group of the substrate (Fauman and Saper 1996, Spinelli and Leslie 2015). PTEN deletion or mutation is largely associated with glioblastomas (Liu *et al.,* 1997). Predominantly glioblastomas display PTEN down-regulation accompanied with EGFR amplification (Liu, James et al. 1997). Reportedly PTEN has been found to be inactivated by mutation in prostate cancer (Cairns *et al.,* 1997). Therefore loss of tumor suppressor function of PTEN contributes to pathogenesis.

2.5 Current Status of the Akt Pathway Inhibition and Limitations

Contemplating the regulatory role of Akt and its frequent de-regulation in pathogenesis, a number of inhibitors have been designed to achieve therapeutic benefit. A number of Akt inhibitors are under pre-clinical and clinical studies, among an extensive number of Akt pathway inhibitors under development, a few have been presented in **Table 2.4**.

Inhibitor	**Target**	**Manufacturer**	**Stage of Development**	**Reference**
Perifosine	Akt, MAPK, JNK pathways	AEterna Zentaris	Phase I and Phase II trials for solid tumors	(Van Ummersen *et al.,* 2004, Guidetti *et al.,* 2014)
MK-2206	Allosteric inhibitor of Akt	Merck & Co	Preclinical trials for solid tumor	(Hirai *et al.,* 2010, Alexander 2011)

GSK690693	All isoforms of Akt	GlaxoSmithKline	Preclinical trials and Phase I for solid tumor	(Aghajanian *et al.*, 2018)
Afuresertib	Reversible Akt kinase inhibitor	GlaxoSmithKline	Phase I for Multiple Myeloma and hematologic malignancies	(Spencer *et al.*, 2013, Spencer *et al.*, 2014)
Ipatasertib	Small-molecule AKT inhibitor	Roche	Phase II trial for breast cancer	(Kim *et al.*, 2017, Saura *et al.*, 2017)
AZD5363	ATP-competitive AKT kinase inhibitor	AstraZeneca	Phase I trials for solid tumors	(Davies *et al.*, 2012, Hyman *et al.*, 2017)
Wortmannin	Irreversible inhibition of PI3K	-	Clinical trial suspended	(Wymann *et al.*, 1996, Marone *et al.*, 2008)
PX-866	Irreversible inhibition of PI3K	ProlX Pharmaceutical	Phase 1 Clinical trial for solid tumors	(Ihle *et al.*, 2004, Jimeno *et al.*, 2009)
SF1126	pan-PI3K inhibitor	Semaphore Pharmaceuticals	Phase I trials for solid tumors	(Garlich *et al.*, 2008, Chiorean *et al.*, 2009)

Table 2.4 List of Akt pathway inhibitors

A plethora of chemical compounds have been tested and a number of them are under development for the inhibition of one of the most important pathological pathway, the Akt/PI3K pathway. However, the small molecule inhibitors show pharmacological limitations. Wortmannin was found to have excellent anti-proliferative activity, however it was unstable in biological fluids, a condition referred to as 'wortmannin paradox' (Yuan *et al.,* 2007). Therefore, poor pharmacological properties, low aqueous solubility, cellular toxicity and limited stability precluded clinical development of this molecule (Wymann *et al.,* 2003). MK-2206 an allosteric inhibitor of Akt induced significant apoptosis in human breast cancer cells. Despite encouraging preclinical trial studies, Ma and colleagues did not observe any significant anti-tumor effect of MK-2206 in combination with hormonal therapy in patients under phase I clinical trial (Jansen *et al.,* 2016, Ma *et al.,* 2016). The treatment with MK-2206 was limited by the development of rash and 17% of patients discontinued treatment due to toxicities. Similarly, numerous preclinical studies demonstrated inhibition of all isoforms of Akt by GSK690693. *In vivo* studies suggested inhibition of SKOV-3 ovarian, LNCaP prostate, and BT474 breast tumors (Kumar Pal *et al.,* 2010). Despite these preclinical findings, phase I trial testing was suspended due to drug-related hyperglycemia (Crouthamel *et al.,* 2009, Kumar Pal, Reckamp et al. 2010). Therefore, it is the side effects associated with small molecule inhibitors that led the drug discovery industry undergo a paradigm shift towards alternative approaches viz gene therapy and protein therapy.

2.6 PTEN Based Therapy

One of the reasons for amplified Akt function is the loss or down-regulation of PTEN function. PTEN mutations have been reported to be a major determinant that influence tumor development across tissues (Dillon and Miller 2014). Missense, nonsense or frameshift mutations occur throughout the gene, however hotspot mutations at specific amino acids have been identified as Arg130, Arg173 and Arg233 (Song *et al.,* 2012). Although PTEN mutations have been associated with wide range of cancers, uterine cancer and glioblastoma multiforme have the highest percentages of PTEN mutations and homozygous loss (Dillon and Miller 2014). The types of PTEN mutations in different tissue samples has been illustrated in **Scheme 2.4** and **Table 2.5**

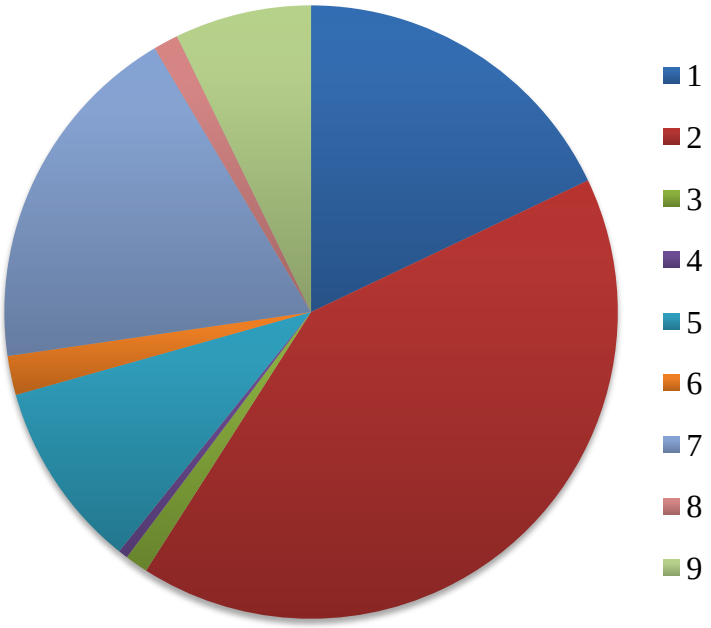

Scheme 2.4 Distribution of PTEN mutations in tissue samples. Data is curated by the Catalogue of Somatic Mutations in Cancer (COSMIC) database (www.sanger.ac.uk/genetics/CGP/cosmic)

Serial Number	Mutation Type	Number of samples (%)
1	Nonsense Substitution	890 (18.19 %)
2	Missense Substitution	2038 (41.66%)
3	Synonymous Substitution	60 (1.23%)
4	Inframe Insertion	25 (0.51%)
5	Frameshift Insertion	490 (10.02%)
6	Inframe Deletion	102 (2.09%)
7	Frameshift Deletion	931 (19.03%)
8	Complex Mutation	65 (1.33%)
9	Other	357 (7.30%)
	Total Unique Samples	4892

Table 2.5 Types of PTEN mutations in different samples. Data is curated by the Catalogue of Somatic Mutations in Cancer (COSMIC) database (www.sanger.ac.uk/genetics/CGP/cosmic)

Therefore, one of the potential therapeutic strategies is replenishment of the PTEN function. Exogenous PTEN function can be mediated via delivery of the correct gene or the gene product. Non-viral and adenoviral mediated PTEN gene therapy effect has been evaluated both *in vitro* cell lines and *in vivo*. Tanaka and colleagues investigated the *in vitro* and *in vivo* effect of adenoviral vector mediated PTEN delivery in bladder cancer cell lines expressing PTEN differentially. PTEN gene therapy resulted in enhanced tumor apoptosis and inhibition of tumor growth *in vivo.* Combination therapy with doxorubicin resulted in chemo-sensitization of doxorubicin resistant cell line UM-UC-6dox (Tanaka *et al.*, 2000, Tanaka and Grossman 2003). Adenoviral vector PTEN gene therapy in combination with radiation (5 Gy) has been reported to inhibit the growth of human prostate tumors xenografts (Anai *et al.*, 2006). Examination of the genetic profile of glioblastoma revealed mutations of the PTEN gene located at 10q23.3 prevail in primary glioblastomas (~25%) (Ohgaki and Kleihues 2013). Therefore, one of the strategies is restoration of PTEN function in gliomas. Adenovirus-PTEN gene transfer resulted in *in vivo* decrease in angiogenesis in orthotopic brain tumors (Abe *et al.*, 2003). The results indicated PTEN's role in regulating angiogenesis in gliomas, in spite of the presence of strong pro-angiogenic signals provided by constitutive EGFR activation or p53 inactivation (Abe, Terada et al. 2003). Co-transfer of two tumor suppressor genes TIMP-2 and PTEN by adenoviral mediated method in U-87 MG cells was attempted by Lu and colleagues (Lu *et al.*, 2004). Combination therapy resulted in enhanced inhibition of invasion as compared to monotherapy, suggesting that adenovirus-mediated combined TIMP-2 and PTEN gene therapy can possibly be valuable for anti-invasion therapy of malignant glioma (Lu, Zhou et al. 2004). *In vitro* and pre-clinical studies of PTEN gene therapy in different tumor systems have provided encouraging results. However, the clinical trials for PTEN gene therapy or even for other tumor suppressor genes are still in the nascent stage and demands further optimization of the current gene therapy protocols to achieve clinical success (Okura *et al.*, 2014).

An alternative strategy to combat disease conditions is protein therapy. A study by Hopkins *et al* (Hopkins et al., 2013), reported successful purification of a translational variant of PTEN, termed as PTEN-Long. PTEN-Long is transcribed from an alternative translation start site (CTG), which is 519 base pairs upstream of the translation start site of PTEN (ATG).

This adds another 173 amino acids at the N-terminal sequence of the protein. The stretch of arginine residues in the additional 173 amino acid region grants a membrane-permeable function to the protein. PTEN-Long has been reported to antagonize the canonical Akt/PI3K pathway and induce apoptosis *in vitro* and *in vivo* (Hopkins, Fine et al. 2013, Wang *et al.,* 2015).

2.7 Delivery Strategies for Intracellular Recombinant Protein Therapy

Protein therapeutics encompasses a major subset of pharmaceutical products applied for the treatment of plethora of diseases. As presented above in **Table 2.1**, there are a number of commercially available protein drugs. However, proteins are the most dynamic and versatile class of macromolecules that perform numerous function inside the body. As discussed above, one of the major functions of proteins is regulation of cellular signaling. This is because disruption in regulatory proteins gives rise to disease conditions. However, the endeavor to use intracellular regulatory proteins as regular therapeutic agent faces challenges due to their inherent complex architecture (Putney and Burke 1998). The macromolecules are generally susceptible to rapid structural disintegration and degradation leading to forfeiture of functionality. Intracellular proteins possess additional limitation of poor membrane permeation (Mitragotri *et al.,* 2014). Therefore, a major quest in protein therapeutics is the formulation of the protein delivery cargo to achieve successful intracellular conveyance of functional protein. This necessitates the application of a suitable stabilization approach to make recombinant proteins acceptable drug candidates (Lu *et al.,* 2006). While a number of formulations are being characterized to stabilize and deliver proteins viz liposome (Herrera Estrada and Champion 2015), nanoparticles (Utama *et al.,* 2012), and injections among others, it is extremely crucial to confirm that the interaction between the protein and carrier does not hamper the active state conformation and activity of the protein. Formulation of proteins for their sustained delivery for pharmaceutical applications has always been a challenging task. Various model as well as therapeutic proteins, such as bovine serum albumin, myoglobin, erythropoietin and rIL-2 have been formulated into polymer coated microparticles to achieve their sustained release for biomedical applications (Geng *et al.,* 2008, Yang *et al.,* 2009, Liu *et al.,* 2012, Xu *et al.,* 2012, Zhao *et al.,* 2013).

- **Silica Nanoparticles**

Among different materials used for synthesis of nanomaterials for biomedical applications, silica nanoparticles has gained attention as drug delivery vehicles due to their excellent properties such as, tunable shape and size, biocompatibility and ease of synthesis (Benezra *et al.,* 2011, Tang and Cheng 2013) Interestingly, silica nanoparticles ranging from 25 to 100 nm in size are reported to cross the blood brain barrier (Hanada *et al.,* 2014). In 2011, FDA approved first-in human clinical trial of small sized nonporous silica nanoparticles highlighting their importance in biomedical applications (Tang and Cheng 2013). Besides silica nanoparticles can be readily modified providing great scope for application dependent alterations, for example fluorescent silica nanoparticles offer an attractive tool for cell labeling purposes (Soenen *et al.,* 2013). Since a large number of signaling proteins are intracellular proteins, there is an ever increasing demand for synthesis of efficient nano-carriers for delivery. Silica nanoparticles functionalized with n-octadecyltrimethoxysilan have been successfully employed for intracellular delivery of phospho-AKT antibody into MCF-7 cells resulting in regulation of cellular signaling indicating successful delivery (Bale *et al.,* 2010, Niu *et al.,* 2015). Owning to their properties silica has always been a preferred material for intended protein stabilization and delivery.

- **Metal Nanoclusters**

Advancement in fabrication of nanomaterials gave rise to a new class of nanomaterials known as metal nanoclusters that comes armed with attractive properties such as optical stability, efficient clearance from the body and low side effects, making them suitable for biomedical applications (Song *et al.,* 2016). Metal nanoclusters constitute an innovative class of nanomaterials that provide the missing link between metal atoms and nanoparticles (Diez and Ras 2011). Ever since the inception of metallic nanoclusters, they have been largely applied as fluorescent probes or labels for bioimaging application (Li *et al.,* 2012, Das *et al.,* 2015, Yang *et al.,* 2015). Along with the commonly developed metal clusters of gold (Au) and silver (Ag) for bioimaging (Shiang *et al.,* 2012), platinum clusters and nanodiamonds are emerging as innovative materials for theranostic applications (Chen *et al.,* 2015, Ryu *et al.,* 2016). Additional exciting avenue of nanoclusters applications involve combination of

fluorescent imaging with delivery of drug or gene to combat disease conditions (Li *et al.*, 2013, Yahia-Ammar *et al.*, 2016).

A single system comprising delivery of therapeutic biomolecules and simultaneous imaging of the delivery makes it promising for all biomedical applications. To accomplish successful medical applications, modification or coating of nanomaterial surface is routinely executed. An array of biodegradable polymers such as polyethylene glycol (PEG), chitosan (Chronopoulou *et al.*, 2013) and poly(lactic-co-glycolic acid) (PLGA) have been employed for the modification of nanomaterial surface. Polymeric coating offers a surplus of advantages such as regulation of size, charge, density and sustained release of payload (Budhian *et al.*, 2008). Addition of PEG coating has been reported to overcome elementary challenges in the clinical applications of nanoparticles, reduced non-specific protein interactions and enhanced circulation time and stability (Jokerst *et al.*, 2011). Nanoparticles coated with PEG are known to efficiently diffuse into the brain tissue as compared to uncoated nanoparticles (Brigger *et al.*, 2002, Nance *et al.*, 2012), perhaps due to the 'sleath' (Jokerst, Lobovkina et al. 2011) behavior of PEG and enhanced circulation time (Calvo *et al.*, 2001). This opens up promising avenues for formulating therapeutic delivery systems for treatment of diseases pertaining to the central nervous system (CNS).

2.8 Key Features and Scope of the Work

The fundamental understanding that targeting cellular signaling can offer substantial therapeutic leverage opens enormous scope to generate recombinant proteins and mediate their cellular delivery. The present research investigation is based on the following scopes as potential research areas.

- Identification and purification of a specific recombinant signaling molecule
- Targeting defective cellular signaling pathways to achieve therapeutic success
- Exploring the application of novel nanomaterials for stabilization and delivery of intracellular proteins
- Exploring the combination therapy of recombinant proteins with anti-cancer drugs with the aim of reducing the drug associated side effects

- Evaluation of the therapeutic efficacy of the recombinant proteins on different screening platforms, such as monolayer cultures and three dimensional cultures to understand the biological relevance of the protein

2.9 Objectives

In the light of the regulatory role of PTEN and formulation of a successful stabilization and delivery vehicle to achieve therapeutic benefit, the following objectives were framed.

- Cloning, expression and purification of key signaling regulator, such as PTEN and PTEN Long
- Functional characterization of the recombinant signaling proteins
- Synthesis, characterization of suitable nanocarrier for stabilization and delivery of the recombinant PTEN to cancer cells
- Deciphering molecular aspects in recombinant PTEN therapy

2.10 References

Abe, T., Terada, K., Wakimoto, H., Inoue, R., Tyminski, E., Bookstein, R., Basilion, J. P. and Chiocca, E. A. (**2003**). PTEN decreases in vivo vascularization of experimental gliomas in spite of proangiogenic stimuli. Cancer Res **63**(9), 2300-2305.

Aghajanian, C., Bell-McGuinn, K. M., Burris, H. A., 3rd, Siu, L. L., Stayner, L. A., Wheler, J. J., Hong, D. S., Kurkjian, C., Pant, S., Santiago-Walker, A., Gauvin, J. L., Antal, J. M., Opalinska, J. B., Morris, S. R. and Infante, J. R. (**2018**). A phase I, open-label, two-stage study to investigate the safety, tolerability, pharmacokinetics, and pharmacodynamics of the oral AKT inhibitor GSK2141795 in patients with solid tumors. Invest New Drugs.

Alessi, D. R. and Cohen, P. (**1998**). Mechanism of activation and function of protein kinase B. Curr Opin Genet Dev **8**(1), 55-62.

Alexander, W. (**2011**). Inhibiting the Akt Pathway in Cancer Treatment: Three Leading Candidates. Pharmacy and Therapeutics **36**(4), 225-227.

Anai, S., Goodison, S., Shiverick, K., Iczkowski, K., Tanaka, M. and Rosser, C. J. (**2006**). Combination of PTEN gene therapy and radiation inhibits the growth of human prostate cancer xenografts. Hum Gene Ther **17**(10), 975-984.

Bale, S. S., Kwon, S. J., Shah, D. A., Banerjee, A., Dordick, J. S. and Kane, R. S. (**2010**). Nanoparticle-Mediated Cytoplasmic Delivery of Proteins To Target Cellular Machinery. ACS Nano **4**(3), 1493-1500.

Bellacosa, A., Testa, J. R., Staal, S. P. and Tsichlis, P. N. (**1991**). A retroviral oncogene, akt, encoding a serine-threonine kinase containing an SH2-like region. Science **254**(5029), 274-277.

Benezra, M., Penate-Medina, O., Zanzonico, P. B., Schaer, D., Ow, H., Burns, A., DeStanchina, E., Longo, V., Herz, E., Iyer, S., Wolchok, J., Larson, S. M., Wiesner, U. and Bradbury, M. S. (**2011**). Multimodal silica nanoparticles are effective cancer-targeted probes in a model of human melanoma. J Clin Invest **121**(7), 2768-2780.

Brigger, I., Morizet, J., Aubert, G., Chacun, H., Terrier-Lacombe, M. J., Couvreur, P. and Vassal, G. (**2002**). Poly(ethylene glycol)-coated hexadecylcyanoacrylate nanospheres display a combined effect for brain tumor targeting. J Pharmacol Exp Ther **303**(3), 928-936.

Budhian, A., Siegel, S. J. and Winey, K. I. (**2008**). Controlling the in vitro release profiles for a system of haloperidol-loaded PLGA nanoparticles. Int J Pharm **346**(1-2), 151-159.

Cairns, P., Okami, K., Halachmi, S., Halachmi, N., Esteller, M., Herman, J. G., Jen, J., Isaacs, W. B., Bova, G. S. and Sidransky, D. (**1997**). Frequent inactivation of PTEN/MMAC1 in primary prostate cancer. Cancer Res **57**(22), 4997-5000.

Calvo, P., Gouritin, B., Chacun, H., Desmaele, D., D'Angelo, J., Noel, J. P., Georgin, D., Fattal, E., Andreux, J. P. and Couvreur, P. (**2001**). Long-circulating PEGylated

polycyanoacrylate nanoparticles as new drug carrier for brain delivery. Pharm Res **18**(8), 1157-1166.

Chen, D., Zhao, C., Ye, J., Li, Q., Liu, X., Su, M., Jiang, H., Amatore, C., Selke, M. and Wang, X. (**2015**). In Situ Biosynthesis of Fluorescent Platinum Nanoclusters: Toward Self-Bioimaging-Guided Cancer Theranostics. ACS Applied Materials & Interfaces **7**(32), 18163-18169.

Chen, W. S., Xu, P.-Z., Gottlob, K., Chen, M.-L., Sokol, K., Shiyanova, T., Roninson, I., Weng, W., Suzuki, R., Tobe, K., Kadowaki, T. and Hay, N. (**2001**). Growth retardation and increased apoptosis in mice with homozygous disruption of the akt1 gene. Genes & Development **15**(17), 2203-2208.

Chiorean, E. G., Mahadevan, D., Harris, W. B., Von Hoff, D. D., Younger, A. E., Rensvold, D. M., Shelton, C. F., Hennessy, B. T., Garlich, J. R. and Ramanathan, R. K. (**2009**). Phase I evaluation of SF1126, a vascular targeted PI3K inhibitor, administered twice weekly IV in patients with refractory solid tumors. Journal of Clinical Oncology **27**(15_suppl), 2558-2558.

Chronopoulou, L., Massimi, M., Giardi, M. F., Cametti, C., Devirgiliis, L. C., Dentini, M. and Palocci, C. (**2013**). Chitosan-coated PLGA nanoparticles: A sustained drug release strategy for cell cultures. Colloids and Surfaces B: Biointerfaces **103**, 310-317.

Crouthamel, M. C., Kahana, J. A., Korenchuk, S., Zhang, S. Y., Sundaresan, G., Eberwein, D. J., Brown, K. K. and Kumar, R. (**2009**). Mechanism and management of AKT inhibitor-induced hyperglycemia. Clin Cancer Res **15**(1), 217-225.

Das, N. K., Ghosh, S., Priya, A., Datta, S. and Mukherjee, S. (**2015**). Luminescent Copper Nanoclusters as a Specific Cell-Imaging Probe and a Selective Metal Ion Sensor. The Journal of Physical Chemistry C **119**(43), 24657-24664.

Davies, B. R., Greenwood, H., Dudley, P., Crafter, C., Yu, D. H., Zhang, J., Li, J., Gao, B., Ji, Q., Maynard, J., Ricketts, S. A., Cross, D., Cosulich, S., Chresta, C. C., Page, K., Yates, J., Lane, C., Watson, R., Luke, R., Ogilvie, D. and Pass, M. (**2012**). Preclinical pharmacology of AZD5363, an inhibitor of AKT: pharmacodynamics, antitumor activity, and correlation of monotherapy activity with genetic background. Mol Cancer Ther **11**(4), 873-887.

Diez, I. and Ras, R. H. A. (**2011**). Fluorescent silver nanoclusters. Nanoscale **3**(5), 1963-1970.

Dillon, L. M. and Miller, T. W. (**2014**). Therapeutic targeting of cancers with loss of PTEN function. Current drug targets **15**(1), 65-79.

Dimitrov, D. S. (2012). Therapeutic Proteins. Therapeutic Proteins: Methods and Protocols. V. Voynov and J. A. Caravella. Totowa, NJ, Humana Press**:** 1-26.

Fauman, E. B. and Saper, M. A. (**1996**). Structure and function of the protein tyrosine phosphatases. Trends Biochem Sci **21**(11), 413-417.

Fresno Vara, J. A., Casado, E., de Castro, J., Cejas, P., Belda-Iniesta, C. and Gonzalez-Baron, M. (**2004**). PI3K/Akt signalling pathway and cancer. Cancer Treat Rev **30**(2), 193-204.

Gao, D., Inuzuka, H., Tseng, A., Chin, R. Y., Toker, A. and Wei, W. (**2009**). Phosphorylation by Akt1 Promotes Skp2 Cytoplasmic Localization and Impairs APC/Cdh1-mediated Skp2 Destruction. Nature cell biology **11**(4), 397-408.

Garlich, J. R., De, P., Dey, N., Su, J. D., Peng, X., Miller, A., Murali, R., Lu, Y., Mills, G. B., Kundra, V., Shu, H. K., Peng, Q. and Durden, D. L. (**2008**). A vascular targeted pan phosphoinositide 3-kinase inhibitor prodrug, SF1126, with antitumor and antiangiogenic activity. Cancer Res **68**(1), 206-215.

Geng, Y., Yuan, W., Wu, F., Chen, J., He, M. and Jin, T. (**2008**). Formulating erythropoietin-loaded sustained-release PLGA microspheres without protein aggregation. J Control Release **130**(3), 259-265.

Gibney, J. and Johannsson, G. (**2004**). Safety of growth hormone replacement therapy in adults. Expert Opin Drug Saf **3**(4), 305-316.

Gonzalez, E. and McGraw, T. E. (**2009**). The Akt kinases: isoform specificity in metabolism and cancer. Cell cycle (Georgetown, Tex.) **8**(16), 2502-2508.

Guidetti, A., Carlo-Stella, C., Locatelli, S. L., Malorni, W., Mortarini, R., Viviani, S., Russo, D., Marchianò, A., Sorasio, R., Dodero, A., Farina, L., Giordano, L., Di Nicola, M., Anichini, A., Corradini, P. and Gianni, A. M. (**2014**). Phase II Study of Perifosine and Sorafenib Dual-Targeted Therapy in Patients with Relapsed or Refractory Lymphoproliferative Diseases. Clinical Cancer Research **20**(22), 5641.

Hanada, S., Fujioka, K., Inoue, Y., Kanaya, F., Manome, Y. and Yamamoto, K. (**2014**). Cell-Based in Vitro Blood–Brain Barrier Model Can Rapidly Evaluate Nanoparticles' Brain Permeability in Association with Particle Size and Surface Modification. International Journal of Molecular Sciences **15**(2), 1812-1825.

Hanahan, D. and Weinberg, R. A. (**2000**). The hallmarks of cancer. Cell **100**(1), 57-70.

Hayakawa, J., Ohmichi, M., Kurachi, H., Kanda, Y., Hisamoto, K., Nishio, Y., Adachi, K., Tasaka, K., Kanzaki, T. and Murata, Y. (**2000**). Inhibition of BAD phosphorylation either at serine 112 via extracellular signal-regulated protein kinase cascade or at serine 136 via Akt cascade sensitizes human ovarian cancer cells to cisplatin. Cancer Res **60**(21), 5988-5994.

Herrera Estrada, L. P. and Champion, J. A. (**2015**). Protein nanoparticles for therapeutic protein delivery. Biomaterials Science **3**(6), 787-799.

Hirai, H., Sootome, H., Nakatsuru, Y., Miyama, K., Taguchi, S., Tsujioka, K., Ueno, Y., Hatch, H., Majumder, P. K., Pan, B. S. and Kotani, H. (**2010**). MK-2206, an allosteric Akt inhibitor, enhances antitumor efficacy by standard chemotherapeutic agents or molecular targeted drugs in vitro and in vivo. Mol Cancer Ther **9**(7), 1956-1967.

Hopkins, B. D., Fine, B., Steinbach, N., Dendy, M., Rapp, Z., Shaw, J., Pappas, K., Yu, J. S., Hodakoski, C., Mense, S., Klein, J., Pegno, S., Sulis, M. L., Goldstein, H., Amendolara, B., Lei, L., Maurer, M., Bruce, J., Canoll, P., Hibshoosh, H. and Parsons, R. (**2013**). A secreted PTEN phosphatase that enters cells to alter signaling and survival. Science **341**(6144), 399-402.

Hyman, D. M., Smyth, L. M., Donoghue, M. T. A., Westin, S. N., Bedard, P. L., Dean, E. J., Bando, H., El-Khoueiry, A. B., Perez-Fidalgo, J. A., Mita, A., Schellens, J. H. M., Chang, M. T., Reichel, J. B., Bouvier, N., Selcuklu, S. D., Soumerai, T. E., Torrisi, J., Erinjeri, J. P., Ambrose, H., Barrett, J. C., Dougherty, B., Foxley, A., Lindemann, J. P. O., McEwen, R., Pass, M., Schiavon, G., Berger, M. F., Chandarlapaty, S., Solit, D. B., Banerji, U., Baselga, J. and Taylor, B. S. (**2017**). AKT Inhibition in Solid Tumors With AKT1 Mutations. J Clin Oncol **35**(20), 2251-2259.

Ihle, N. T., Williams, R., Chow, S., Chew, W., Berggren, M. I., Paine-Murrieta, G., Minion, D. J., Halter, R. J., Wipf, P., Abraham, R., Kirkpatrick, L. and Powis, G. (**2004**). Molecular pharmacology and antitumor activity of PX-866, a novel inhibitor of phosphoinositide-3-kinase signaling. Mol Cancer Ther **3**(7), 763-772.

Jansen, V. M., Mayer, I. A. and Arteaga, C. L. (**2016**). Is There a Future for AKT Inhibitors in the Treatment of Cancer? Clinical cancer research : an official journal of the American Association for Cancer Research **22**(11), 2599-2601.

Jimeno, A., Hong, D. S., Hecker, S., Clement, R., Kurzrock, R., Pestano, L. A., Hiscox, A., Leos, R. A., Kirkpatrick, D. L., Eckhardt, S. G. and Herbst, R. S. (**2009**). Phase I trial of PX-866, a novel phosphoinositide-3-kinase (PI-3K) inhibitor. Journal of Clinical Oncology **27**(15_suppl), 3542-3542.

Jokerst, J. V., Lobovkina, T., Zare, R. N. and Gambhir, S. S. (**2011**). Nanoparticle PEGylation for imaging and therapy. Nanomedicine (London, England) **6**(4), 715-728.

Jones, P. F., Jakubowicz, T., Pitossi, F. J., Maurer, F. and Hemmings, B. A. (**1991**). Molecular cloning and identification of a serine/threonine protein kinase of the second-messenger subfamily. Proc Natl Acad Sci U S A **88**(10), 4171-4175.

Keniry, M. and Parsons, R. (**2008**). The role of PTEN signaling perturbations in cancer and in targeted therapy. Oncogene **27**, 5477.

Kim, S.-B., Dent, R., Im, S.-A., Espié, M., Blau, S., Tan, A. R., Isakoff, S. J., Oliveira, M., Saura, C., Wongchenko, M. J., Kapp, A. V., Chan, W. Y., Singel, S. M., Maslyar, D. J., Baselga, J., Kim, S.-B., Lee, K. S., Im, S.-A., Espié, M., Wang, H.-C., Blau, S., Dent, R., Tan, A., Sohn, J. H., De Laurentiis, M., Estevez, L. G., Huang, C.-S., Romieu, G., Velez, M., Villanueva, R., Conte, P. F., Dakhil, S., Debled, M., Martin, A. G., Hurvitz, S., Kim, J. H., Levy, C., Oliveira, M., Rovira, P. S., Seo, J. H., Valero, V., Vidal, G., Wong, A., Allison, M. A. K., Figlin, R., Chan, D., Chen, S.-C., Chen, Y.-H., Cobleigh, M., De Braud, F., Dirix, L., Hansen, V., Bessard, A. H., Iannotti, N., Isakoff, S., Lawler, W., Montaño, A., Salkini, M. and Seigel, L. (**2017**). Ipatasertib plus paclitaxel versus placebo plus paclitaxel as first-line

therapy for metastatic triple-negative breast cancer (LOTUS): a multicentre, randomised, double-blind, placebo-controlled, phase 2 trial. The Lancet Oncology **18**(10), 1360-1372.

Kumar Pal, S., Reckamp, K., Yu, H. and Figlin, R. A. (**2010**). Akt inhibitors in clinical development for the treatment of cancer. Expert opinion on investigational drugs **19**(11), 1355-1366.

Leader, B., Baca, Q. J. and Golan, D. E. (**2008**). Protein therapeutics: a summary and pharmacological classification. Nat Rev Drug Discov **7**(1), 21-39.

Lee, J.-O., Yang, H., Georgescu, M.-M., Di Cristofano, A., Maehama, T., Shi, Y., Dixon, J. E., Pandolfi, P. and Pavletich, N. P. (**1999**). Crystal Structure of the PTEN Tumor Suppressor: Implications for Its Phosphoinositide Phosphatase Activity and Membrane Association. Cell **99**(3), 323-334.

Lee, J. and Kim, S. S. (**2009**). The function of p27(KIP1) during tumor development. Experimental & Molecular Medicine **41**(11), 765-771.

Li, J., Wang, W., Sun, D., Chen, J., Zhang, P.-H., Zhang, J.-R., Min, Q. and Zhu, J.-J. (**2013**). Aptamer-functionalized silver nanoclusters-mediated cell type-specific siRNA delivery and tracking. Chemical Science **4**(9), 3514-3521.

Li, J., Zhong, X., Cheng, F., Zhang, J.-R., Jiang, L.-P. and Zhu, J.-J. (**2012**). One-Pot Synthesis of Aptamer-Functionalized Silver Nanoclusters for Cell-Type-Specific Imaging. Analytical Chemistry **84**(9), 4140-4146.

Li, M., Rao, C., Pei, D., Wang, L., Li, Y., Gao, K., Wang, M. and Wang, J. (**2014**). Novaferon, a novel recombinant protein produced by DNA-shuffling of IFN-α, shows antitumor effect in vitro and in vivo. Cancer Cell International **14**(1), 8.

Liang, J. and Slingerland, J. M. (**2003**). Multiple roles of the PI3K/PKB (Akt) pathway in cell cycle progression. Cell Cycle **2**(4), 339-345.

Liras, A. (**2008**). Recombinant proteins in therapeutics: haemophilia treatment as an example. International Archives of Medicine **1**, 4-4.

Liu, G., Hong, X., Jiang, M. and Yuan, W. (**2012**). Sustained-release G-CSF microspheres using a novel solid-in-oil-in-oil-in-water emulsion method. Int J Nanomedicine **7**, 4559-4569.

Liu, W., James, C. D., Frederick, L., Alderete, B. E. and Jenkins, R. B. (**1997**). PTEN/MMAC1 mutations and EGFR amplification in glioblastomas. Cancer Res **57**(23), 5254-5257.

Lu, W., Zhou, X., Hong, B., Liu, J. and Yue, Z. (**2004**). Suppression of invasion in human U87 glioma cells by adenovirus-mediated co-transfer of TIMP-2 and PTEN gene. Cancer Lett **214**(2), 205-213.

Lu, Y., Yang, J. and Sega, E. (**2006**). Issues related to targeted delivery of proteins and peptides. The AAPS Journal **8**(3), E466-E478.

Ma, C. X., Sanchez, C., Gao, F., Crowder, R., Naughton, M., Pluard, T., Creekmore, A., Guo, Z., Hoog, J., Lockhart, A. C., Doyle, A., Erlichman, C. and Ellis, M. J. (**2016**). A Phase I Study of the AKT Inhibitor MK-2206 in Combination with Hormonal Therapy in Postmenopausal Women with Estrogen Receptor-Positive Metastatic Breast Cancer. Clin Cancer Res **22**(11), 2650-2658.

Marone, R., Cmiljanovic, V., Giese, B. and Wymann, M. P. (**2008**). Targeting phosphoinositide 3-kinase: moving towards therapy. Biochim Biophys Acta **1784**(1), 159-185.

Mayo, L. D. and Donner, D. B. (**2001**). A phosphatidylinositol 3-kinase/Akt pathway promotes translocation of Mdm2 from the cytoplasm to the nucleus. Proceedings of the National Academy of Sciences **98**(20), 11598.

Mitragotri, S., Burke, P. A. and Langer, R. (**2014**). Overcoming the challenges in administering biopharmaceuticals: formulation and delivery strategies. Nat Rev Drug Discov **13**(9), 655-672.

Mitragotri, S., Burke, P. A. and Langer, R. (**2014**). Overcoming the challenges in administering biopharmaceuticals: formulation and delivery strategies. Nat Rev Drug Discov **13**(9), 655-672.

Myers, M. P., Stolarov, J. P., Eng, C., Li, J., Wang, S. I., Wigler, M. H., Parsons, R. and Tonks, N. K. (**1997**). P-TEN, the tumor suppressor from human chromosome 10q23, is a dual-specificity phosphatase. Proceedings of the National Academy of Sciences **94**(17), 9052-9057.

Nance, E. A., Woodworth, G. F., Sailor, K. A., Shih, T.-Y., Xu, Q., Swaminathan, G., Xiang, D., Eberhart, C. and Hanes, J. (**2012**). A Dense Poly(Ethylene Glycol) Coating Improves Penetration of Large Polymeric Nanoparticles Within Brain Tissue. Science Translational Medicine **4**(149), 149ra119.

Niu, Y., Yu, M., Zhang, J., Yang, Y., Xu, C., Yeh, M., Taran, E., Hou, J. J. C., Gray, P. P. and Yu, C. (**2015**). Synthesis of silica nanoparticles with controllable surface roughness for therapeutic protein delivery. Journal of Materials Chemistry B **3**(43), 8477-8485.

Ohgaki, H. and Kleihues, P. (**2013**). The Definition of Primary and Secondary Glioblastoma. Clinical Cancer Research **19**(4), 764.

Okura, H., Smith, C. A. and Rutka, J. T. (**2014**). Gene therapy for malignant glioma. Molecular and cellular therapies **2**, 21.

Pawson, T. and Nash, P. (**2000**). Protein-protein interactions define specificity in signal transduction. Genes Dev **14**(9), 1027-1047.

Putney, S. D. and Burke, P. A. (**1998**). Improving protein therapeutics with sustained-release formulations. Nat Biotech **16**(2), 153-157.

Robertson, G. P. (**2005**). Functional and therapeutic significance of Akt deregulation in malignant melanoma. Cancer Metastasis Rev **24**(2), 273-285.

Russell, C. S. and Clarke, L. A. (**1999**). Recombinant proteins for genetic disease. Clin Genet **55**(6), 389-394.

Ryu, T.-K., Baek, S. W., Kang, R. H. and Choi, S.-W. (**2016**). Selective Photothermal Tumor Therapy Using Nanodiamond-Based Nanoclusters with Folic Acid. Advanced Functional Materials **26**(35), 6428-6436.

Saura, C., Roda, D., Roselló, S., Oliveira, M., Macarulla, T., Pérez-Fidalgo, J. A., Morales-Barrera, R., Sanchis-García, J. M., Musib, L., Budha, N., Zhu, J., Nannini, M., Chan, W. Y., Sanabria Bohórquez, S. M., Meng, R. D., Lin, K., Yan, Y., Patel, P., Baselga, J., Tabernero, J. and Cervantes, A. (**2017**). A First-in-Human Phase I Study of the ATP-Competitive AKT Inhibitor Ipatasertib Demonstrates Robust and Safe Targeting of AKT in Patients with Solid Tumors. Cancer discovery **7**(1), 102-113.

Shiang, Y.-C., Huang, C.-C., Chen, W.-Y., Chen, P.-C. and Chang, H.-T. (**2012**). Fluorescent gold and silver nanoclusters for the analysis of biopolymers and cell imaging. Journal of Materials Chemistry **22**(26), 12972-12982.

Soenen, S. J., Manshian, B., Doak, S. H., De Smedt, S. C. and Braeckmans, K. (**2013**). Fluorescent non-porous silica nanoparticles for long-term cell monitoring: Cytotoxicity and particle functionality. Acta Biomaterialia **9**(11), 9183-9193.

Song, G., Ouyang, G. and Bao, S. (**2005**). The activation of Akt/PKB signaling pathway and cell survival. J Cell Mol Med **9**(1), 59-71.

Song, M. S., Salmena, L. and Pandolfi, P. P. (**2012**). The functions and regulation of the PTEN tumour suppressor. Nature Reviews Molecular Cell Biology **13**, 283.

Song, X.-R., Goswami, N., Yang, H.-H. and Xie, J. (**2016**). Functionalization of metal nanoclusters for biomedical applications. Analyst **141**(11), 3126-3140.

Spencer, A., Sutherland, H. J., Dwyer, M. E., Huang, S.-Y., Stewart, K., Chb, Chari, A., Rosenzweig, M., Nooka, A. K., Rosenbaum, C. A., Hofmeister, C. C., Smith, D. A., Antal, J. M., Santiago-Walker, A., Gauvin, J., Opalinska, J. B. and Trudel, S. (**2013**). Novel AKT Inhibitor Afuresertib In Combination With Bortezomib and Dexamethasone Demonstrates Favorable Safety Profile and Significant Clinical Activity In Patients With Relapsed/Refractory Multiple Myeloma. Blood **122**(21), 283.

Spencer, A., Yoon, S. S., Harrison, S. J., Morris, S. R., Smith, D. A., Brigandi, R. A., Gauvin, J., Kumar, R., Opalinska, J. B. and Chen, C. (**2014**). The novel AKT inhibitor afuresertib shows favorable safety, pharmacokinetics, and clinical activity in multiple myeloma. Blood **124**(14), 2190-2195.

Spinelli, L. and Leslie, N. R. (**2015**). Assaying PTEN catalysis in vitro. Methods **77–78**, 51-57.

Staal, S. P., Hartley, J. W. and Rowe, W. P. (**1977**). Isolation of transforming murine leukemia viruses from mice with a high incidence of spontaneous lymphoma. Proceedings of the National Academy of Sciences of the United States of America **74**(7), 3065-3067.

Stambolic, V., Suzuki, A., de la Pompa, J. L., Brothers, G. M., Mirtsos, C., Sasaki, T., Ruland, J., Penninger, J. M., Siderovski, D. P. and Mak, T. W. (**1998**). Negative regulation of PKB/Akt-dependent cell survival by the tumor suppressor PTEN. Cell **95**(1), 29-39.

Stochholm, K. and Johannsson, G. (**2015**). Reviewing the safety of GH replacement therapy in adults. Growth Horm IGF Res **25**(4), 149-157.

Swiech, K., Picanço-Castro, V. and Covas, D. T. (**2017**). Production of recombinant coagulation factors: Are humans the best host cells? Bioengineered **8**(5), 462-470.

Tanaka, M. and Grossman, H. B. (**2003**). In vivo gene therapy of human bladder cancer with PTEN suppresses tumor growth, downregulates phosphorylated Akt, and increases sensitivity to doxorubicin. Gene Therapy **10**, 1636.

Tanaka, M., Koul, D., Davies, M. A., Liebert, M., Steck, P. A. and Grossman, H. B. (**2000**). MMAC1/PTEN inhibits cell growth and induces chemosensitivity to doxorubicin in human bladder cancer cells. Oncogene **19**(47), 5406-5412.

Tang, L. and Cheng, J. (**2013**). Nonporous silica nanoparticles for nanomedicine application. Nano Today **8**(3), 290-312.

Tokunaga, E., Oki, E., Egashira, A., Sadanaga, N., Morita, M., Kakeji, Y. and Maehara, Y. (**2008**). Deregulation of the Akt pathway in human cancer. Curr Cancer Drug Targets **8**(1), 27-36.

Tschopp, O., Yang, Z. Z., Brodbeck, D., Dummler, B. A., Hemmings-Mieszczak, M., Watanabe, T., Michaelis, T., Frahm, J. and Hemmings, B. A. (**2005**). Essential role of protein kinase B gamma (PKB gamma/Akt3) in postnatal brain development but not in glucose homeostasis. Development **132**(13), 2943-2954.

Utama, R. H., Guo, Y., Zetterlund, P. B. and Stenzel, M. H. (**2012**). Synthesis of hollow polymeric nanoparticles for protein delivery via inverse miniemulsion periphery RAFT polymerization. Chemical Communications **48**(90), 11103-11105.

Van Ummersen, L., Binger, K., Volkman, J., Marnocha, R., Tutsch, K., Kolesar, J., Arzoomanian, R., Alberti, D. and Wilding, G. (**2004**). A phase I trial of perifosine (NSC 639966) on a loading dose/maintenance dose schedule in patients with advanced cancer. Clin Cancer Res **10**(22), 7450-7456.

Wang, H., Zhang, P., Lin, C., Yu, Q., Wu, J., Wang, L., Cui, Y., Wang, K., Gao, Z. and Li, H. (**2015**). Relevance and Therapeutic Possibility of PTEN-Long in Renal Cell Carcinoma. PLoS ONE **10**(2), e114250.

Wu, D. and Pan, W. (**2010**). GSK3: a multifaceted kinase in Wnt signaling. Trends in Biochemical Sciences **35**(3), 161-168.

Wymann, M. P., Bulgarelli-Leva, G., Zvelebil, M. J., Pirola, L., Vanhaesebroeck, B., Waterfield, M. D. and Panayotou, G. (**1996**). Wortmannin inactivates phosphoinositide 3-kinase by covalent modification of Lys-802, a residue involved in the phosphate transfer reaction. Mol Cell Biol **16**(4), 1722-1733.

Wymann, M. P., Zvelebil, M. and Laffargue, M. (**2003**). Phosphoinositide 3-kinase signalling--which way to target? Trends Pharmacol Sci **24**(7), 366-376.

Xu, D., Hu, Z., Su, J., Wu, F. and Yuan, W. (**2012**). Micro and Nanotechnology for Intracellular Delivery Therapy Protein. Nano-Micro Letters **4**(2), 118-123.

Yahia-Ammar, A., Sierra, D., Mérola, F., Hildebrandt, N. and Le Guével, X. (**2016**). Self-Assembled Gold Nanoclusters for Bright Fluorescence Imaging and Enhanced Drug Delivery. ACS Nano **10**(2), 2591-2599.

Yang, J., Xia, N., Wang, X., Liu, X., Xu, A., Wu, Z. and Luo, Z. (**2015**). One-pot one-cluster synthesis of fluorescent and bio-compatible Ag14 nanoclusters for cancer cell imaging. Nanoscale **7**(44), 18464-18470.

Yang, S., Yuan, W. and Jin, T. (**2009**). Formulating protein therapeutics into particulate forms. Expert Opin Drug Deliv **6**(10), 1123-1133.

Yuan, H., Barnes, K. R., Weissleder, R., Cantley, L. and Josephson, L. (**2007**). Covalent reactions of wortmannin under physiological conditions. Chem Biol **14**(3), 321-328.

Zhang, L., Ren, J., Zhang, H., Cheng, G., Xu, Y., Yang, S., Dong, C., Fang, D., Zhang, J. and Yang, A. (**2016**). HER2-targeted recombinant protein immuno-caspase-6 effectively induces apoptosis in HER2-overexpressing GBM cells in vitro and in vivo. Oncol Rep **36**(5), 2689-2696.

Zhang, X., Tang, N., Hadden, T. J. and Rishi, A. K. (**2011**). Akt, FoxO and regulation of apoptosis. Biochimica et Biophysica Acta (BBA) - Molecular Cell Research **1813**(11), 1978-1986.

Zhao, H., Wu, F., Cai, Y., Chen, Y., Wei, L., Liu, Z. and Yuan, W. (**2013**). Local antitumor effects of intratumoral delivery of rlL-2 loaded sustained-release dextran/PLGA-PLA core/shell microspheres. Int J Pharm **450**(1-2), 235-240.

Materials and Methods

Section 3

Materials and Methods

3.1 Materials

Sigma-Aldrich (USA) Dulbecco's modified eagle's medium (DMEM), Erlotinib hydrochloride, Fetal bovine serum (FBS), Gel extraction kit, Plasmid mini prep kit, Glutathione-agarose beads, Hydroxycinnamic acid, Lysozyme (chicken egg white), o-phenylenediamine dihydrochloride (OPD), ponceauS, Propidium Iodidie (PI), Reduced glutathione, RIPA buffer, Tamoxifen, Temozolomide, Triton X-100, Tetraethylorthosilicate (TEOS), Trizma base (Tris), Tween 20, Tetra methyl ethylene diamine (TEMED), Tri reagent, Trypsin-EDTA, 3-(4,5-dimethyl-2-thiazolyl)-2,5-diphenyl-2H-tetrazolium bromide (MTT)

Sisco Research Laboratories (SRL, India) para-Nitrophenylphosphate disodium salt (PNPP) N-(2-Hydroxyethylo) piperazine-N-(2-ethanesulphonicacid) (HEPES)

HiMedia (India) Bovine serum albumin (BSA), Isopropyl-β-D-1-thiogalactopyranoside (IPTG), Luria Bertani (LB) broth, polyethylene glycol (PEG) 4000

Fluka (Sweden) Dichloromethane

NEB (USA) Restriction enzymes (*Bam HI, Xho I, Eco RI)*

Merck (Germany) Ammonium hydroxide (NH_4OH) and Ethanol

GE health care Thrombin and Anti-GST antibody, PGEX-4T-2 vector

Echelon Biosciences Inc (USA) Dioctanoyl Phosphatidylinositol 3,4,5-triphosphate (PIP_3 diC8) and Malachite green assay kit

Promega (USA) PCR master mix, pGEM-T easy vector kit and Quick ligation kit

CST Signaling Technology (USA) anti-PTEN antibody (raised in rabbit), anti-Akt antibody (raised in rabbit), anti-pAktS473 antibody (raised in rabbit), anti-GAPDH antibody (raised in rabbit) and HRP conjugated anti-rabbit antibody

Invitrogen anti-pFAKTyr397 antibody (raised in rabbit)

Amresco RNase

Corning Inc. (USA) Tissue culture dishes

National Centre for Cell Science (NCCS) cell repository (India) U-87 MG and MCF7 cell lines

Integrated DNA technologies (IDT) (USA) Primers for all PCR reactions **(Table 3.1)**

Name	Primer Sequence
PTEN-pGEMT Easy Cloning Primers	Forward 5'-CGGGATCCGACATGACAGCCATCATCAAAG-3' Reverse 5'-CCCTCGAGGACTTTTGTAATTTGTGTATGC-3'
PTEN-PGEX-4T-2 Cloning Primers	Forward 5'-CGGGATCCGACATGACAGCCATCATCAAAG-3' Reverse 5'-CCCTCGAGGACTTTTGTAATTTGTGTATGC-3'
PTEN-Long -pGEMT Easy Cloning Primers	Forward 5'-AGGAGGTAAAACATATGAGCGAGTC-3' Reverse 5'-CCCTCGAGGACTTTTGTAATTTGTGTATGC-3'
PTEN-Long -PGEX-4T-2 Cloning Primers	Forward 5'- AGGAGGTAAAACATATGAGCGAGTC-3' Reverse 5'-CCCTCGAGGACTTTTGTAATTTGTGTATGC-3'
Cyclin A	Forward 5'- TCAGCTGGGAAGGACCGGGG-3' Reverse 5'-GGGGGCTCTTGGACCCCACA-3'
Cyclin B1	Forward 5'-TCTGGATAATGGTGAATGGACA-3' Reverse 5'-CGATGTGGCATACTTGTTCTTG-3'
Cyclin B2	Forward 5'-AAAGTTGGCTCCAAAGGGTCCTT-3' Reverse 5'-GAAACTGGCTGAACCTGTAAAAAT-3'
Cyclin D1	Forward 5'- CGCCCCACCCCTCCAG-3' Reverse 5'- CCGCCCAGACCCTCAGACT-3'
BAX	Forward 5'- CGCCCCACCCCTCCAG-3' Reverse 5'- CCGCCCAGACCCTCAGACT-3'

FOXO3a	Forward 5'-GCGTGCCCTACTTCAAGGATAAG-3' Reverse 5'-GACCCGCATGAATCGACTATG-3'
GAPDH	Forward 5'-GAAGGTGAAGGTCGGAGTC-3' Reverse 5'-GAAGATGGTGATGGGATTTC-3'
EGFR1	Forward 5'-TGGAGAACTGCCAGAAACTGACC-3' Reverse 5'- GCCTGCAGCACACTGGTTG-3'
EGFR2	Forward 5'-TGTGACTGCCTGTCCCTACAA-3' Reverse 5'-CCAGACCATAGCACACTCGG-3'
EGFR3	Forward 5'-AGTCATGAGGGCGAACGAC-3' Reverse 5'-TCACACTCAGGCCATTCAGA-3'
EGFR4	Forward 5'-ACAGGACTTTGGGTCTGGGT-3' Reverse 5'-CAAGGCTCGGTACTGCTGTT-3'

3.2 Maintenance of Cell Lines

Breast cancer cell line (MCF7) and glioblastoma (U-87 MG) were procured from the National Centre for Cell Science (NCCS) cell repository, Pune, India. The cells were maintained in DMEM supplemented with 10% FBS, 20 U/mL penicillin and 50 mg/mL streptomycin in 5% CO_2 humidity at 37 °C in a humidified incubator. The media were periodically changed and the cells were sub-cultured.

3.3 Cloning of Human PTEN-Long and PTEN

The coding sequence of human PTEN gene in pANT_cGST vector and PTEN-long gene in JpExpress404 vector was procured from DNASU plasmid repository (USA) and Addgene (USA), respectively. For cloning of PTEN-Long gene the PCR amplification conditions consisted of 30 cycles of 95 °C for 30 seconds, 55 °C for 1 min and 72 °C for 1 min 40 seconds using gene specific forward primer 5'-AGGAGGTAAAACATATGAGCGAGTC-3' with a *BamHI* overhang and reverse primer 5'-CCCTCGAGGACTTTTGTAATTTGT-GTATGC-3' with a *XhoI* overhang. The 1.8 kb PCR product was purified from agarose gel by gel extraction method using manufacturer's protocol and cloned into pGEMT easy vector

by TA ligation method. The legated product was transformed to competent *Escherichia coli* DH5α by standard heat shock process. Transformed cells were spread onto ampicillin-LB agar plates coated with X-gal/ IPTG for assisting in blue-white screening. Following overnight growth in incubator at 37 °C selected white and blue colonies were screened for positive clones by restriction digestion with *BamHI* and *XhoI* restriction enzymes. The clones with insert were stored as glycerol stocks in -80°C until further use.

The PCR amplification conditions for cloning of PTEN gene consisted of 30 cycles of 95 °C for 30 seconds, 50 °C for 1 min and 72 °C for 1 min 20 seconds using gene specific forward primer 5'-CGGGATCCGACATGACAGCCATCATCAAAG-3' with a *BamHI* overhang and reverse primer 5'-CCCTCGAGGACTTTTGTAATTTGTGTATGC-3' with a *XhoI* overhang. The 1.2 kb PCR product was purified from agarose gel by gel extraction method using manufacturer's protocol and cloned into pGEMT easy vector by TA ligation method. Competent *Escherichia coli* DH5α was prepared by employing TSS buffer. The legated product was transformed to competent *Escherichia coli* DH5α by standard heat shock process. Transformed cells were spread onto ampicillin-LB agar plates coated with X-gal/ IPTG for assisting in blue-white screening. Following overnight growth in incubator at 37 °C selected white and blue colonies were screened for positive clones by restriction digestion with *BamHI* and *XhoI* enzymes. The clones with insert were stored as glycerol stocks in -80 °C until further use.

3.4 Cloning into Bacterial Expression Vector

PTEN-Long and PTEN genes cloned into pGEMT easy vector were further cloned into bacterial expression vector PGEX-4-T2 for bacterial expression and purification of the recombinant proteins. PTEN-Long gene and PTEN gene were PCR amplified from the pGEMT-PTEN-Long and pGEMT-PTEN constructs, respectively. The PCR product purified by gel extraction method was subsequently digested by *BamHI* and *XhoI restriction* enzymes. Simultaneously the PGEX-4T-2 vector was also digested by the same set of enzymes. The digested gene and vector product were then legated by quick ligation method following manufacturer's protocol. The legated product was then transformed into competent *Escherichia coli* BL21 (DE3) by standard heat shock process. The transformed cells were spread onto amplicillin-LB agar plates and allowed to grow overnight at 37 °C. Selected

colonies were screened for positive clones by restriction digestion with *BamHI* and *XhoI* enzymes. The clones with insert were stored as glycerol stocks in -80 °C until further use.

3.5 Bacterial Expression of the Recombinant PTEN-Long and PTEN Proteins

A single colony of *Escherichia coli* BL21 (DE3) containing the cloned construct was inoculated in 5 mL LB medium containing 100 µg/ mL ampicillin and allowed to grow overnight in incubator shaker at 37 °C , 180 rpm to generate the primary culture. This primary culture was used as inoculum for secondary culture of 500 mL LB media. The expression of recombinant PTEN-Long was induced at an OD_{600} of 0.6 by addition of IPTG at a final concentration of 0.5 mM. Culture was then shifted to 21 °C and allowed to further grow for 12 h. The cells were harvested by centrifugation at 7000 rpm for 8 min and stored at -20 °C until further use.

To induce the expression of recombinant PTEN at an OD_{600} of 0.6, IPTG was added to a final concentration of 0.5 mM. Culture was then shifted to 28 °C and allowed to further grow for 4 h. The cells were harvested by centrifugation at 7000 rpm for 8 min and stored at -20 °C until further use.

3.6 Purification of the Recombinant PTEN-Long and PTEN Proteins

The frozen bacterial pellet of *Escherichia coli* BL21 (DE3) containing the pGEX-4T-2-PTEN-Long construct was re-suspended in chilled lysis buffer of 50 mM Tris pH 7.4, 1 mM EDTA, 1 mM PMSF and 150 mM NaCl. The bacteria were lysed by probe sonication on ice at 30 % amplitude for 10 cycles of 1 minute ON and 1 minute OFF. Supernatant collected after centrifugation at 12000 rpm for 20 min was diluted with an equal amount of HBS (50 mM Hepes and 150 mM NaCl, pH 7.4) and filtered through 0.45 µm syringe filter. The lysate was allowed to bind to glutathione-agarose beads under slow rocking conditions on ice for 45 min followed by several washes with HBS. Bound recombinant PTEN-Long was eluted using 10 mM L-reduced glutathione in 50 mM Hepes pH 8.0. Eluted fractions were subjected to buffer exchange by dialysis against 25 mM Hepes pH 7.4 at 4 °C for 4 h. The dialyzed protein was concentrated by centrifugation at 5000 rpm (30kDa MWCO) Spin-X UF concentrator and verified by 12 % SDS-PAGE analysis.

The lysis buffer for PTEN protein purification consisted of 20 mM Tris pH 7.4, 1 mM EDTA, 1 mM PMSF and 150 mM NaCl. The bacteria were lysed by probe sonication on ice at 30 % amplitude for 30 cycles of 2 seconds ON and 25 seconds OFF. Supernatant collected after centrifugation at 12000 rpm for 20 min was diluted with an equal amount of HBS (50 mM Hepes and 150 mM NaCl, pH 7.4) and filtered through 0.45 µm syringe filter. The lysate was allowed to bind to glutathione-agarose beads under slow rocking conditions on ice for 1 h followed by 8 washes of 5 min each with HBS. Bound recombinant PTEN was eluted using 10 mM L-reduced glutathione in 50 mM Hepes pH 8.0. Eluted fractions were subjected to buffer exchange by dialysis against 25 mM Hepes pH 7.4 at 4 °C for 4 h. The dialyzed protein was concentrated by centrifugation at 5000 rpm (30kDa MWCO) Spin-X UF concentrator and verified by 12 % SDS-PAGE analysis. The method for protein purification is illustrated in **Scheme 3.1**

3.7 Thrombin Cleavage of the Recombinant Proteins

To excise the GST tag, on-column thrombin cleavage was performed where the protein PTEN-Long or PTEN was cleaved from GST while it was still bound to glutathione-agarose beads. The cell lysate after binding and washing with HBS was incubated with thrombin cleavage buffer composed of 50 mM Hepes pH 7.4, 150 mM NaCl and 15 µl of thrombin (0.0004 NIH Units/µl) for 6 h at room temperature. Cleaved protein (PTEN-Long or PTEN) was finally eluted and analyzed on 12 % SDS-PAGE.

3.8 Characterization of the Recombinant Proteins

3.8.1 Western Blot

Purified GST-PTEN-Long and GST-PTEN were separated on 12% SDS-PAGE followed by transfer onto a PVDF membrane. After verifying the transfer of protein using ponceauS stain, the membrane was washed with TBST (50 mM Tris pH 7.4 and 150 mM NaCl) several times to remove the stain. Blocking was performed at room temperature for 2 h using 3 % BSA in TBST. Subsequently, the membrane was incubated overnight at 4 °C with anti-PTEN primary antibody raised in rabbit (Dilution 1:2000). The membrane was washed with TBST four times of 20 min each followed by incubation with HRP conjugated anti-rabbit secondary

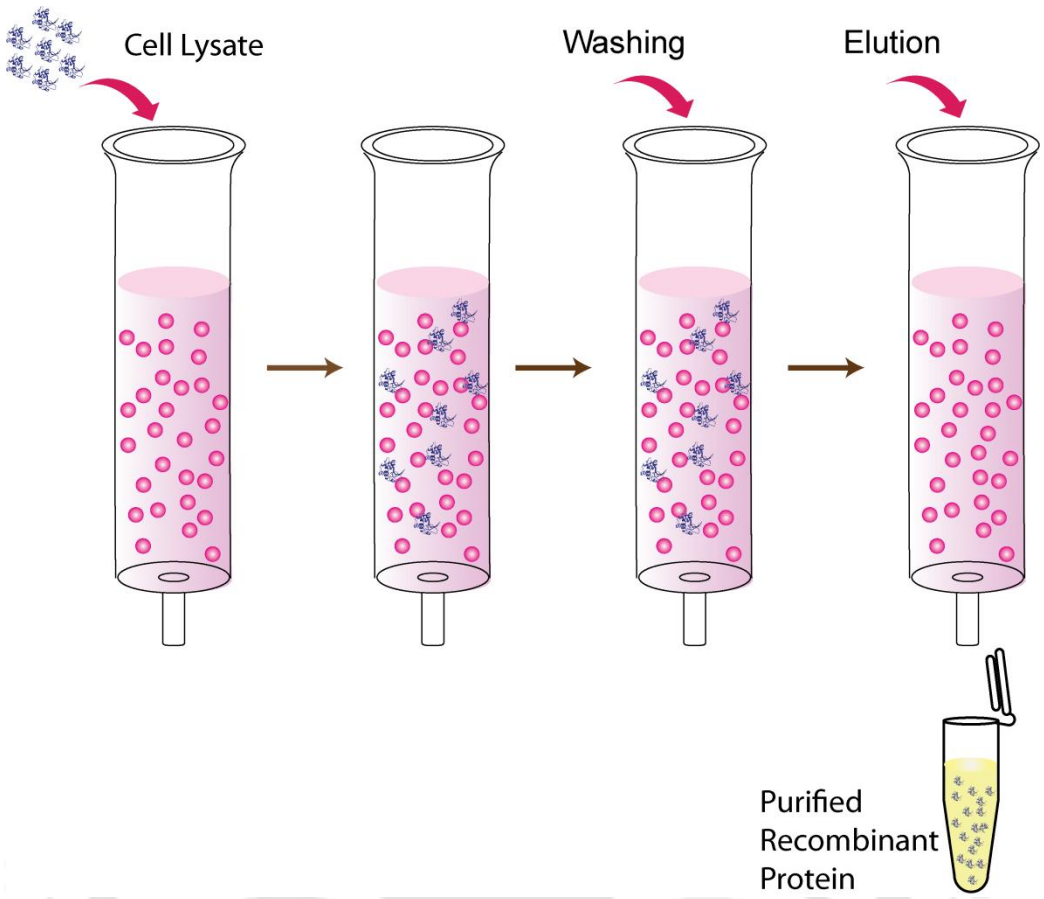

Scheme 3.1 Schematic representation of protein purification employing affinity column chromatography.

antibody (Dilution 1:2000) at room temperature for 2 h and then the washing step was repeated. Blot was developed using chemiluminescent peroxidase substrate. GST was also probed using anti-GST antibody (raised in rat) and anti-rat as the primary and secondary antibody (Dilution 1:2000), respectively.

3.8.2 MALDI TOF-TOF Analysis

Purified GST-PTEN-Long and GST-PTEN proteins separated on 12% SDS gel was stained with colloidal coomassie G-250. Following staining the desired band was excised into small pieces from the SDS-PAGE gel. The gel pieces were de-stained using de-staining solution from the IGD kit (Sigma). In gel trypsin digestion was performed, using trypsin profile IGD kit (Sigma), according to manufacturer's protocol. Peptide samples were then desalted using

ziptip C18 column. The desalted samples were mixed with the matrix α-Cyano-4-Hydroxycinnamic acid (10 mg/ml) in the ratio of 3:1(Sample: Matrix) and spotted onto the MALDI analyzer plate. MS-MS analysis was done using 4800 proteomics analyzer with TOF-TOF optics, Applied Biosystems. The results were analyzed using Expasy proteomics Findpept program (Yip *et al.,* 2005).

3.8.3 Secondary Structure Analysis by Circular Dichroism Spectroscopy

The purified proteins GST-PTEN-Long and GST-PTEN were dialyzed against 10 mM Tris pH 7.4, and further concentrated by centrifugation at 5000 rpm for desired time using (30 kDa MWCO) Spin-X UF concentrator. Samples in 10 mM Tris pH 7.4, taken in cuvette with 5 mm pathlength were analyzed using JASCO-815 spectrometer. The CD spectra were recorded from 190 nm to 240 nm in 0.5 nm steps under constant nitrogen gas purging at a flow rate of 5 L/min and 25 °C temperatures. The reading for sample buffer was subtracted from the experimental data. The data points accumulated in millidegree were converted to mean residue ellipticity (expressed in deg cm^2 $dmol^{-1}$) by using the following formula (Greenfield 2006)

$$Mean\ Residue\ Ellipticity\ (\theta) = \frac{Millidegree\ X\ Mean\ Residue\ Weight}{Pathlength\ X\ Concentration}$$

Where, mean residue weight is molecular weight divided by number of amino acids, pathlength in mm and protein concentration in mg ml^{-1}.

3.8.4 Protein Phosphatase Assay

Assessment of *in vitro* phosphatase activity of GST tagged and untagged PTEN-Long and PTEN was done using para-Nitrophenylphosphate (PNPP) as substrate. The reaction buffer was composed of 25 mM Hepes pH 7.4, 10 mM DTT and 1 µg of purified GST tagged and untagged enzymes. The reaction mixture was incubated at 37 °C for desired time. Stop solution consisting of 1N NaOH added after the specified incubation period served dual purpose; terminate the reaction and intensify the colour of the product that was measured by

colorimetric analysis (McAvoy and Nairn 2010). Under alkaline conditions the product para-nitrophenol (PNP) is converted to para-nitrophenolate which was measured by absorbance at 405 nm (Martin *et al.,* 2014) using Perkin Elmer Victor X3 multiplate reader. Only substrate control was kept to eliminate potential nonspecific phosphate release. The amount of phosphate released was estimated against a standard curve by linear regression analysis. The schematic representation of the protocol for PNPP phosphatase assay is depicted in **Scheme 3.2**.

3.9 Cellular Internalization Study of PTEN-Long

To study the cellular uptake of PTEN-Long , U-87 MG cells were seed in 96 well plates in DMEM media supplement with 10% FBS and was allowed to attached overnight. Following attachment, the cells were treated with 100 nM of PTEN-Long for different time intervals (15, 30, 60, 120, 240 min). After incubation with PTEN-Long for the desired time, the media containing the protein was removed and supplemented with fresh DMEM serum media. The cells were then incubated at 37 °C under humidified atmosphere of 5% CO_2 for 48 h. After incubation, fresh serum media containing 5 µl of 5 mg/ml MTT solution was added to each well and the plates were incubated at 37 °C under CO_2 humidified atmosphere. Subsequently, the media was discarded and DMSO was added to dissolve the formazan crystals formed by enzymatic conversion by live cells. The product was measured by absorbance at 570 nm along with background measurement at 690 nm using multiplate reader (Tecan, Infinite M200PRO).

3.10 Cell Viability Assay

The effect of the recombinant proteins alone or in combination with drugs was evaluated on two cell lines expressing PTEN differentially, PTEN null glioblastoma cell line U-87 MG and breast cancer cell line MCF7. U-87 MG and MCF7 cell lines were seed in 96 well plate DMEM media supplemented with 10% FBS was allowed to attach overnight. Following adherence, the media was removed and fresh serum media containing varying concentrations of the protein alone or in combination with drugs were added and incubated at 37 °C under humidified atmosphere of 5% CO_2 for desired time. After incubation, fresh serum media containing 5 µl of 5 mg/ml MTT solution was added to each well and the plates were

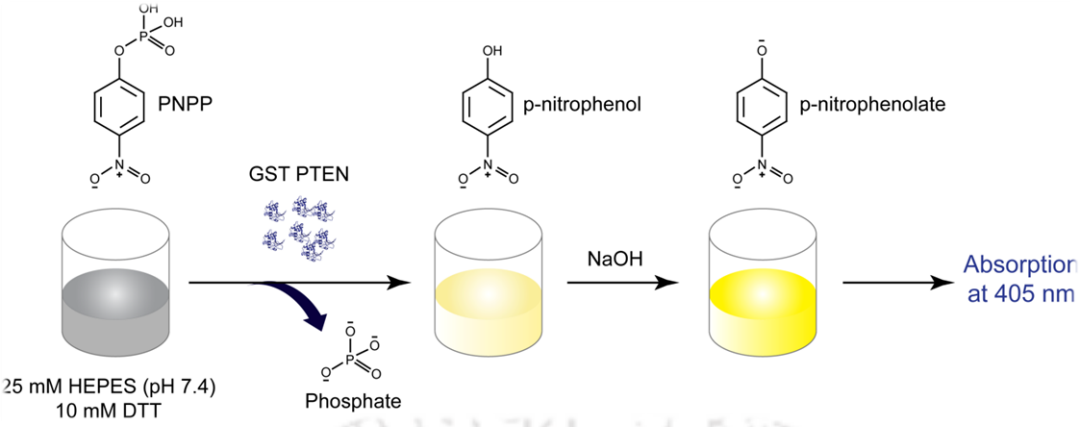

Scheme 3.2 Schematic representation of the para-nitrophenylphosphate (PNPP) phosphatase assay protocol.

incubated at 37 °C under CO_2 humidified atmosphere. Subsequently, the media was discarded and DMSO was added to dissolve the formazan crystals formed by enzymatic conversion by live cells. The product was measured by absorbance at 570 nm along with background measurement at 690 nm using multiplate reader (Tecan, Infinite M200PRO). Cell viability (%) relative to the control untreated cells was calculated using the following formula-

$$Cell\ viability\ (\%) = \frac{(Abs\ 570 - Abs\ 690)\ Sample}{(Abs\ 570 - Abs\ 690)\ Control} X\ 100$$

For all experiments with PTEN-Long, U-87 MG cells were seeded at a cell density of 3500 cells per well in 96 well plate. For all experiments with PTEN, U-87 MG cells and MCF7 cells were seeded at a cell density of 4000 and 6000 cells per well in 96 well plate, respectively.

3.11 Scratch Assay

For wound healing assay, U-87MG and MCF7 cells were seeded in 35 mm tissue culture dishes at a density of $1x10^5$ cells per well and allowed to grow to 85-90% confluence in DMEM serum media. The confluent cell monolayer was scraped with a sterile pipette tip to create a 'scratch' (Liang *et al.*, 2007). Wounded monolayer was then washed with PBS to

remove any cell debris. Immediately after the wound was created, images of the wound were acquired using Nikon ECLIPSE Ti microscope. Cells were then treated with the recombinant proteins and incubated at 37 °C, under humidified condition of 5% CO_2 for the desired period of time. Subsequently, the control and treated tissue culture dishes at the end of the experiment were examined under the microscope. The schematic representation depicting the protocol of the scratch assay is illustrated in **Scheme 3.3**.

3.12 Determination of Cell Cycle Pattern

The effect of the recombinant proteins on the cell cycle pattern of U-87 MG cells and MCF7 cells were determined by flow cytometry using propidium iodide (PI) DNA staining dye. Cells seeded in 6 well plates at a density of $1x10^5$ cells per ml were allowed to attach overnight. Prior to treatment the cells were synchronized by serum starvation for 48 h. Cells were then treated with varying concentrations of the recombinant proteins for the desired time in serum DMEM media. For experiments with PTEN-Long, U-87 MG cells were treated with 100 nM of the protein for 48 h in serum DMEM media. For experiments with PTEN, U-87 MG were treated with PTEN (72 nM)-Cluster (60 µg/ml) composite and MCF7 cells were treated with PTEN (36 nM)-Cluster (30 µg/ml) composite for 48 h in serum DMEM media. The cell collected by trypsinization were fixed by adding chilled 70% ethanol drop wise while vortexing the pellet, and stored at -20 °C until further analysis. The samples were processed as per the protocol described by Riccardi *et al* (Riccardi and Nicoletti 2006) The fixed samples were centrifuged at 650 rcf for 6 min.

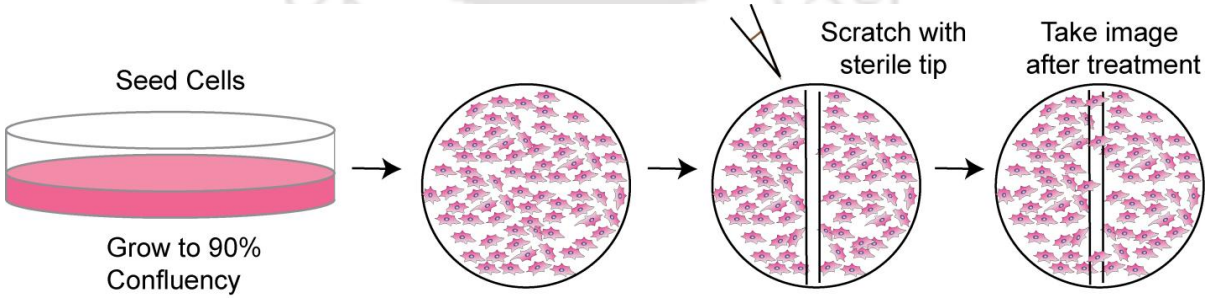

Scheme 3.3 The schematic representation of the scratch assay.

The pellet was washed with chilled 1X PBS following incubation with RNase at 37 °C for 1 h. Samples were then incubated with PI staining dye and 0.01% Trition X-100 until analysis using BD FACSCalibur. The samples were recorded using Cell Quest programme and the data collected was examined using FCS express software.

3.13 Modulation of Cellular Signalling

The expression of intracellular signalling proteins upon treatment with the recombinant proteins was determined by the Western blot analysis. U-87 MG and MCF7 cells seeded in 6 well plates at a density of $1x10^5$ cells per ml were allowed to attach overnight. For experiments with PTEN-Long, U-87 MG cells were treated with 100 nm of the protein for 2 h and 4 h in serum DMEM media. For experiments with PTEN, U-87 MG Cells were treated with PTEN (72 nM)-Cluster (60 μg/ml) composite and MCF7 cells were treated with PTEN (36 nM)-Cluster (30 μg/ml) composite for 8 h in serum DMEM media.

Upon treatment, the total protein from the mammalian cells was extracted using RIPA buffer. To each well 150 μL of RIPA buffer was added along with protease inhibitors (Sodium orthovandate, Sodium fluoride and PMSF) and incubated for 20 min under rocking conditions on ice. Following incubation, the cells were scraped and collected. The collected cells were sonicated for 10 sec on ice at 25% amplitude and then stored in -80 °C until further application.

The total protein was estimated using lowry protein estimation method. A total of 12 μg of protein for each sample was separated on 12% SDS gel and subsequently transferred onto PVDF membrane. The membrane was stained with ponceauS to verify protein transfer. Blocking was performed at room temperature for 2 h using 3% BSA in TBST following overnight incubation at 4 °C with respective primary antibody (Dilution 1:2000). The membrane was washed with TBST several times and incubated with secondary antibody (Dilution 1:2000) at room temperature for 2 h. Following washing with TBST, the blot was developed using chemiluminescent peroxidase substrate using chemi gel doc (Biorad).

3.14 Calcein-AM/ Ethidium Bromide (EtBr) Dual Staining

MCF7 and U-87 MG cells were cultured in 96 well plates, in DMEM media supplemented with 10% FBS. Cells were left untreated or treated with the recombinant proteins for desired time. The cells were washed with 1X PBS pH 7.4 and dual staining solution in PBS containing calcein-AM and EtBr was added and incubated for 5 min. After incubation the cell were washed twice with 1X PBS pH 7.4 and visualized using fluorescence microscope (Nikon ECLIPSE Ti).

3.15 Synthesis of Silica Nanoparticles

To study stabilization of GST-PTEN protein for intracellular delivery, silica nanoparticles were synthesized. Synthesis of silica nanoparticles were carried out by modification of Stober's process (Clemments *et al.,* 2015). Ethanol was mixed with NH_4OH at room temperature and the mixture was stirred for about 5 min to attain homogeneity. TEOS was then added to the solution under stirring condition and allowed to stir for 3 h. Nanoparticles formed were collected by centrifugation at 12000 rpm for 10 min and re-suspended in EtOH using water bath sonicator for 4 min. This process was repeated three times to remove any unreacted reagents. Finally the nanoparticles were washed twice with Milli-Q and stored at 4 °C until further use. Stored nanoparticles were sonicated prior to any applications.

3.16 Characterization of Silica Nanoparticles

3.16.1 Surface Morphology Study

To determine the morphology of the synthesized silica nanoparticles FESEM and TEM study was performed. For FESEM, synthesized silica NPs were drop coated on aluminum foil, air dried overnight, double coated with gold (SC7620"Mini", Polaron Sputter Coater, Quorum Technologies, Newhaven, England) and analyzed in a Carl Zeiss, SIGMA VP, instrument. For TEM, 7 µl of sample was drop coated on carbon coated copper grid, air dried overnight and observed in JEM 2100 (Jeol, Peabody, MA; accelerating voltage of 200 keV). The same study was repeated after binding of the protein onto the nanoparticles.

3.16.2 Hydrodynamic Diameter and Zeta Potential Measurements

For DLS and zeta potential analysis, silica nanoparticles diluted in Milli-Q was analyzed using Malvern Zeta sizer Nano ZS to determine the hydrodynamic diameter and surface charge, respectively. The same study was performed after binding of the protein onto the nanoparticles.

3.17 Determination of Immobilization of GST-PTEN onto Silica NPs

Interaction between protein and nanoparticles can be monitored by various analytical strategies like fluorescence spectroscopy, FTIR spectroscopy, dynamic light scattering, Zeta potential and Enzyme Linked Immunosorbent Assay (ELISA). To immobilize GST-PTEN on Silica NPs, varying concentrations (6 nM to 30 nM) of GST-PTEN was incubated with constant concentration of silica NPs (0.8 mg/ml) at room temperature for 2 h. The final volume was made to 1 ml using 25 mM Hepes pH 7.4. Following incubation, the samples were centrifuged at 10000 rpm for 10 min, and the pellet was re-dispersed in 1 ml Milli-Q water. To determine binding, fluorescence intensity of protein was recorded at a wavelength of 340 nm for an excitation wavelength of 280 nm using Fluoromax-4, Horiba JobinYvon, Edison, NY, USA.

Binding percentage was calculated as follows

$$Binding\ (\%) = \frac{Emission\ of\ Total\ Protein - Emission\ of\ Unbound\ Protein}{Emission\ of\ Total\ Protein} \text{ X } 100$$

To corroborate successful interaction between the recombinant protein and nanoparticles, ELISA was performed. The overall strategy was similar to bead-based ELISA platform (Scholler *et al.*, 2006), where the silica nanoparticles were used as beads to capture recombinant PTEN **(Scheme 3.4)**. This method was advantageous due to requirement of relatively small amount of protein sample. ELISA was performed with maximum binding ratio of protein to nanoparticles. After binding 100 µl of the samples in triplicate were distributed in 1.5 ml

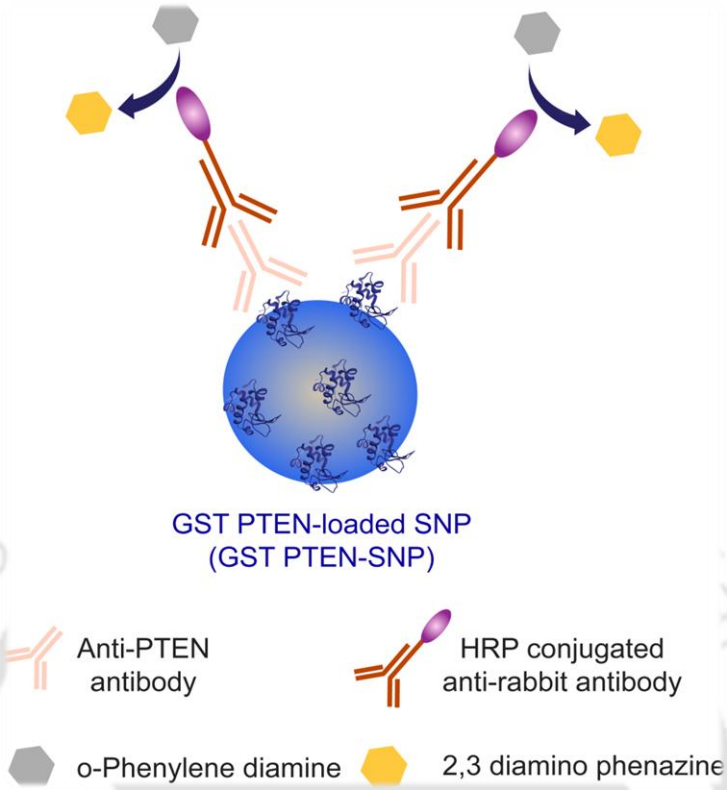

Scheme 3.4 Illustration of bead based ELISA study for determining recombinant PTEN-silica nanoparticles binding.

eppendorf tubes previously treated with blocking buffer consisting of TBS (50 mM Tris pH 7.4 and 150 mM NaCl) with 2% BSA for 12 h. Samples were incubated at room temperature under slow rocking conditions for 4 h and washed with TBS and finally centrifuged. The pellet was re-dispersed in blocking buffer and incubated at room temperature for 2 h. Following washing with TBS, 100 µl of TBS containing anti-PTEN primary antibody raised in rabbit (1:1000 dilution) was added to each sample and incubated overnight at 4 °C. Subsequently, the samples were washed with TBS twice followed by addition of HRP conjugated anti-rabbit secondary antibody. After washing with TBS twice, the samples were incubated with o-phenylenediaminedihydrochloride (OPD) substrate. The product developed was measured at 450 nm using Tecan infinite M200 PRO multiplate reader. All centrifugation was performed at 8000 rpm for 5 min. Protein binding was also studied by Fourier Transform Infrared (FTIR) Spectroscopy, Zeta and DLS measurements. FTIR analyses of the lyophilized samples were carried out by mixing the samples with KBr to form

pellet and the spectra was recorded in the frequency range of 4000-500 cm^{-1} using Perkin Elmer Spectrum One machine. The peaks obtained were analyzed to study binding of the recombinant protein to the silica nanoparticles. For DLS measurement, diluted and thoroughly mixed samples were analyzed using Malvern Zeta sizer Nano ZS.

3.18 Release Studies of GST-PTEN from Silica NPs

To study the cumulative protein release of GST-PTEN from the surface of silica nanoparticles, the ratio of protein to nanoparticles exhibiting maximum binding percentage was selected. After binding, the samples were centrifuged at 10000 rpm for 10 min and the pellet was re-distributed in 10 mM Tris pH 7.4. The sealed tubes were placed in water bath maintaining temperature at 37 °C. Samples taken out at specific time intervals ranging from 1 to 72 h were centrifuged at 10000 rpm for 10 min. The supernatant was collected and intrinsic fluorescence of the protein was probed at 280 nm to determine the amount of protein released using Fluoromax-4, Horiba JobinYvon, Edison, NY, USA.

3.19 Evaluating GST-PTEN-Silica Nanoparticles Interaction

3.19.1 Evaluation of Structural Integrity

To study the structural changes induced upon nanoparticles interaction, the secondary structure of the GST-PTEN released from the nanoparticles surface was analyzed by circular dichroism spectroscopy. After binding, the sample was centrifuged at 10000 rpm for 10 min and the pellet was re-distributed in 10 mM Tris pH 7.4. Samples taken in cuvette with 5 mm pathlength were analyzed using JASCO-815 spectrometer. The CD spectra were recorded from 190 nm to 240 nm in 0.5 nm steps under constant nitrogen gas purging at a flow rate of 5 L/min and 25 °C temperatures. The reading for sample buffer was subtracted from the experimental data after measurement. The spectra obtained were further analyzed by Yang's reference.

2.19.2 Assessment of Functional Integrity

Assessment of *in vitro* phosphatase activity of GST-PTEN bound to silica nanoparticles was performed using both protein and lipid substrates. The reaction buffer for PNPP phosphatase assay was composed of 25 mM Hepes pH 7.4, 10 mM DTT and 1 µg of purified GST-PTEN or GST-PTEN bound to silica nanoparticles (GST-PTEN-SNP). DTT is an important component of reaction buffer, as it is required to maintain the cysteine residue in the active site of the enzyme in the reduced state (Spinelli and Leslie 2015). The reaction was incubated at 37 °C for desired time. After incubation, stop solution consisting of 1 N NaOH was added to terminate the reaction and intensify the colour of the product, para-Nitrophenol (PNP). The product was measured by colorimetric analysis at 405 nm using Perkin Elmer Victor X3 multiplate reader. Only substrate control was kept to eliminate potential nonspecific phosphate release. The amount of phosphate released was estimated against a standard curve by linear regression analysis.

Lipid phosphatase assay was performed using water soluble phosphatidylinositol 3,4,5-trisphosphate diC8 (PIP_3 diC8) (Rodriguez-Escudero *et al.*, 2011) ranging from 15 to 150 µM in 25 µl of reaction mixture consisting of 25 mM Hepes pH 7.4, 10 mM DTT, 2 mM EDTA and 1 µg of purified GST-PTEN and GST-PTEN-SNP. The phosphate released was quantified by colorimetric assay using malachite green solution. Detection of phosphate is based on formation of complex between free phosphate and molybdate (malachite green) which was quantified by absorbance at 660 nm using Perkin Elmer Victor X3 multiplate reader. The amount of phosphate released was determined by standard linear regression analysis. The principle of the phosphates assay is illustrated in **Scheme 3.5**.

3.19.3 Protease Protection Assay

Free and silica nanoparticles bound GST-PTEN (exhibiting maximum binding percentage) were incubated with 0.5 µg/ml of Proteinase K for 30 min at 37 °C. After Proteinase K digestion the samples were analyzed by phosphatase assay using PNPP as substrate. Phosphatase assay of the treated and untreated protein samples was

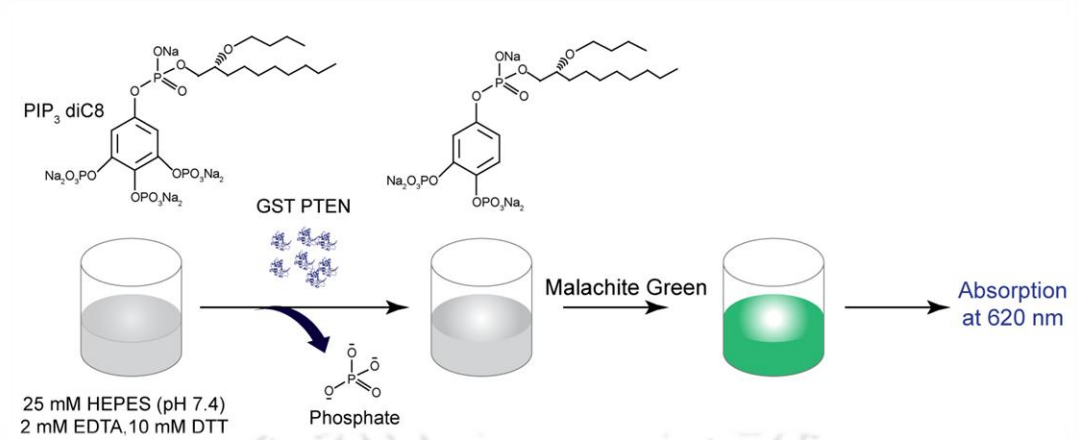

Scheme 3.5 Schematic representation of the lipid (PIP_3 diC8) phosphatase assay protocol.

performed using 50 mM PNPP at 37 °C for 60 min following colorimetric quantification of the product formed at 405 nm using multiplate reader (Tecan, Infinite M200PRO). The overall principle of the assay is illustrated in **Scheme 3.6**

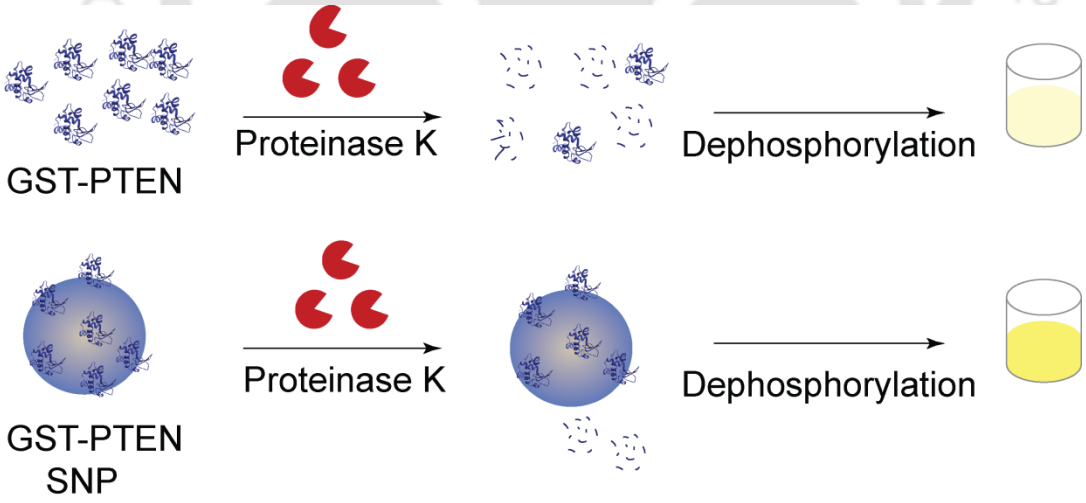

Scheme 3.6 Schematic representation of the protease protection assay design.

3.20 Synthesis of Lysozyme Stabilized Silver Nanoclusters

Lysozyme stabilized silver nanoclusters were synthesized by slight modification of the protocol developed by Zhou *et al* (Zhou *et al.,* 2012). To 5 ml of Milli-Q, 75 mg of lysozyme (chicken white egg) was added with stirring conditions. To the same solution 1 ml of silver nitrate (10 N) was added drop wise and allowed to stir for 5 min. Alkaline environment was created by addition of 300 µL of 1 N NaOH and allowed to stir. To mediate reduction of silver, 40 µL of sodium borohydride was added drop wise. Change in the colour of the solution from colourless to brown indicated the reduction of silver.

3.21 Characterization of Silver Nanoclusters

The synthesis of lysozyme stabilized silver nanoclusters was characterized by TEM and spectroscopy based analysis. For TEM analysis, 7 µl of sample was drop coated on carbon coated copper grid, air dried overnight and observed in JEM 2100 (Jeol, Peabody, MA; accelerating voltage of 200 keV). To determine the absorbance profile of synthesized silver nanoclusters, 1 ml of nanoclusters was taken in cuvette and the absorbance was recorded from 380 nm to 700 nm using Cary 300 UV-Vis spectrophotometer. The fluorescence spectrum of the synthesized nanoclusters was recorded from 500 nm to 800 nm upon excitation at 480 nm using Fluoromax-4, Horiba JobinYvon, Edison, NY, USA. For DLS and zeta potential analysis, silver nanoclusters diluted in Milli-Q was analyzed using Malvern Zeta sizer Nano ZS to determine the hydrodynamic diameter and surface charge, respectively.

3.22 Binding Study of GST tagged PTEN and Silver Nanoclusters

The interaction between protein and nanoclusters was determined by probing the fluorescence of the nanoclusters. To achieve binding of GST-PTEN to silver nanoclusters, fixed concentration of nanoclusters was incubated with varying concentrations of protein (6-48 nM) at room temperature for 2 h. The final volume was made up to 1 ml using 25 mM Hepes, pH 7.4. Following incubation, the samples were centrifuged at 10000 rpm at 4 °C for 10 min. The pellet was re-dispersed in 25

mM Hepes, pH 7.4. The pellet was probed at 480 nm and the fluorescence was recorded at 650 nm using Fluoromax-4, Horiba JobinYvon, Edison, NY, USA. Binding percentage was calculated as follows-

$$Binding\ (\%) = \frac{Fluorescence\ Intensity_{NCs} - \ Fluorescence\ Intensity_{Bound\ NCs}}{Fluorescence\ Intensity_{NCs}}\ x\ 100$$

Where, Fluorescence $Intensity_{NCS}$ is the fluorescence of the nanoclusters and Fluorescence $Intensity_{Bound\ NCS}$ is the fluorescence of the nanoclusters after binding to GST-PTEN.

3.23 Polymer Encapsulation and Characterization of PTEN Bound Nanoclusters

GST-PTEN bound silver nanoclusters (GST-PTEN-AgNCs) as well as free silver nanoclusters were coated with polyethylene glycol 4000 (PEG) by double emulsion technique according protocol described by Samadi *et al* (Samadi *et al.,* 2014), with small modifications. Protein bound nanoclusters (GST-PTEN-AgNCs) solution was emulsified in Dichloromethane (DCM) containing (5% w/v) PEG 4000 using a probe sonicator for 4 min at 40% amplitude. The water-in-oil emulsion (w/o) was further emulsified in aqueous phase of NaCl solution (0.9% w/v) to form water-in-oil-in-water emulsion (w/o/w) in an ice bath using probe sonicator for 5 min at 60% amplitude. DCM was evaporated in a vacuum desiccator overnight. The solution was then centrifuged at 12000 rpm for 20 min at 4 °C to collect the nanoparticles formed. The nanoparticles formed were washed twice with Milli-Q. The pellet was finally dispersed in Milli-Q for further applications. The strategy for PEG encapsulation is depicted in **scheme 3.7**.

Protein loading efficiency was determined by method involving dimethyl sulphoxide (DMSO), sodium hydroxide (NaOH) and SDS that allowed solubilization of both PEG polymer and protein in a single phase, as described by Sah *et al* (Sah 1997). Following coating of the ensemble with PEG, the pellet obtained was dried. The dried pellet of the samples was mixed with DMSO and 0.05 M NaOH containing 0.05% SDS.

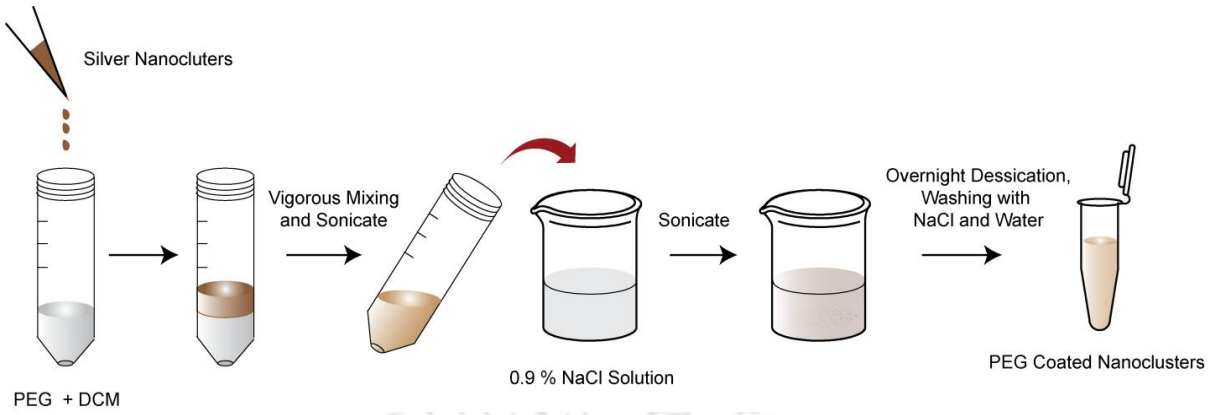

Scheme 3.7 Schematic representation of PEG coating protocol of GST-PTEN-AgNCs ensemble.

Upon incubation at 37 °C for 12 h, clear solution was obtained. The solution obtained was analyzed for protein estimation.

Protein loading efficiency was determined by applying the following definition-

$$Protein\ Loading\ Efficiency\ (\%) = \frac{Amount\ of\ Protein\ Entraped}{Nominal\ Protein}\ X\ 100$$

The silver nanoclusters coated with PEG have been named as nanocomposites and the silver nanoclusters bound with the GST-PTEN protein have been referred to as PTEN-nanocomposites. The concentration of the nanocomposites is expressed as nM of protein (PTEN) and μg/ml of silver in the cluster. The formation of nanocomposites and PTEN-nanocomposites was confirmed by TEM analysis, hydrodynamic diameter and zeta potential measurements as mentioned above.

3.24 Cellular Internalization of the PTEN-Nanocomposites

The luminescent property of silver nanoclusters was capitalized to study the intracellular delivery of the protein cargo. Intracellular uptake was investigated employing flow cytometry, confocol microscopy and fluorescence spectroscopy. For flow cytometry based analysis, glioblastoma cell line U-87 MG and breast cancer cell line MCF7 were seeded in 6 well plates at a cell density of $1x10^5$ cells per well in DMEM media supplemented with 10 % FBS and incubated at 37 ˚C under humidified condition of 5% CO_2 for cell adherence.

Following attachment, PTEN-nanocomposites [PTEN (12nM)-Cluster (10µg/ml) composite] was added to cells and incubated in CO_2 incubator. At different time points of 2 h, 4 h and 8 h cells were trypisinized and washed with 1X PBS followed by analysis using Beckman coulter. For confocal microscopy, MCF7 and U-87 MG cells grown on cover slip were incubated with PTEN-nanocomposites. After 4 h of incubation, the serum media was removed and the cells were washed with PBS thrice. The cells were then fixed using chilled absolute ethanol. The cover slip was mounted on a clean glass side and the sides were sealed. The fixed cells were then analyzed using Zeiss LSM 880 microscope with excitation at 488 nm, accompanied by z-stacking analysis. For fluorescence spectroscopy study, following incubation with the PTEN-nanocomposites the cells were trypsinized and collected by centrifugation at 650 rcf for 7 min. The pellet was washed with 1X PBS pH 7.4 thrice and finally re-dispersed in 1X PBS pH 7.4. Uptake was determined using multiplate reader Tecan infinite M200PRO at 480 nm and 650 nm excitation and emission wavelength, respectively.

To understand the mode of cellular internalization, U-87 MG and MCF7 were seeded in 6 well plates at a cell density of $1x10^5$ cells per well in DMEM media supplemented with 10 % FBS and incubated at 37 °C under humidified condition of 5% CO_2 for cell adherence. Following adherence the cells were either incubated with sodium azide or incubated at low temperature of 4 °C for 30 min. U-87 MG and MCF7 cells were incubated with 10 mM and 3 mM of sodium azide, respectively. Following incubation the cells were treated with PTEN (12nM)-Cluster (10µg/ml) composite for different time points. After incubation at different time points of 30 min, 120 min and 480 min the cells were trypisinized and washed with 1X PBS followed by analysis using multiplate reader Tecan infinite M200PRO at 480 nm and 650 nm excitation and emission wavelength, respectively.

3.25 RNA Isolation and Expression Study

U-87 MG and MCF7 cells were seeded in 6 well plates at a cell density of $1x10^5$ cells per well in DMEM media supplemented with 10% FBS and incubated at 37 °C under humidified condition of 5% CO_2 for cell adherence. For experiments with PTEN-Long, U-87 MG cells were treated with 100 nM of the protein for 2 h and 4 h in serum DMEM media. For experiments with PTEN, U-87 MG cells were treated with PTEN (72 nM)-Cluster (60 µg/ml) composite and MCF7 cells were treated with

PTEN (36 nM)-Cluster (30 μg/ml) for 8 h in serum DMEM media. To study the modulation of cyclins upon treatment, total mammalian RNA was isolated using tri reagent based method from the treated and untreated cells. Total RNA isolated from the treated and control cells using tri reagent based method was quantified using nanodrop (Eppendorf). A total of 0.5 μg of RNA was used for cDNA synthesis using verso cDNA synthesis kit (Thermo scientific). Cyclins and apoptotic genes were amplified in PCR reaction using gene specific primers with 27 amplification cycles. GAPDH was also amplified as internal control. The PCR product was run on 1% agarose gel to analyze gene expression.

3.26 Generation of Spheroids

The U-87 MG and MCF7 spheroids were generated by a facile and reproducible method to obtain single spheroid in individual well (Ivascu and Kubbies 2006, Friedrich *et al.*, 2009). U-87 MG and MCF7 cells were cultured as 2D monolayer to confluency in DMEM media supplemented with 10% FBS (DMEM serum media). The cells were harvested by trypsinization and finally re-suspended in DMEM serum media. To 96 well plates, 50 μL of serum free media containing agarose was added to each well. Prior to addition to the wells, agarose (1.5% w/v) in serum free DMEM media was sterilized by autoclaving. To the agarose coated 96 well plates, U-87 MG and MCF7 cells were seeded at a cell density of $1x10^4$ cells per well with final media volume of 200 μL. Followed by seeding, the 96 well plates were centrifuged at 400 rcf for 10 min at room temperature. Subsequently, the plates were incubated in 37 °C incubator with 5% CO_2 and humidified atmosphere for 96 h. The growth of the spheroids was monitored each day using NIKON microscope. The spheroids generated after 96 h incubation, were subsequently used for all experimental purpose.

3.27 Calcein-AM/ PI Dual Staining of U-87 MG and MCF7 Spheroids

The spheroids generated after 96 h incubation were subsequently used for all experimental analysis. The spheroids were treated with PTEN-nanocomposite [PTEN (96 nM)-Cluster (60 μg/ml) composite) and nanocomposite [Cluster (60 μg/ml) composite] for 48 h. Following treatment, the spheroids transferred to fresh flat-bottomed 96 well plates. The plates were then centrifuged at 400 rcf for 10 min at room temperature to spin down spheroids, clusters

and single cells. The spheroids were then washed carefully by replacing the media with 1X PBS pH 7.4. The plates were then again centrifuged under similar conditions and the washing process was repeated thrice. Finally the spheroids were incubated for 30 min with 100 µL of 1X PBS pH 7.4 containing calcein-AM and PI to a final concentration of 2 µM and 4 µM, respectively. After incubation, the spheroids were washed with 1X PBS pH 7.4 twice and imaged using using Zeiss LSM 880 microscope, accompanied by z-stacking analysis.

3.28 Alamar Blue Assay for Spheroid Viability Study

The resazurin reduction assay was performed to determine the presence of metabolically active cells in the treated and untreated spheroids (Walzl *et al.*, 2014). The detection is based on the principle of reduction of resazurin into resorufin, which can be measured by colorimetric method to determine the number of viable cells. Following treatment of the U-87 MG and MCF7 spheroids with PTEN-nanocomposites and nanocomposites, the alamar blue assay was performed. To each 96 well plate 50 µL of alamar blue solution was added and incubated for 4 h at 37 °C under 5% CO_2 humidified condition. Following incubation, the product was measured at 570 nm along with background measurement at 600 nm using multiplate reader (Tecan, Infinite M200 pro). The cell viability (%) relative to the untreated control spheroids was determined using the following formula

$$Cell\ viability(\%) = \frac{(abs570\ -abs600)Sample}{(abs570\ -abs600)Control} X\ 100$$

3.29 Cell Cycle Analysis of the Spheroids

Followed by treatment with PTEN-nanocomposite and nanocomposite, the spheroids were collected in 1.5 ml centrifuge tubes. The spheroid was then dislodged by trypsinization and collected by centrifugation at 400 rcf for 10 min at room temperature. The cells were fixed by drop wise addition of 70% chilled ethanol, and stored at -20 °C until further analysis. The fixed samples were prepared for cycle analysis using propidium iodide dye by following the protocol as mentioned above.

Briefly, the samples were centrifuged at 650 rcf for 10 min and washed with chilled 1X PBS pH 7.4. Following washing, the samples were incubated with RNAse for 1 h at 37 °C. The samples were then incubated with PI and stored in dark on ice until further analysis using BD FacsCalibur. The samples were recorded using Cell Quest programme and the data collected was examined using FCS express software.

3.30 Statistical analysis

All statistical analyses performed in this study were executed using Graphpad prism software where *p<0.05, **p<0.001, ***p<0.001.

3.31 References

Clemments, A. M., Botella, P. and Landry, C. C. (**2015**). Protein Adsorption From Biofluids on Silica Nanoparticles: Corona Analysis as a Function of Particle Diameter and Porosity. ACS Applied Materials & Interfaces **7**(39), 21682-21689.

Friedrich, J., Seidel, C., Ebner, R. and Kunz-Schughart, L. A. (**2009**). Spheroid-based drug screen: considerations and practical approach. Nat Protoc **4**(3), 309-324.

Greenfield, N. J. (**2006**). Using circular dichroism spectra to estimate protein secondary structure. Nature protocols **1**(6), 2876-2890.

Ivascu, A. and Kubbies, M. (**2006**). Rapid generation of single-tumor spheroids for high-throughput cell function and toxicity analysis. J Biomol Screen **11**(8), 922-932.

Liang, C.-C., Park, A. Y. and Guan, J.-L. (**2007**). In vitro scratch assay: a convenient and inexpensive method for analysis of cell migration in vitro. Nature Protocols **2**, 329.

Martin, K. R., Narang, P., Medina-Franco, J. L., Meurice, N. and MacKeigan, J. P. (**2014**). Integrating virtual and biochemical screening for protein tyrosine phosphatase inhibitor discovery. Methods **65**(2), 219-228.

McAvoy, T. and Nairn, A. C. (**2010**). Serine/Threonine Protein Phosphatase Assays. Current protocols in molecular biology / edited by Frederick M. Ausubel et. al. **CHAPTER**, Unit18.18-Unit18.18.

Riccardi, C. and Nicoletti, I. (**2006**). Analysis of apoptosis by propidium iodide staining and flow cytometry. Nat. Protocols **1**(3), 1458-1461.

Rodriguez-Escudero, I., Oliver, M. D., Andres-Pons, A., Molina, M., Cid, V. J. and Pulido, R. (**2011**). A comprehensive functional analysis of PTEN mutations: implications in tumor- and autism-related syndromes. Hum Mol Genet **20**(21), 4132-4142.

Sah, H. (**1997**). A new strategy to determine the actual protein content of poly(lactide-co-glycolide) microspheres. J Pharm Sci **86**(11), 1315-1318.

Samadi, N., van Steenbergen, M. J., van den Dikkenberg, J. B., Vermonden, T., van Nostrum, C. F., Amidi, M. and Hennink, W. E. (**2014**). Nanoparticles based on a hydrophilic polyester with a sheddable PEG coating for protein delivery. Pharm Res **31**(10), 2593-2604.

Scholler, N., Crawford, M., Sato, A., Drescher, C. W., O'Briant, K. C., Kiviat, N., Anderson, G. L. and Urban, N. (**2006**). Bead-based ELISA assays for validation of ovarian cancer early detection markers. Clinical cancer research : an official journal of the American Association for Cancer Research **12**(7 Pt 1), 2117-2124.

Spinelli, L. and Leslie, N. R. (**2015**). Assaying PTEN catalysis in vitro. Methods **77–78**, 51-57.

Walzl, A., Unger, C., Kramer, N., Unterleuthner, D., Scherzer, M., Hengstschlager, M., Schwanzer-Pfeiffer, D. and Dolznig, H. (**2014**). The Resazurin Reduction Assay Can Distinguish Cytotoxic from Cytostatic Compounds in Spheroid Screening Assays. J Biomol Screen **19**(7), 1047-1059.

Yip, C. K., Kimbrough, T. G., Felise, H. B., Vuckovic, M., Thomas, N. A., Pfuetzner, R. A., Frey, E. A., Brett Finlay, B., Miller, S. I. and Strynadka, N. C. J. (**2005**). Structural characterization of the molecular platform for type III secretion system assembly. Nature **435**(7042), 702-707.

Zhou, T., Huang, Y., Li, W., Cai, Z., Luo, F., Yang, C. J. and Chen, X. (**2012**). Facile synthesis of red-emitting lysozyme-stabilized Ag nanoclusters. Nanoscale **4**(17), 5312-5315.

Results and Discussion

Section 4

भारतीय प्रौद्योगिकी संस्थान गुवाहाटी
Indian Institute of Technology Guwahati

Cloning, Expression and Purification of Recombinant proteins PTEN and PTEN-Long

4.1 Cloning of PTEN and PTEN-Long

The coding sequence of PTEN-Long was procured from addgene (USA) in JpExpress404 vector. Similarly, the coding sequence of PTEN was purchased from DNASU plasmid repository in pANT_cGST vector. The genes were PCR amplified using respective gene specific primers to optimize the PCR conditions. The genes were then PCR amplified with primers containing *BamHI* and *XhoI* restriction enzyme overhangs at the 5' and 3' end, respectively. After amplification, the genes were cloned into pGEMT easy vector and transformed into competent *Escherichia coli* DH5α. The TA cloning was confirmed by release of the 1.8 kb fragment for PTEN-Long and 1.2 kb fragment for PTEN upon restriction digestion **(Figure 4.1A and 4.1B)**.

The pGEMT-PTEN-Long and the pGEMT-PTEN constructs were used as template to amplify the genes and sub-clone into bacterial expression vector PGEX-4T-2 vector. After amplification and sub cloning into PGEX-4T-2 vector, the construct was transformed into competent *Escherichia coli* BL21 (DE3). The cloning into bacterial expression system was confirmed by release of the 1.8 kb fragment for PTEN-Long and 1.2 kb fragment for PTEN upon restriction digestion **(Figure 4.1C and 4.1D)**.

4.2 Bacterial Expression, Purification and Physical Characterization of the Recombinant Proteins

Upon confirmation of cloning, the expression of the evaluated proteins was induced. The expression was first optimized in small scale 5 ml cultures. PGEX-4T-2 vector system contains the Lac Z gene, which makes it an Isopropyl-β-D-1-thiogalactopyranoside (IPTG) inducible vector system. The transformed bacteria were grown on LB agar plates containing ampicillin. Primary culture of 3 ml grown from isolated single colony overnight at 37 °C was used as an inoculum for secondary culture of 5 ml LB media. The protein expression was induced by IPTG at different temperatures for different time periods. The expression conditions optimized for GST-PTEN-Long protein were 0.5 mM IPTG concentration, 12 h induction time at a temperature of 21 °C. Optimal conditions for expression of the

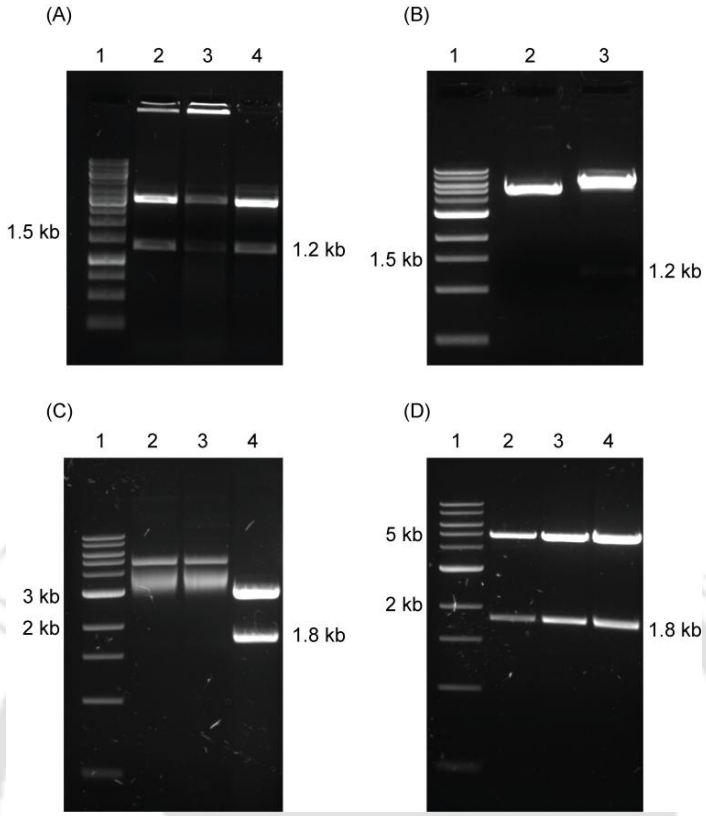

Figure 4.1 Cloning of PTEN and PTEN-Long genes (A) Lane 1 shows 1 kb DNA ladder, Lane 2-4 shows digestion of pGEMT-PTEN by *EcoRI* (B) Lane 1 shows 1 kb DNA ladder, Lane 2 shows the uncut PGEX-4T-2 plasmid and Lane 3 shows restriction digestion of PGEX-4T-2-PTEN by *BamHI* and *XhoI* (C) Lane 1 shows 1 kb DNA ladder, Lane 2-3 shows uncut digestion pGEMT-PTEN-Long, Lane 4 shows restriction digestion of pGEMT-PTEN-Long by *EcoRI* (D) Lane 1 shows 1 kb DNA ladder, Lane 2-4 shows restriction digestion of PGEX-4T-2-PTEN-Long by *BamHI* and *XhoI*.

recombinant GST-PTEN were 0.5 mM IPTG concentration, 4 h induction time at a temperature of 28 °C. The expression of the induced recombinant proteins were analyzed on 12% SDS gel **(Figure 4.2A and 4.2B)**.

For both the recombinant proteins, at small scale of 5 ml secondary cultures when the cells were lysed and analyzed on SDS gel, most of the induced protein was found to be in the insoluble fraction with a small amount in the soluble fraction. However, upon increasing the culture volume to 500 ml, considerable amount of induced recombinant protein was found in the soluble fraction. Therefore, the supernatant fraction was used without solubilizing the

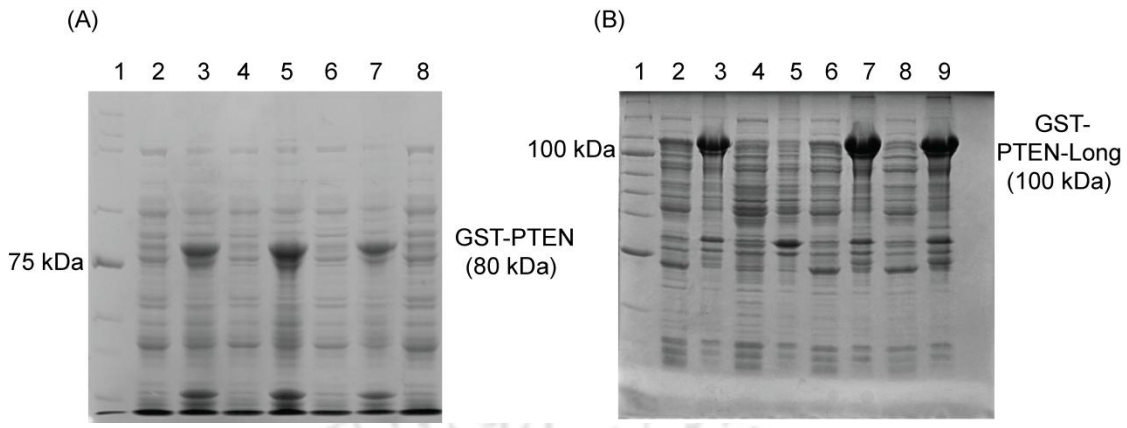

Figure 4.2 Induction of PTEN and PTEN-Long proteins expression (A) Lane 1 shows 2-212 kDa protein ladder, Lane 2,4,6 displays supernatant fraction of induced cell lysate of different clones, Lane 3,5,7 displays expression of GST-PTEN in pellet fraction of induced cell lysate of different clones (around 81 kDa) and Land 8 shows uninduced cell lysate (B) Lane 1 shows 2-212 kDa protein ladder, Lane 2,6,8 displays supernatant fraction of induced cell lysate of different clones, Lane 3,7,9 displays expression of GST-PTEN in pellet fraction of induced cell lysate of different clones (around 81 kDa) and Land 4,5 shows uninduced cell lysate.

pellet so as to avoid the use of detergents during the course of purification. The bacterial cells from 500 ml culture were harvested by centrifugation at 7000 rpm for 8 min and stored at -20 $^{\circ}$C until further use. The frozen bacterial pellet were lysed and processed for purification.

Purification was carried out using glutathione-agarose affinity chromatography. The protein was purified on ice under slow rocking conditions by following binding, washing and elution steps. A band of around 100 kDa and 81 kDa corresponding to GST-PTEN-Long and GST-PTEN, respectively was observed when the purified fraction was run on 12% SDS-PAGE **(Figure 4.3A and 4.3B)**. Protein yield determined by Bradford assay was approximately 5 to 10 mg per litre of *E.coli* culture for the recombinant proteins. GST tag was also excised by on-column thrombin cleavage and the cleaved fractions were analyzed on 12% SDS-PAGE **(Figure 4.3C and 4.3D).** The purified recombinant proteins were further confirmed by MALDI TOF-TOF and Western blot analysis. The MS/MS profile obtained by MALDI TOF-TOF analysis of trypsin digested peptide fragments inspected using findpept expasy tool, generated match of the peptide sequence EKVENGSL with sequence query coverage of 14% for GST-PTEN-Long protein.

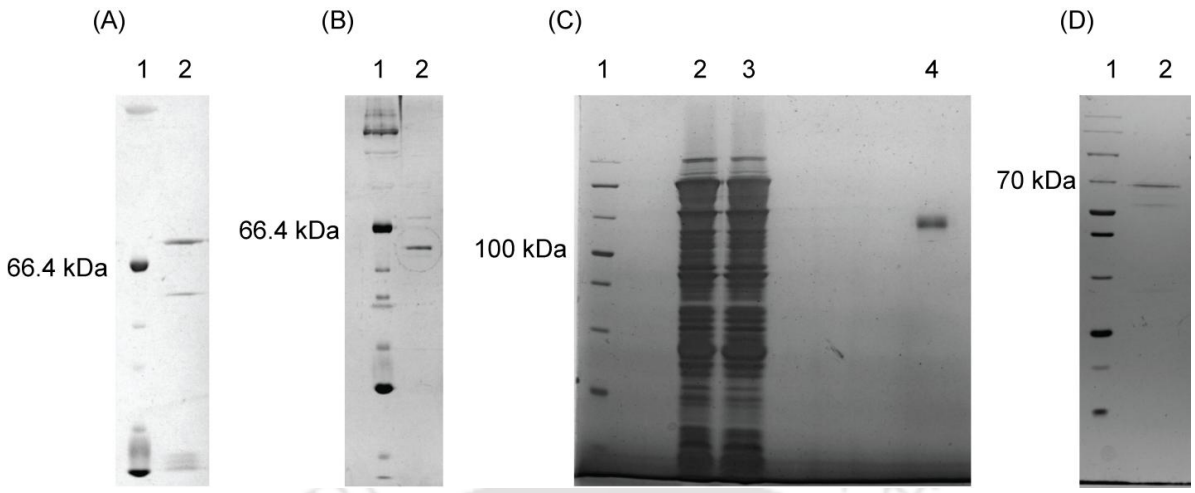

Figure 4.3 Purification profile of PTEN and PTEN-Long (A) Lane 1 shows 2-212 kDa protein ladder and Lane 2 shows purified GST-PTEN (B) Lane 1 shows 2-212 kDa protein ladder and Lane 2 shows purified PTEN (C) Lane 1 shows 2-212 kDa protein ladder, Lane 2 and 3 flow through fractions, Lane 4 purified GST-PTEN-Long (D) Lane 1 shows 2-212 kDa protein ladder and Lane 2 shows purified PTEN-Long.

For GST-PTEN protein the peptide sequence match NDLDKANKDKANRYFSPNFKVK was generated with sequence query coverage of 16.13% **(Figure 4.4A and 4.4B)**. Protein purified to homogeneity was investigated by the Western blotting using anti-PTEN antibody and anti-GST antibody. HRP-conjugated with the secondary antibody was used to develop the blots, which generated bands at legitimate molecular weight of 100 kDa and 81 kDa corresponding to GST-PTEN-Long and GST-PTEN, respectively. For GST band was developed at legitimate molecular weight around 26 kDa **(Figure 4.4C and 4.4D)**.

Following bacterial purification, it is important to study the secondary structure integrity of the recombinant proteins. Secondary structure of GST-PTEN-Long and GST-PTEN was characterized by far-UV circular dichroism spectroscopy. The spectrum investigated by Yang's reference (Chen and Yang 1971), revealed the content of secondary structural elements to be 45.5% α-helix and 25.5% β-sheet for GST-PTEN-Long. The spectrum investigated revealed the content of secondary structural elements to be 24.5% α-helix, 25.6 % β-sheet for GST-PTEN, as determined by Yang's reference **(Figure 4.5A and 4.5B)**.

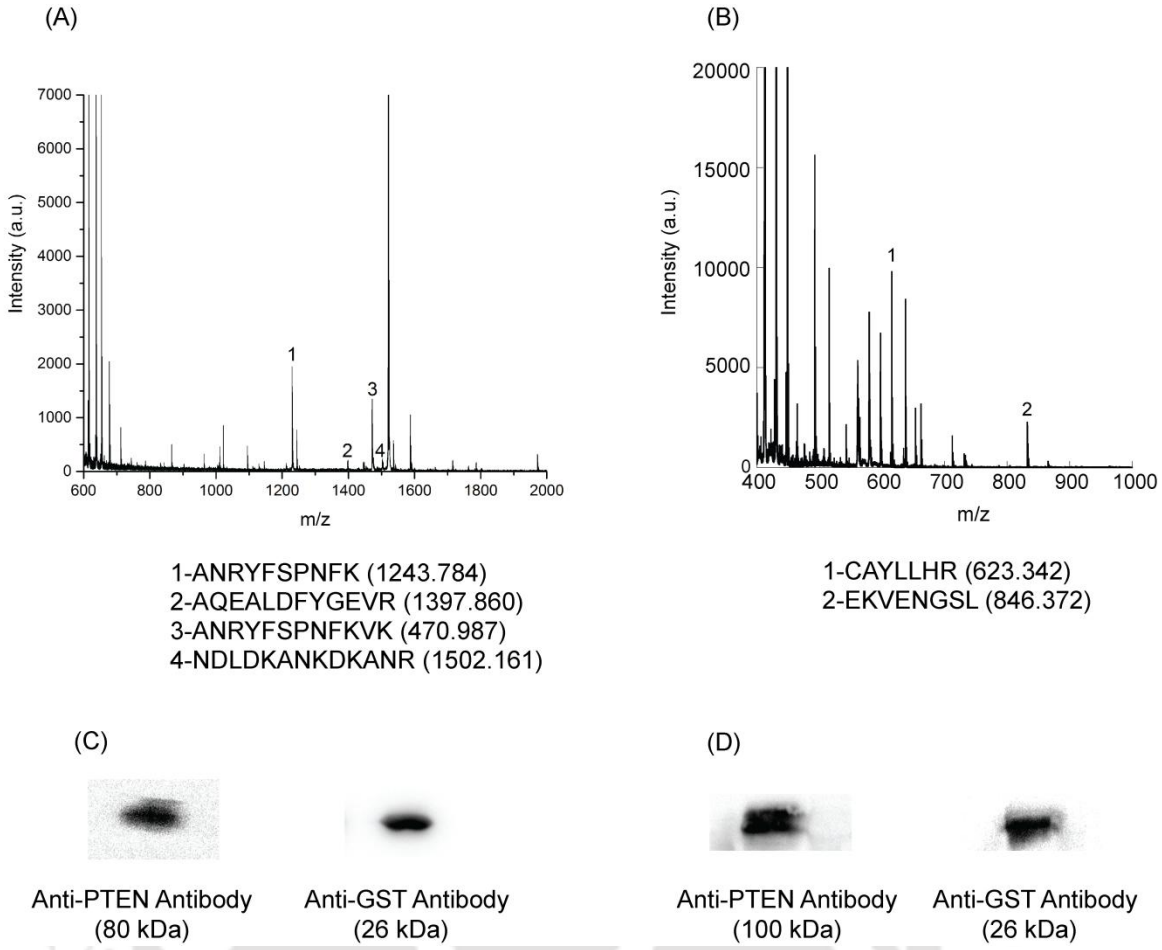

Figure 4.4 Characterization of the recombinant proteins (A) MALDI TOF-TOF analysis of purified GST-PTEN (B) MALDI TOF-TOF analysis of purified GST-PTEN-Long (C) Western blot with Anti-PTEN antibody and Anti-GST antibody for GST-PTEN (D) Western blot with Anti-PTEN antibody and Anti-GST antibody for GST-PTEN-Long.

The result was in accordance with the available crystal structure of PTEN in PDB (1D5R), where the estimated secondary structural elements were 19.603 % α-helix and 24.5 % β-sheet. Once the secondary structure was intact as evident by circular dichroism, the function of the recombinant enzymes were determined by phosphatase assay.

4.3 Functional Characterization of the Recombinant Proteins

PTEN, a dual specificity phosphatase, contains the signature motif HCXXGXXR in consensus with the family of PTPase (Myers *et al.*, 1997). Although PTEN de-phosphorylates artificial protein substrates such as para-nitrophenylphosphate (PNPP),

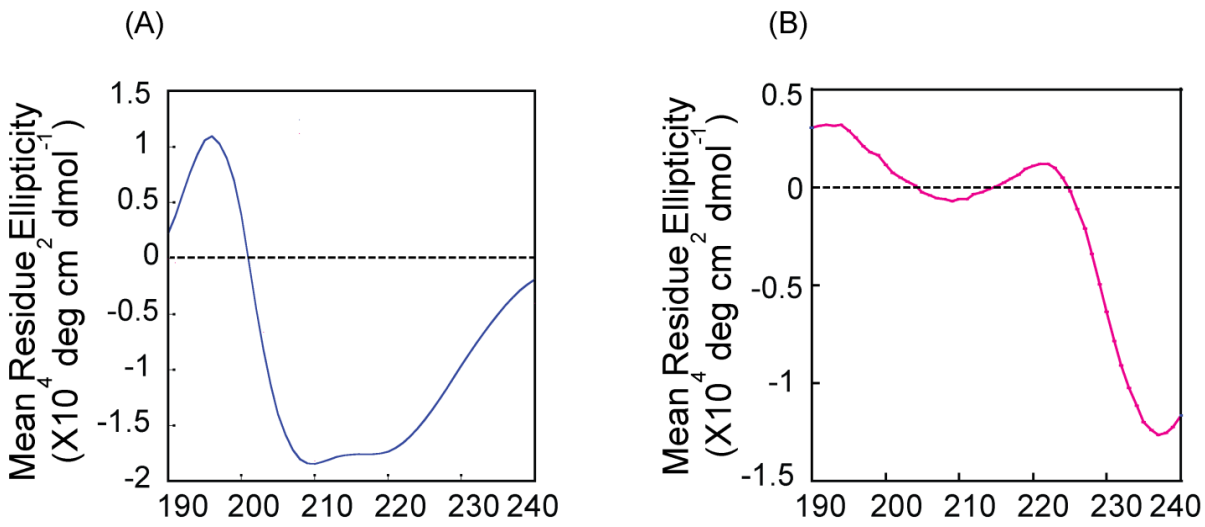

Figure 4.5 Characterization of secondary structure by circular dichroism (A) GST tagged PTEN (B) GST tagged PTEN-Long.

it has higher catalytic affinity towards lipid substrates (Maehama and Dixon 1998). Assaying PTEN requires a reducing environment to retain the active-site cysteine residue in its reduced state (Spinelli and Leslie 2015).Therefore, dithiothreitol (DTT) was an important component of the reaction buffer mixture. However, the phosphatase activity of PTEN-Long was previously not known. Therefore, its activity was established using PNPP assay in this current work. Assay results indicated that activity of PTEN-Long and PTEN (nanomole of phosphate released) over increasing concentration of PNPP substrate fits Michaelis-Menten kinetics **(Figure 4.6A and 4.6B)**. Kinetic parameters K_m and k_{cat}/K_m assessed using GraphPad Prism software were K_m and k_{cat}/K_m as 3767 µM and 0.22 x 10^{-3} $min^{-1}µM^{-1}$ for PTEN and 4216 µM and 0.24 x 10^{-3} $min^{-1}µM^{-1}$ for PTEN-Long, respectively. The kinetic parameters are illustrated in **Table 4.1**. The kinetic analysis essentially revealed no significant difference between the catalytic efficiency of GST-PTEN and PTEN and GST-PTEN-Long and PTEN-Long towards PNPP substrate, suggesting that the presence of GST tag did not hinder the enzymatic function of the proteins.

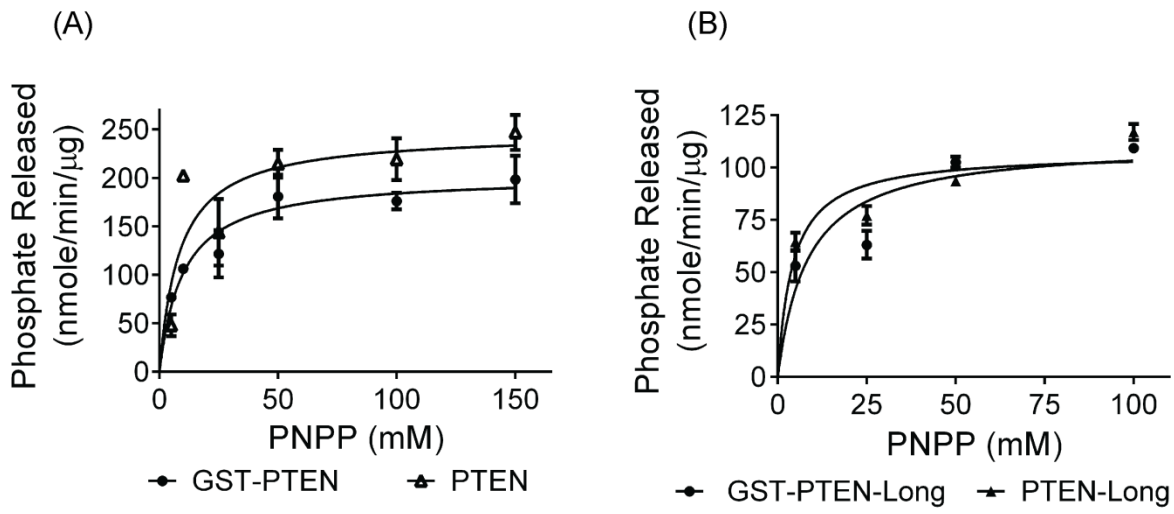

Figure 4.6 Kinetic profile of the recombinant proteins towards para-Nitrophenylphosphate (A) GST tagged and untagged PTEN (B) GST tagged and untagged PTEN-Long.

Additional considerations for presence of GST in the protein is that the affinity tag may also assist in protein folding, protein immobilization onto nanoparticles, facile one step purification and stabilization of the enzyme (Terpe 2003, Harper and Speicher 2011).Therefore the GST tag was retained and the effect of GST tagged PTEN-Long and GST tagged PTEN were further evaluated by performing cellular assays.

Sample	K_m (µM)	k_{cat}/ K_m (min^{-1} $µM^{-1}$)
GST-PTEN	6881	0.16×10^{-3}
PTEN	3767	0.22×10^{-3}
GST-PTEN-Long	8387	0.12×10^{-3}
PTEN-Long	4216	0.24×10^{-3}

Table 4.1 Kinetic parameters of the recombinant proteins towards para-Nitrophenylphosphate.

In vitro Effects of Recombinant PTEN-Long

4.4 Evaluation of Therapeutic Potential of PTEN-Long

A recent report suggested (Hopkins *et al.*, 2013) membrane-permeable function of PTEN-Long that would allow it to enter other cells. Therefore, the therapeutic efficacy of GST-PTEN-Long was evaluated on two different cancer cell lines, PTEN Null glioblastoma (U-87 MG) and PTEN expressing breast cancer cell line (MCF7). Upon 48 h treatment with varying concentration of GST-PTEN-Long, a dose-dependent reduction in cell viability of the two cell lines was observed **(Figure 4.7A and 4.7B)**, however IC_{50} was not achieved for either case. One possible inference could be the presence of GST tag; the 26 kDa negatively charged GST protein present at the N- Terminal of PTEN-Long may hinder its cellular entry. To verify the same, the GST tag was excised by on-column thrombin cleavage and PTEN-Long was purified. Prior to study the effect of PTEN-Long on the U-87 MG, the cellular internalization of the protein was assessed. To achieve the same, U-87 MG cells were incubated with 100 nM of PTEN-Long for different time intervals of 15, 30, 60, 120 and 240 min, followed by MTT assay of the cells after 48 h. It was observed that there was incubation-time dependent reduction in cell viability **(Figure 4.8)**.

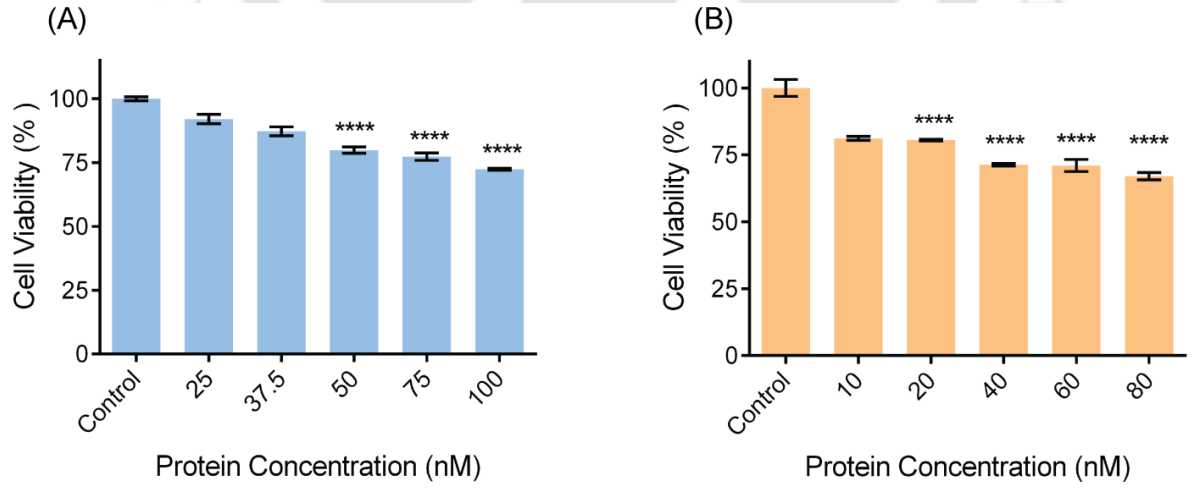

Figure 4.7 Assessment of viability of (A) U-87 MG Cells (B) MCF7 cells upon treatment with GST-PTEN-Long recombinant protein for 48 h by MTT assay.

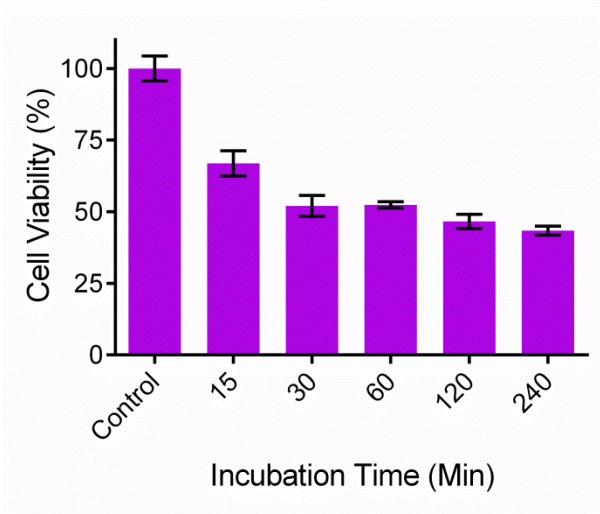

Figure 4.8 Time dependent uptake study of PTEN-Long in U-87 MG cells based on determination of cell viability by MTT assay.

The cell viability was same for 60, 120, and 240 min incubation indicating that the cellular entry of PTEN-Long protein is complete around 60 min to 120 min. Subsequently, treatment with PTEN-Long was performed, which led to dose-dependent reduction in cell viability of U-87 MG, with IC_{50} at 100 nm **(Figure 4.9A)**. However for MCF7, an estrogen-dependent cancer, there was no change in the reduction of the viability of the cells **(Figure 4.9B)**.

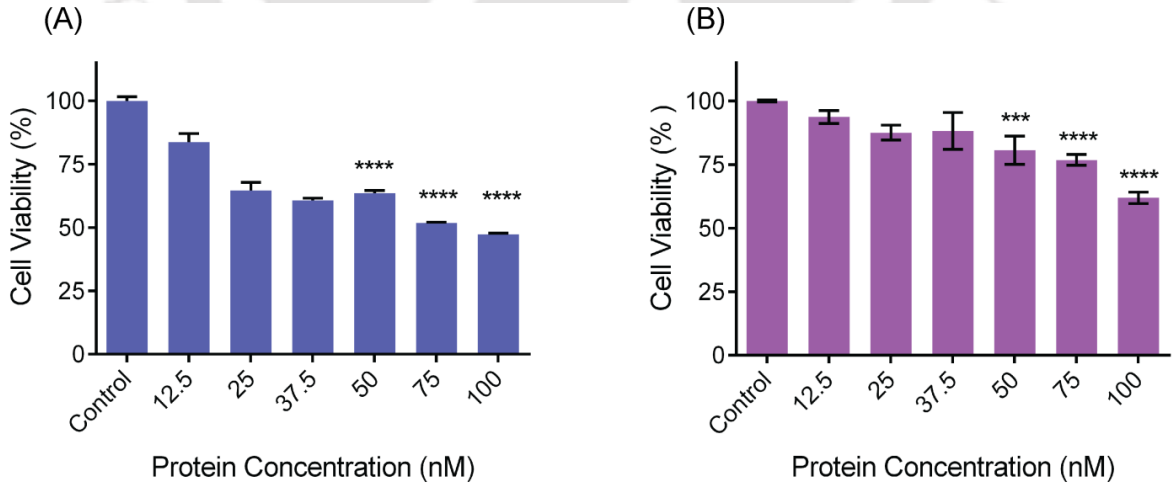

Figure 4.9 Assessment of viability of (A) U-87 MG cells (B) MCF7 cells upon treatment with PTEN-Long recombinant protein for 48 h by MTT assay.

A plausible explanation is the multiple facet regulation of estrogen signaling. Estrogen receptor exerts action by regulation of multiple transduction pathways (ERK/MAPK, p38/MAPK, PI3K/AKT, PLC/PKC) (Marino *et al.*, 2006). As a result, blocking the PI3K/AKT pathway may not be ample to influence cell growth and survival. All further experiments were then carried on U-87 MG cell line. The reduction in cell viability was corroborated with calcein-AM/ EtBr dual staining, where calcein-AM stains the viable cells and EtBr stains dead cells. Treatment with PTEN-Long resulted in reduction of viable cells as compared to buffer treated or untreated cells **(Figure 4.10)**.

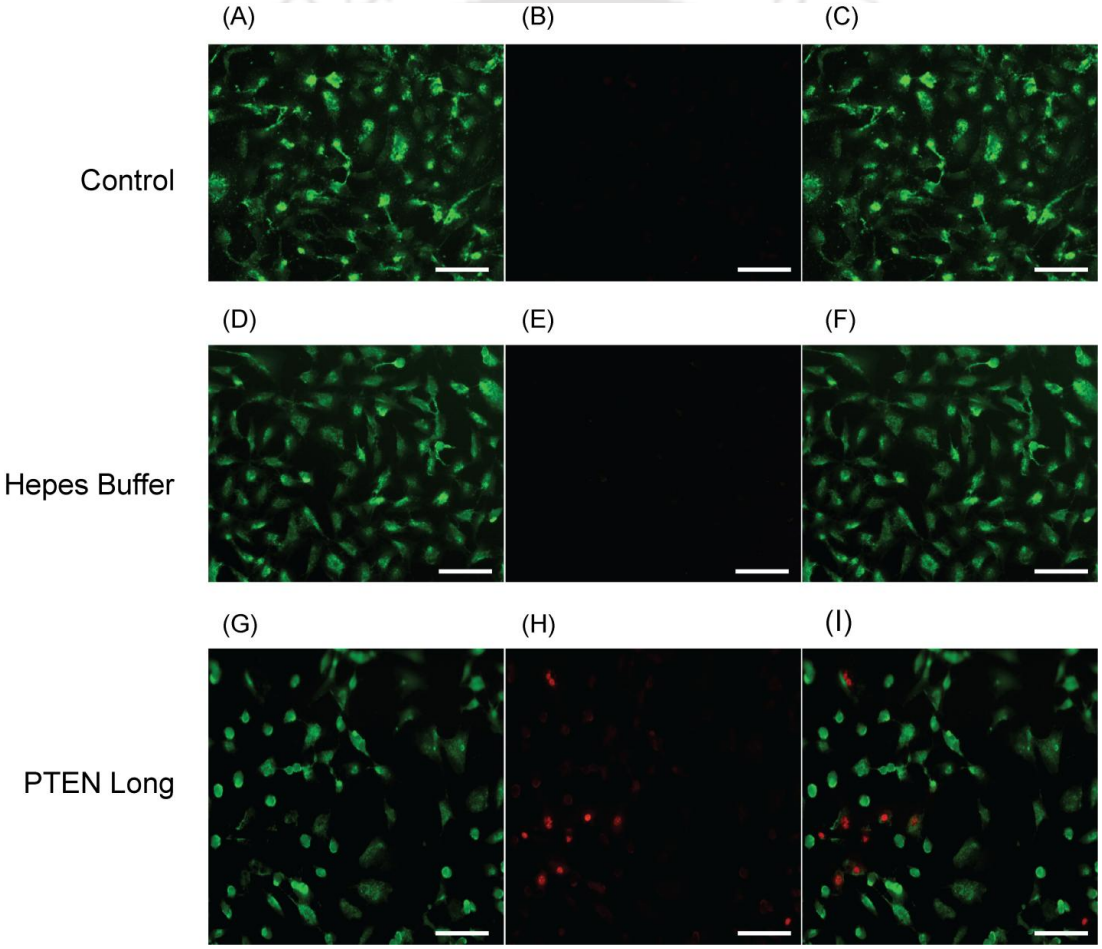

Figure 4.10 Calcein-AM/ EtBr dual staining for assessing U-87 MG cell viability where A, B, C are calcein-AM stained control cells, EtBr stained control cells and Merged cells, respectively. D, E, F are buffer treated calcein-AM stained cells, buffer treated EtBr stained cells and Merged cells, respectively. G, H, I are PTEN-Long protein treated calcein-AM stained cells, PTEN-Long protein treated EtBr stained cells and Merged cells, respectively. (Scale bar 25 µm).

Post verification of cellular entry of the recombinant protein, it was crucial to determine its cellular role. The effect of PTEN-Long on the AKT signaling pathway has been previously established (Hopkins *et al.,* 2013). Therefore the expression of pAKT(Ser473) was determined by western blot analysis of the total cell protein upon PTEN-Long treatment. It was seen that there was reduction in the expression of pAKT(Ser473) after treatment with 100 nM PTEN-Long **(Figure 4.11)**. This indicates the regulation of the AKT expression by PTEN-Long. Since PTEN-Long de-phosphorylated non-specific protein substrate *in vitro*, we embarked on the study of determining the cellular protein phosphatase role of PTEN-Long. Intracellular role of PTEN-Long may involve de-phosphorylation of focal adhesion kinase (FAK), like its PTEN counterpart. Therefore the modulation of pFAK expression was studied. Treatment with PTEN-Long resulted in down-regulation of pFAK(Tyr397) expression, a protein tyrosine kinase involved in cellular migration (Mitra *et al.,* 2005, Zhao and Guan 2011), as compared to untreated cells. AKT and FAK are key checkpoints to regulate signal transduction pathways and play a decisive role in controlling diverse array of functions including cell survival, cell proliferation and motility. Therefore, it was essential to determine the subsequent implications of the altered signaling on U-87 MG cell line.

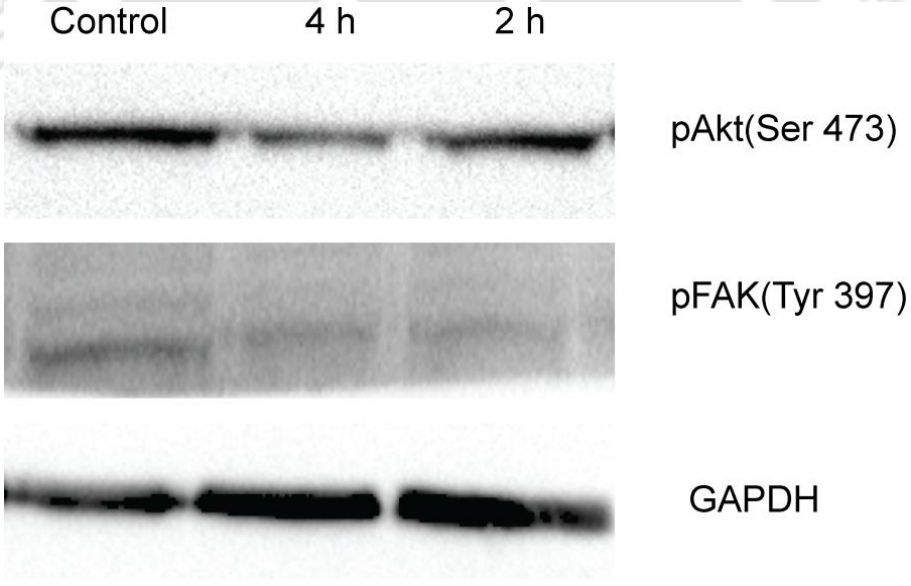

Figure 4.11 Western blot analyses of pAKT, pFAK and GAPDH in U-87 MG cells.

Since pFAK is involved in integrin signaling pathway regulated cell motility and cell migration, scratch assay was performed to determine the role of PTEN-Long in cell migration **(Figure 4.12)**.

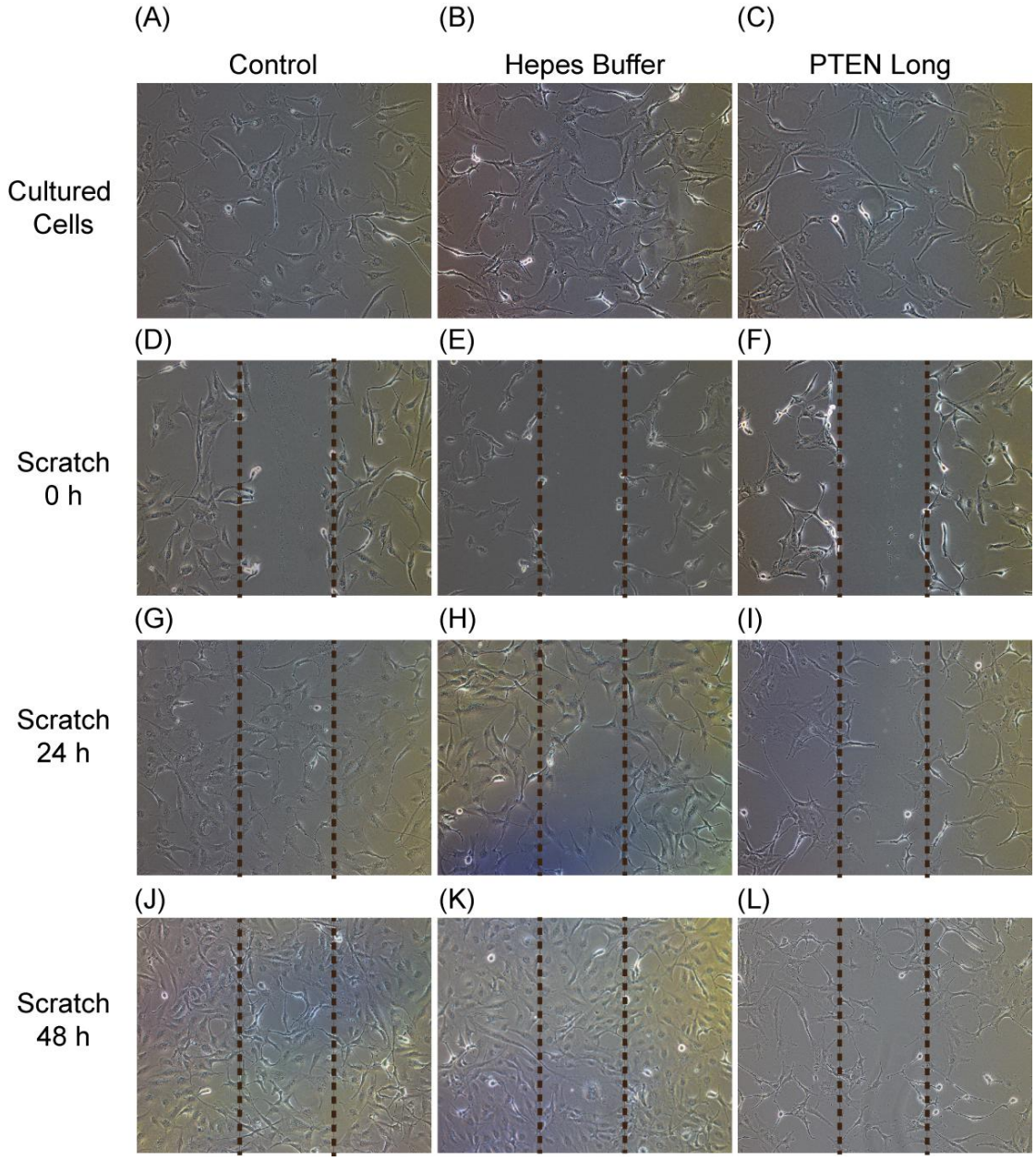

Figure 4.12 Scratch healing assays where A, B and C represents cultured U-87 MG cells, D, E and F represents control, buffer treated and PTEN-Long treated at 0 h. G, H and I represents control, buffer treated and PTEN-Long treated at 24 h. J, K and L represents control, buffer treated and PTEN-Long treated at 48 h.

A scratch was made with sterile pipette tip and the recovery of the wound was monitored using Nikon ECLIPSE Ti microscope at 0 h, 24 h and 48 h. It was observed that the cells treated with PTEN-Long displayed slow healing as compared to buffer treated or untreated control cells. Therefore the down-regulation of pFAK by PTEN-Long correlated with the reduced migration of cells. The reduction in pAKT(Ser473) expression of recombinant protein treated cells reflected in their cycle pattern as determined by propidium iodide (PI) based flow cytometry. Analyzing the cell cycle pattern of U-87 MG cell line revealed S-phase arrest upon treatment with 50 nM and 100 nM of recombinant protein, with a 1.54 fold increase in the S-phase cells in treated cells (29.75 %) as compared to untreated control cells (19.25 %). Cell cycle analysis was performed using FCS express flow cytometry software **(Figure 4.13A)**. The regulation of cell progression from G1 to S to G2 phases and finally to the mitotic phase is controlled by cell cyclins also known as cell cycle check points. To study the expression of the cyclins in the treated and untreated cells, total RNA was

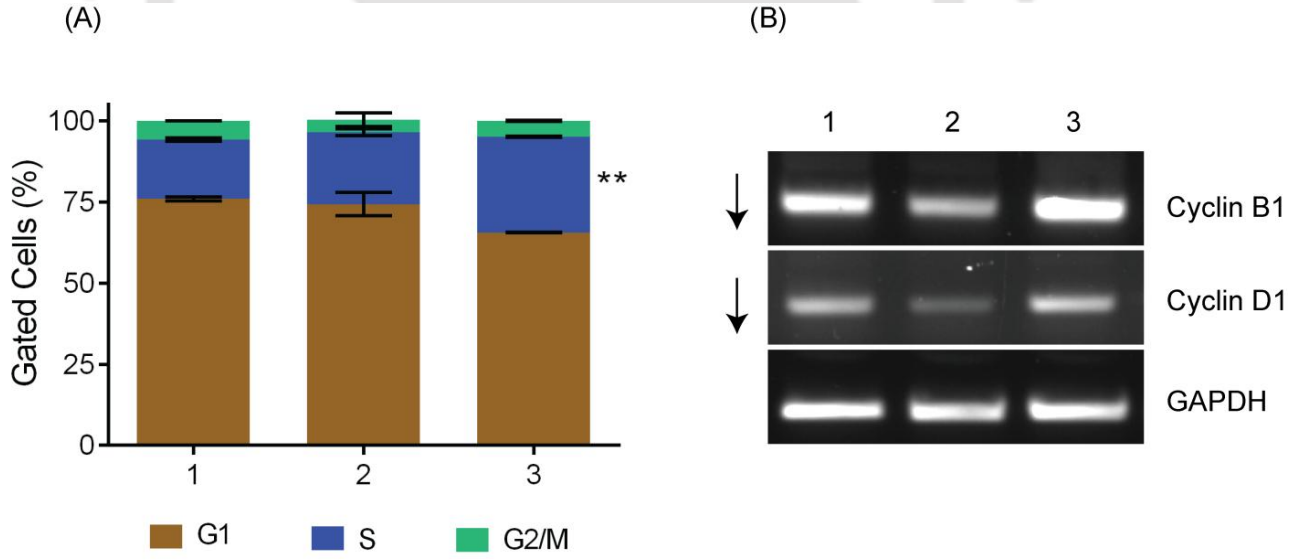

Figure 4.13 Assessment of cell cycle regulation of U-87 MG cells (A) Cell cycle analysis by flow cytometry upon treatment for 48 h where 1, 2 and 3 are control, 50 nM GST-PTEN-Long and 100 nM GST-PTEN-Long treated cells, respectively (B) Expression of cyclin B1, cyclin D1 and GAPDH upon treatment for 48 h where 1, 2 and 3 are control, 100 nM GST-PTEN-Long treated and buffer treated cells, respectively.

isolated and cDNA was synthesized. Semi-quantitative PCR analysis of cyclins using gene specific primers, revealed a decrease in the expression of cyclin B1 and cyclin D1 expression **(Figure 4.13B)**. Cyclin B1 is an important component of the cell cycle, which promote S Phase and G2/M phase transitions (Moore *et al.,* 2003) culminating into cell division. Inhibition of cyclin B1 resulted in accumulation of the PTEN-Long treated cells in the S phase. The fold change of cyclins is presented in the annexure. The results demonstrated anti-proliferative activity of PTEN-Long in U-87 MG cells, with modulation of cellular signaling ensuing reduced cell survival and cell migration.

4.5 Assessment of Co-therapy Module with PTEN-Long

Another approach to combat diseased condition is the possibility of PTEN-Long to act in combination with commercially applied anti-cancer drugs. The combination therapy was first attempted with tamoxifen. Treatment of U-87 MG with tamoxifen did not bring about significant difference in viability of cells in the presence or absence of PTEN-Long **(Figure 4.14A)**. Tamoxifen principally acts by binding to the estrogen receptor and blocking the proliferative action of estrogen. One of the possible outcomes of blocking estrogen is down-regulation of the AKT pathway; therefore further adding of PTEN-Long did not cause any profound effect due to the same target pathway. Therefore, the combinatorial therapy was further evaluated with anti-cancer drug temozolomide (TMZ) **(Figure 4.14B)**.

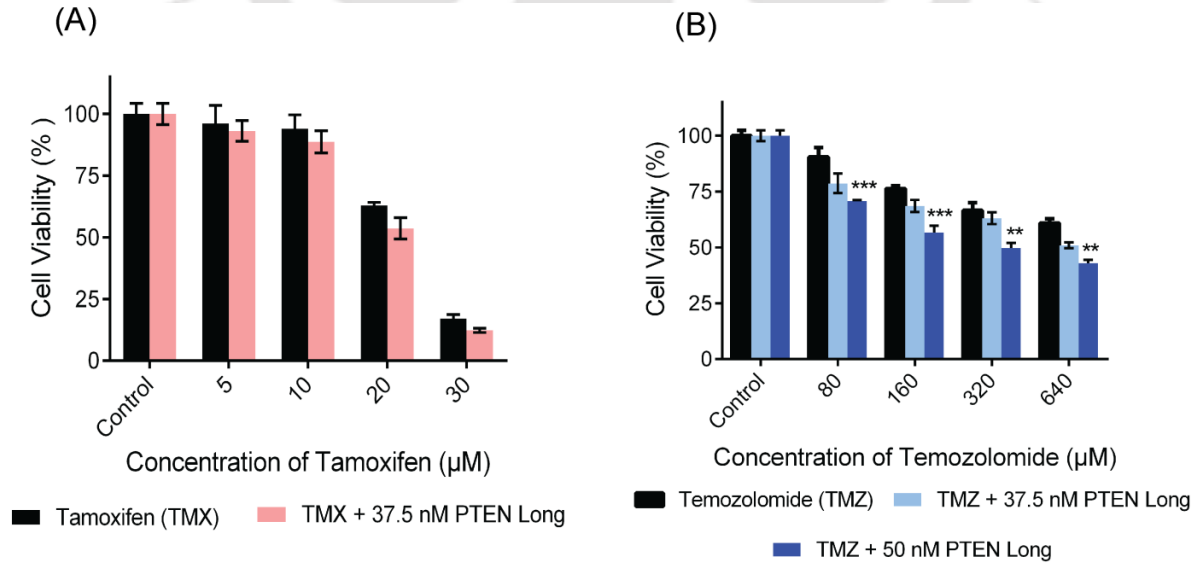

Figure 4.14 Assessment of viability of U-87 MG cells upon treatment with PTEN-Long for 48 h in combination with (A) Tamoxifen drug (B) Temozolomide drug.

PTEN-Long in combination with temozolomide, an alkylating agent used as first-line treatment for glioblastoma (2017, Lee 2017), displayed dose-dependent cell viability reduction with change in IC_{50} of TMZ from 960 μM to 640 μM in presence of 50 nM PTEN-Long protein. Therefore, the combination therapy was successful in reducing the concentration of drug used for treatment of glioblastoma, which can be possibly applied in future to reduce the drug-associated side effects.

In Vitro Effects of Recombinant PTEN

PTEN-Long is a membrane permeable protein as previous reported and demonstrated in this current investigation by the uptake study and ability to modulate cellular environment upon exogenous addition to the U-87 MG cells. However for PTEN there exists sufficient literature evidence that it is an intracellular protein (Leslie 2012). To ensure the same, GST tagged PTEN was added onto different cell lines U-87 MG, A549 and HeLa and the viability was determined by MTT cell viability assay. No significant reduction in cell viability was observed upon 48 h treatment **(Figure 4.15).** Contemplating the regulatory role of PTEN, it was vital to internalize the functional enzyme to capitalize on its biomedical value.

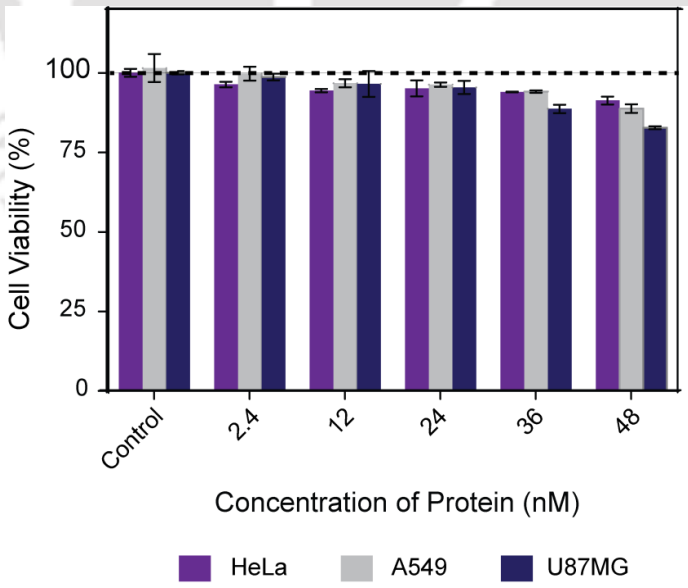

Figure 4.15 Assessment of viability of HeLa, A549 and U-87 MG cells upon treatment with GST-PTEN for 48 h by MTT assay.

This necessitated the application of a suitable approach for stabilization and delivery of the recombinant protein. Nevertheless, it is extremely crucial to confirm that the interaction between the protein and carrier does not hamper the active state conformation and activity of the protein. Among different existing strategies, employing nanoparticles for optimal protein stabilization has attracted great interest. In this prospective, silica nanoparticles gained huge impetus as drug delivery vehicles due to their excellent properties such as, tunable shape and size, biocompatibility and ease of synthesis (Benezra *et al.*, 2011, Tang and Cheng 2013). The facile synthesis of silica nanoparticles with diverse structure and morphologies has always attracted researchers to employ silica for a plethora of biomaterial purposes. Interestingly, silica nanoparticles ranging from 25 to 100 nm in size have been reported to cross the blood brain barrier (Hanada *et al.*, 2014). Therefore, in efforts to stabilize PTEN, silica nanoparticles were synthesized and characterized.

4.6 Synthesis and characterization of Silica Nanoparticles for Recombinant PTEN Immobilization

Silica nanoparticles were synthesized by modification of the Stober's process employing poly-condensation of tetraethylorthosilicate (TEOS) under alkaline environment. The size and shape of the nanoparticles were examined by TEM and FESEM analysis. TEM analysis of the silica nanoparticles displayed synthesis of spherical particles with average diameter of 55 ±10 nm **(Figure 4.16A)**. The size and morphology of nanoparticles was further confirmed by FESEM **(Figure 4.16B)**, which validated the TEM results with average diameter of 60±10 nm. Average diameter was calculated from several images consisting of 100 particles using ImageJ software **(Figure 4.16C and 4.16D)**. Once the synthesis of spherical silica nanoparticles were confirmed, the stabilization of the GST tagged PTEN onto the nanoparticles was evaluated.

Adsorption of GST-PTEN on silica nanoparticles was determined by fluorescence spectroscopy, DLS measurements, ELISA and FTIR study. Binding was determined by probing the intrinsic fluorescence of protein in 25 mM Hepes pH 7.4 **(Figure 4.17A)**. Following binding, the supernatant was probed to determine the binding percentage. The maximum binding percentage was calculated to be 49 %, at a protein concentration of 12 nM

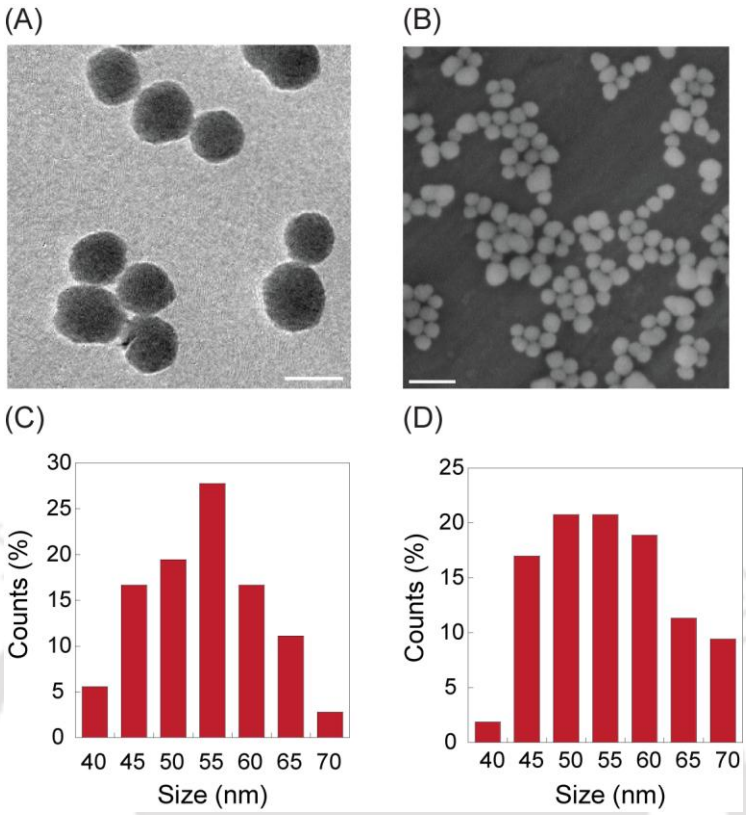

Figure 4.16 Characterization of silica nanoparticles (A) TEM image of silica nanoparticles (Scale bar 50 nm, Average diameter 55 ± 10 nm) (B) FESEM image of silica nanoparticles (Scale bar 100 nm, Average diameter 60± 10 nm) (C) Particle size distribution of silica nanoparticles calculated from TEM images using ImageJ software (D) Particle size distribution of silica nanoparticles calculated from FESEM images using ImageJ software.

at silica nanoparticles concentration of 0.8 mg/ml **(Figure 4.17B)**. Bead-based ELISA was performed using anti-PTEN primary antibody, HRP-conjugated secondary antibody and o-phenylenediamine dihydrochloride (OPD) as substrate. The product measured at 450 nm showed substantial difference between GST-PTEN-SNP and SNP control, indicating successful interaction between the recombinant PTEN and the silica nanoparticles **(Figure 4.17C)**. Protein-nanoparticles interactions are controlled by a number of factors including charge of the moieties, pH, and surface functionalization among others which can be tuned based on the prospective application (Saptarshi *et al.*, 2013). Based on electrostatic affinity, one would assume negatively charged protein to interact with positively charged nanoparticles. However, electrostatic interactions alone does not represent the major driving force regulating the silica–protein interactions (Clemments *et al.*, 2015). The interaction of

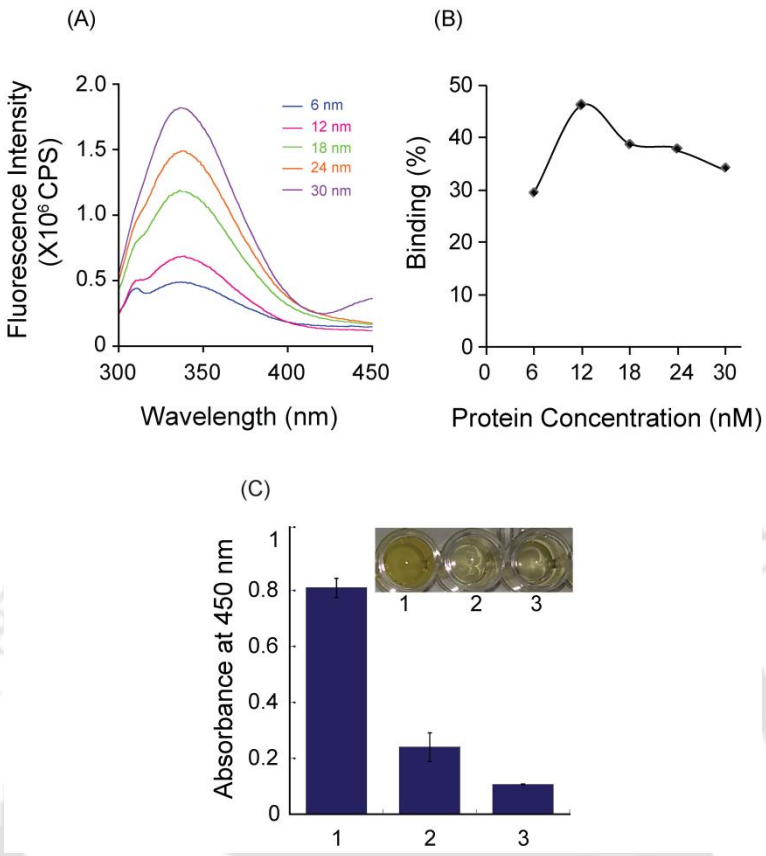

Figure 4.17 Immobilization of GST tagged PTEN onto silica nanoparticles (A) Binding of GST-PTEN onto silica nanoparticles as determined by probing the intrinsic fluorescence of protein (B) Percentage binding of GST-PTEN onto silica nanoparticles at varying concentration of proteins, maximum binding obtained was 49 % at a protein concentration of 12 nM (C) ELISA for analysis of binding of GST-PTEN to silica nanoparticles, where 1 is GST-PTEN immobilized on silica nanoparticles, 2 is only silica nanoparticles and 3 is only buffer control.

GST-PTEN and silica nanoparticles may be predominantly based on large number of surface exposed hydroxyl (OH) groups (Marucco *et al.*, 2014), which provided reactive sites to interact with the protein by several non-covalent interactions, such as Vander Waal's force, hydrogen bonding leading to adsorption of protein onto its surface with minimal structural disruption.

Once interaction was confirmed it was important to verify that the nanoparticles shape and structure is intact. TEM images of GST-PTEN immobilized silica nanoparticles revealed no significant change in the average size and morphology of the nanoparticles after binding of the protein **(Figure 4.18A).**

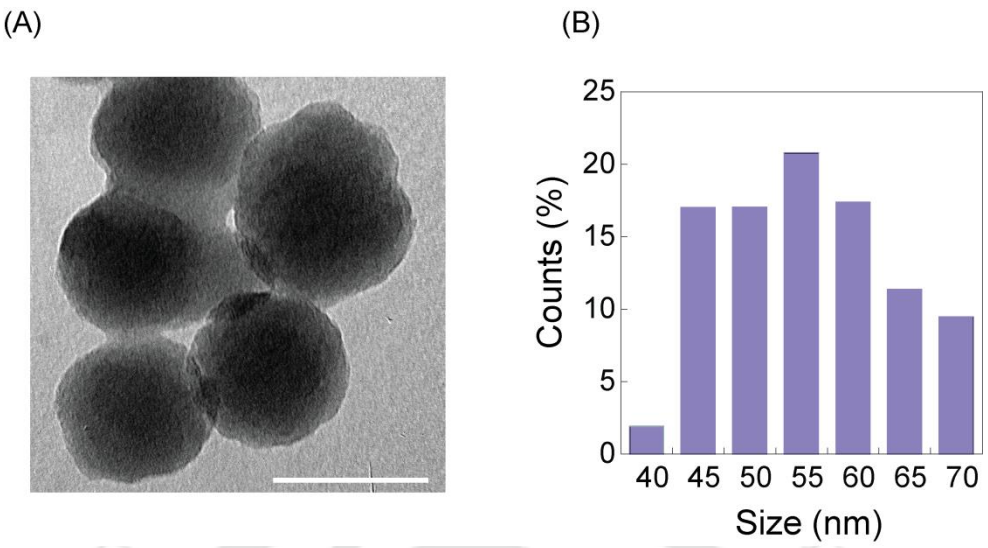

Figure 4.18 Characterization of GST-PTEN-SNPs (A) TEM image of GST-PTEN bound silica NPs (Scale bar 50 nm, Average diameter 58± 10 nm) (B) Particle size distribution of GST-PTEN-SNPs calculated using ImageJ software.

Average diameter calculated from several images consisting of 100 particles using Image J software **(Figure 4.18B)** was in the range of 58 ±10 nm. The binding was further analyzed by zeta potential measurements, dynamic light scattering (DLS) and FTIR study. Zeta potential measurements show a slight shift in the zeta potential of the nanoparticles upon incubation with GST-PTEN as compared to free nanoparticles indicating protein-nanoparticle interactions **(Figure 4.19A and 4.19B).** Hydrodynamic diameter of GST-PTEN immobilized silica nanoparticles was found to be 133.4 nm. The increase in the diameter as compared to free silica nanoparticles (116.5 nm) was indicative of binding of protein with the nanoparticles **(Figure 4.19C and 4.19D)**. The FTIR spectrum of silica nanoparticles demonstrated peaks at 3441 cm^{-1} , 1096 cm^{-1} and 803 cm^{-1} corresponding to Si-OH stretching, Si-O-Si asymmetric stretching and Si-O-Si bending, respectively (Moncada *et al.*, 2007). The FTIR spectrum of recombinant PTEN displayed signature peaks at 1642 cm^{-1} (Amide I), 1538 cm^{-1} (Amide II), 1318 cm-1 (Amide III), 668 cm^{-1} (Amide IV) arising from C=O stretching CN stretching, NH bending, OCN bending, respectively (Barth 2007, Kong and Yu 2007). Observation of peaks corresponding to characteristic bands of peptide linkage in the FTIR spectra of recombinant protein incubated with silica nanoparticles (Shang *et al.*, 2007) indicated the binding of the recombinant PTEN protein to the nanoparticles **(Figure 4.20)**.

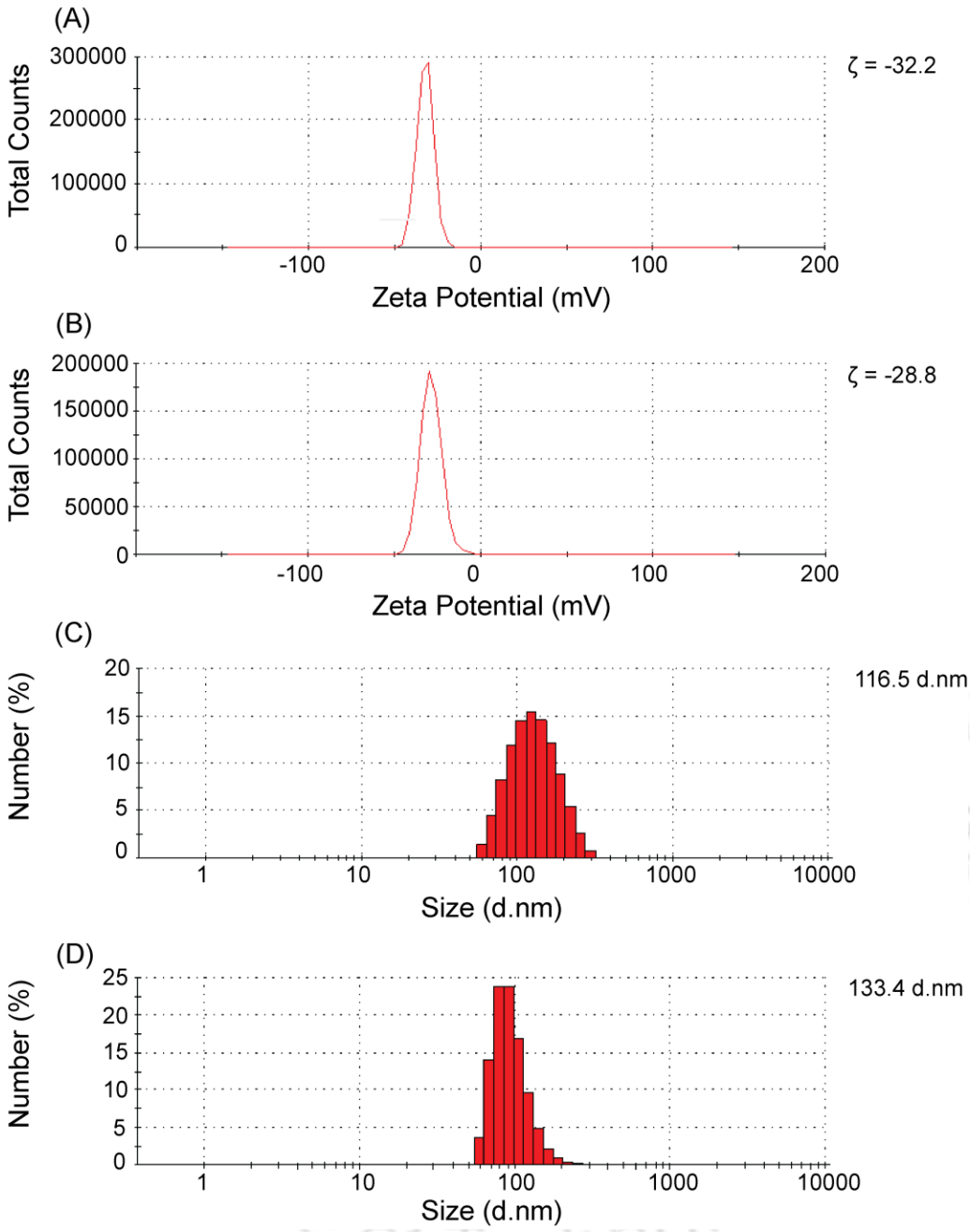

Figure 4.19 Immobilization of GST-PTEN onto silica nanoparticles (A) Zeta potential of silica nanoparticles (B) Zeta potential recombinant GST-PTEN bound silica nanoparticles (C) Dynamic light scattering data of silica nanoparticles (Average diameter of 116.5 nm) (D) Dynamic light scattering data of GST-PTEN bound silica nanoparticles (Average diameter of 133.4 nm).

,

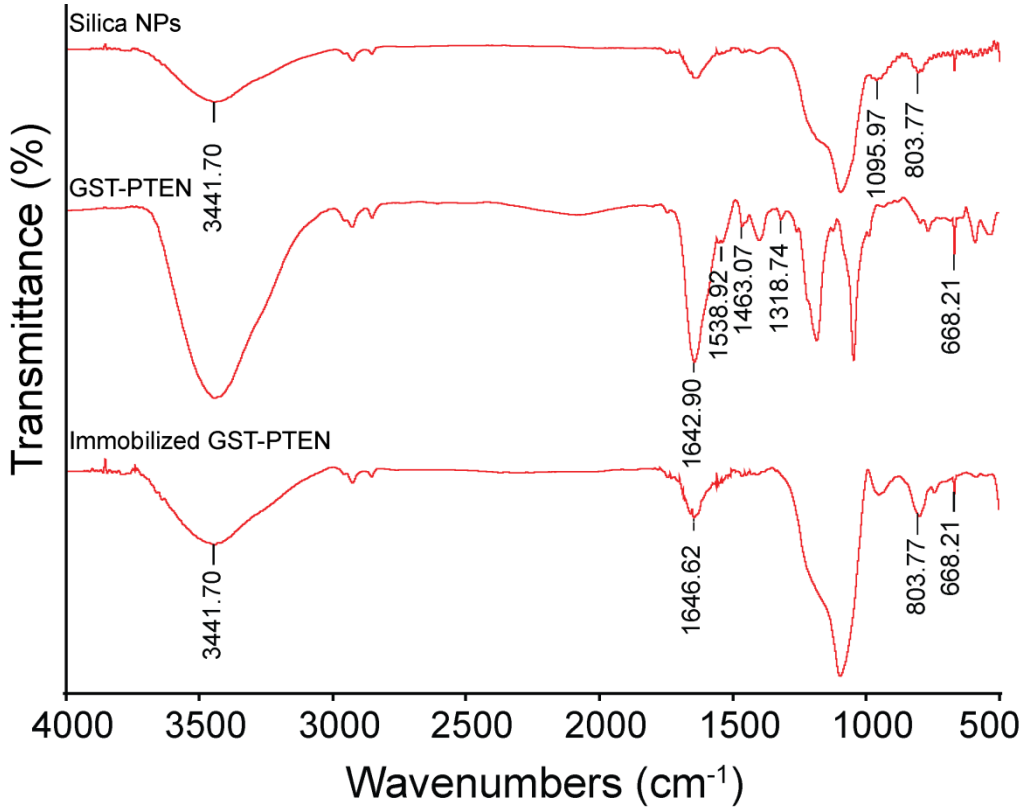

Figure 4.20 FTIR spectra of silica nanoparticles, GST-PTEN and GST-PTEN SNP indicating protein loading.

4.7 Evaluation of Structural and Functional parameters of Recombinant PTEN immobilized onto Silica Nanoparticles

Following binding of the GST-PTEN onto silica nanoparticles, the release of the protein from the nanoparticles surface was evaluated. To investigate release, protein bound silica nanoparticles were re-dispersed in 10 mM Tris pH 7.4 and incubated at 37 °C. The release profile demonstrates an increase in release with increasing time with 55 % release of recombinant PTEN within 72 h **(Figure 4.21A)**. The release pattern ensures rapid release of the protein within stipulated time of 72 h at physiological pH.

However, surface interactions can be further tuned to obtain sustained release for prolonged period (Huang and Brazel 2001). Modifications such as polymeric microencapsulation of the protein may also significantly improve the sustained release of the protein as in case of sustained release of erythropoietin, a recombinant protein used for anemia treatment, from PLGA microspheres for prolonged period suitable for pharmaceutical applications (Geng *et*

al., 2008). Structural framework of protein holds the essence for its function. Adsorption of proteins on solid surfaces may induce structural changes depending upon nature and size of nanomaterials (Billsten *et al.,* 1995, Satzer *et al.,* 2015). The structural changes influenced by interaction of protein with the nanoparticles dictate the functional behaviour of the protein. Hence, preservation of macromolecule structure is essential to achieve intended biological applications. Stability of the protein can be further enhanced by conjugation of protein to solvents such as glycerol or Polyethylene glycol (PEG) (Yuan *et al.,* 2009). Stabilization of protein is crucial during protein delivery to avoid aggregation upon release in aqueous medium to maintain its biological applications. To track the structural changes induced by immobilization of GST-PTEN onto silica nanoparticles, secondary structures of free GST-PTEN and GST-PTEN released from silica nanoparticles in 10 mM Tris pH 7.4 were analyzed by circular dichroism **(Figure 4.21B)**. Structural elements were determined using Yang's reference **(Figure 4.21C)**, which essentially revealed no pronounce difference between the secondary structural elements of released GST-PTEN (22.4 % α-helix, 15.2 % β-sheet) compared to free GST-PTEN (24.5 % α-helix, 25.6 % β-sheet) indicating nominal structural reorganization upon interaction with silica nanoparticles (Billsten, Wahlgren et al. 1995). Decrease in helical content may be attributed to the adsorption of protein onto the nanoparticles as reported previously (Billsten, Wahlgren et al. 1995). Structural changes in protein influenced by interaction with silica nanoparticles have been previously documented for BSA and myoglobin (Satzer, Svec et al. 2015). Both the proteins displayed nanoparticle size dependent conformational change with no significant structural alteration for smaller sized nanoparticles. However, there is no such study for interaction of the PTEN with silica nanoparticles.

Additional experiment was performed to assess the conformational change of the protein immediately upon interaction with the nanoparticles. Monitoring shift at 222 nm of protein bound to silica nanoparticles by circular dichroism study revealed that the initial conformational change was slow indicating that the interaction between the recombinant protein and silica nanoparticles did not rapidly perturb the folding and stability of the protein **(Figure 4.22)**. The analysis of secondary structural elements of free GST-PTEN and released GST-PTEN revealed that the interaction between the protein and the nanoparticles did not

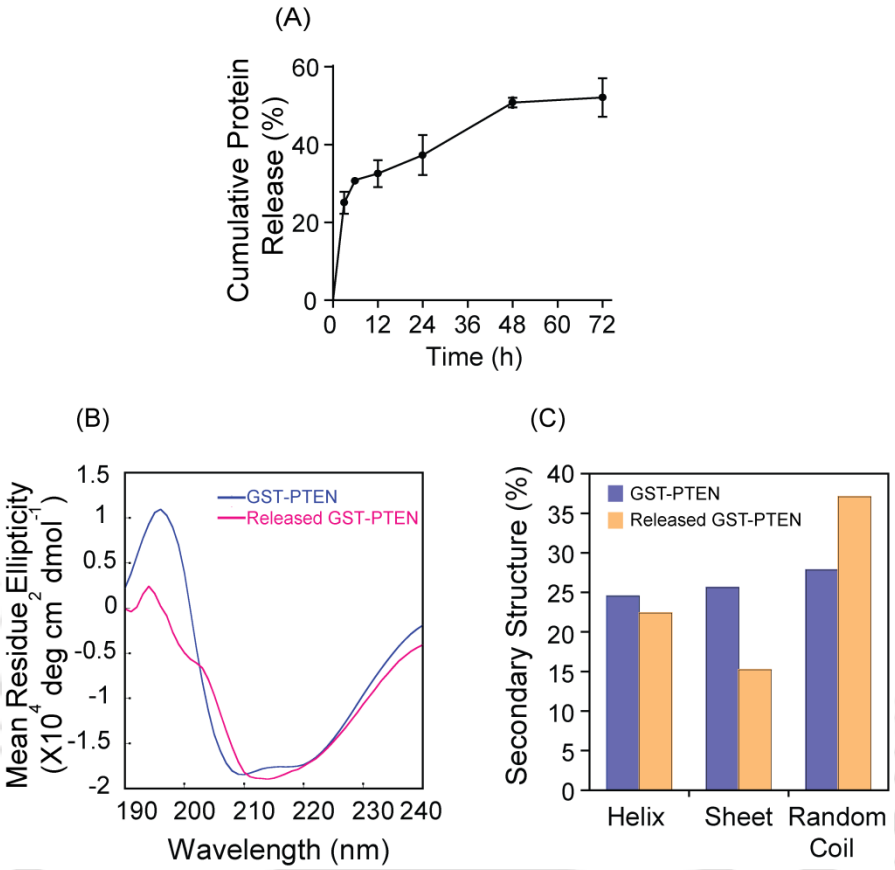

Figure 4.21 Characterization of protein release (A) Release profile of GST-PTEN over a period of 72 h in 10 mM Tris pH 7.4 at 37 °C (B) Circular dichroism spectra of purified GST-PTEN and released GST-PTEN (C) Comparative study of content of secondary structural elements of purified GST-PTEN and GST-PTEN released from silica nanoparticles.

cause profound change in the structural properties of GST-PTEN released from nanoparticles surface. Structural reorganization is inevitable during protein-nanoparticles interactions. Nonetheless in case of interaction between GST-PTEN and silica nanoparticles the minimal framework reorganization, ubiquitous for all protein-nanoparticles interactions, provided a strong motivation for further kinetic evaluation of the bound protein.

To study the effect on enzymatic activity of GST tagged PTEN post immobilization, the bound protein was assayed against lipid and protein substrate, PIP_3 diC8 and PNPP, respectively. Phosphatase activity of GST-PTEN towards PNPP and PIP_3 diC8 was

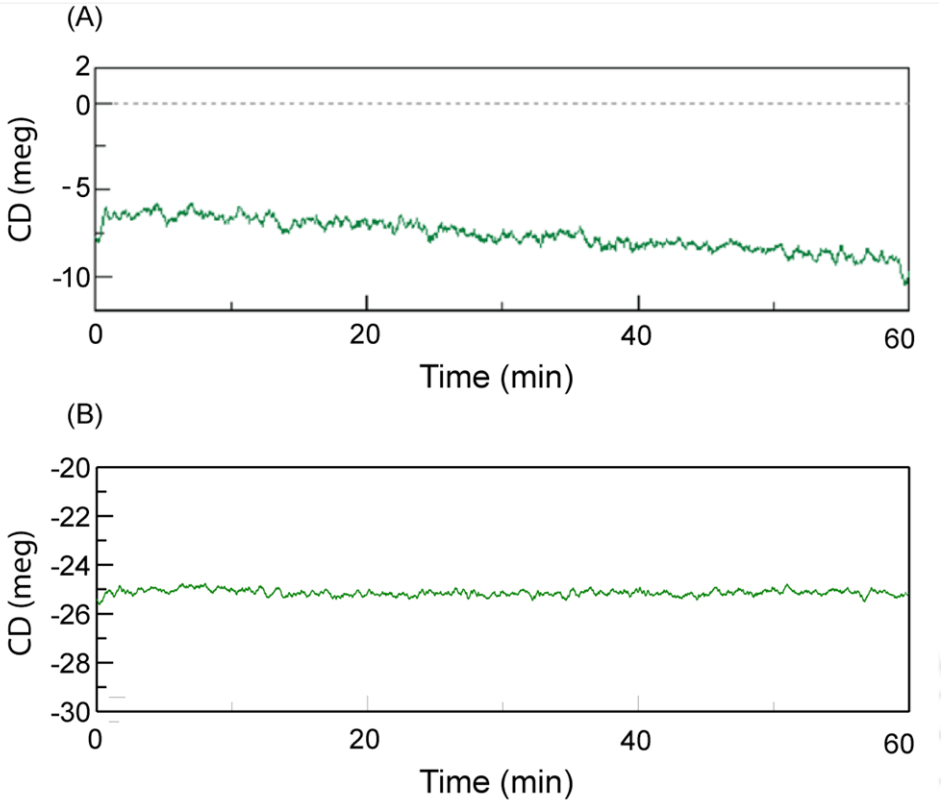

Figure 4.22 Protein-nanoparticles interaction studies (A) Monitoring shift at 222 nm by circular dichroism of GST-PTEN immobilized onto silica nanoparticles (B) Monitoring shift at 222 nm by circular dichroism of GST-PTEN.

determined. Assay results for both the substrates PNPP and PIP_3 diC8 indicated that activity (nanomole of phosphate released) over increasing concentration of substrate fits Michaelis-Menten kinetics **(Figure 4.23)**. PTEN catalysis has been extensively evaluated using lipid substrates such as, Inositol phosphate I(1,3,4,5)P4 and diC6 PIP_3. The kinetic parameters K_m and k_{cat}/K_m reported for Inositol phosphate I(1,3,4,5)P4 and diC6 PIP_3 were 98.6 µM and 67 µM and 0.005 and 0.038 min^{-1} μM^{-1}, respectively (Maehama and Dixon 1998, Bolduc *et al.*, 2013). The experimentally obtained kinetic parameters of GST-PEN are comparable to previous reports with K_m of 16.40 µM and k_{cat}/K_m of 0.0108 min^{-1} μM^{-1}. Thus, comparative study of the kinetic values towards the lipid substrate confirms that GST-PTEN is catalytically active and can be subjected to immobilization onto silica nanoparticles. Immobilization of PTEN onto silica nanoparticles was also conducted, which revealed a maximum binding percentage of 30 % as compared to maximum binding percentage of 49 % for GST-PTEN immobilization suggesting that GST may facilitate in protein-nanoparticle

interaction. Also, GST tag does not contribute to any phosphatase activity as determined by PNPP assay of GST **(Figure 4.24)**. Therefore, it was decided to proceed with GST tagged PTEN for immobilization onto silica nanoparticles. Surface morphology, size and type of nanoparticles greatly influence the activity of the adsorbed protein. In many cases, interaction between nanoparticles and protein causes dramatic loss of enzymatic activity (Vertegel *et al.*, 2004, Gagner *et al.*, 2011). Nevertheless, maintenance of released GST-PTEN structure could possibly entail maintenance of native function as well. Therefore, we embarked on the study of phosphatase activity of immobilized protein towards the same substrates PNPP and PIP_3 diC8. It was interesting to observe that the phosphatase activity of immobilized GST-PTEN followed Michaelis-Menten kinetics with kinetic values as illustrated in **Table 4.2**.

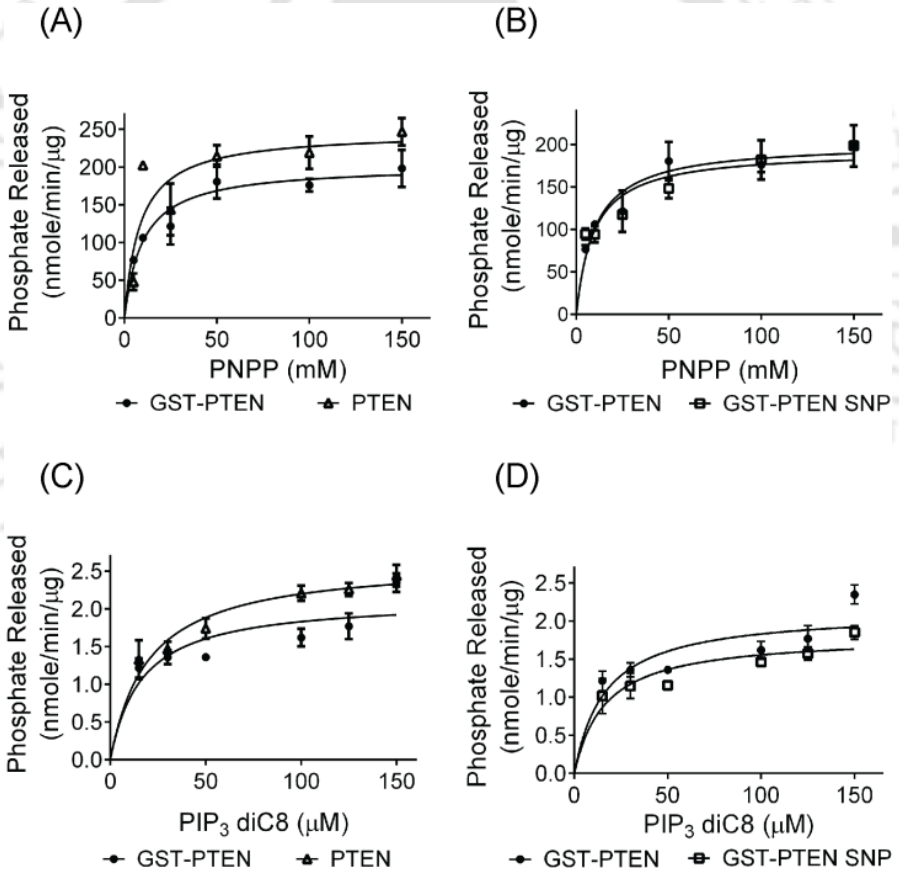

Figure 4.23 Kinetic profile towards PNPP of (A) GST tagged and untagged PTEN (B) Free and silica immobilized GST tagged PTEN, Kinetic profile towards diC8 PIP_3 of (C) GST tagged and untagged PTEN (D) Free and silica immobilized GST tagged PTEN.

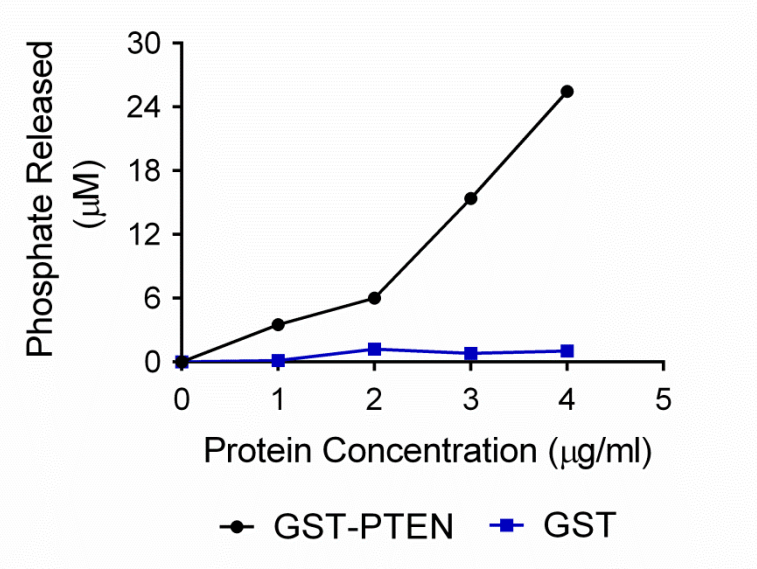

Figure 4.24 PNPP phosphatase activity of GST-PTEN and GST.

Substrate	Sample	K_m (μM)	k_{cat}/ K_m (min^{-1} μM^{-1})
PNPP	GST-PTEN	6881	0.16×10^{-3}
	PTEN	3767	0.22×10^{-3}
	GST-PTEN-SNP	6102	0.15×10^{-3}
PIP_3 diC8	GST-PTEN	16.40	0.0108
	PTEN	19.90	0.0110
	GST-PTEN-SNP	16.31	0.0092

Table 4.2 Kinetic parameters of GST-PTEN, PTEN and GST-PTEN immobilized onto silica nanoparticles.

The kinetic parameters of immobilized GST-PTEN were comparable to its free counterpart implying retention of functional integrity upon immobilization. The results are also consistent with evidences available that smaller sized nanoparticles are known to uphold the native properties of the protein. Our studies bestow a positive lead towards utilization of small sized silica nanoparticles as a suitable vehicle for stabilization and delivery of recombinant PTEN for potential remedial functions. Further, to assess the stability of the GST-PTEN protein bound onto silica nanoparticles, the nanoparticles bound and free protein was subjected to protease digestion using Proteinase K. Following Proteinase K digestion of free and silica bound GST-PTEN; the samples were analyzed by phosphatase assay to understand the effect of the protease digestion on the enzymatic activity of the protein. The overall strategy of the experiment is explained in the materials and method section. Protease treated and untreated GST-PTEN and treated silica bound GST-PTEN was subjected to PNPP catalysis using 50 mM of the substrate at 37 °C for 60 min. The assay results indicated that the catalysis of treated silica bound GST-PTEN was higher as compared to treated free GST- PTEN **(Figure 4.25)**. For silica nanoparticles bound GST-PTEN, the protein cleavage sites may not be as easily accessible to proteinase K for digestion as compared to the free enzyme. Therefore, lower digestion of the nanoparticles bound enzyme (GST-PTEN) replicated in higher phosphatase activity as compared to free enzyme.

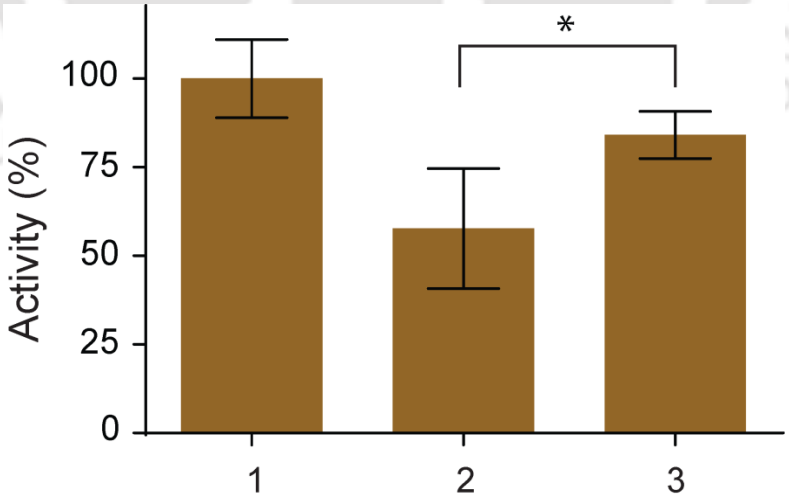

Figure 4.25 Phosphatase assay of Proteinase K treated and untreated samples, 1 is untreated GST-PTEN, 2 is Proteinase K treated GST-PTEN and 3 is Proteinase K treated silica bound GST-PTEN.

4.8 Evaluation of Therapeutic Potential of PTEN loaded Silica Nanoparticles

Once the structural and functional integrity of the GST-PTEN immobilized onto silica nanoparticles was determined to be intact, the cellular investigation of the conjugate was initiated. PTEN alterations in gliomas and particularly glioblastoma result in translation of truncated and non-functional protein products. PTEN expression was checked in glioblastoma cell line U-87 MG and no expression of PTEN was detected **(Figure 4.26A)**. PTEN over-expression by gene therapy approaches has shown promising results in inhibiting tumour growth both *in vitro* and *in vivo* (Tanaka and Grossman 2003, Wu *et al.*, 2008). However, the stabilization and direct delivery of exogenous PTEN protein using suitable delivery vehicle is an area of research still unexplored. To attain this, GST-PTEN was immobilized onto silica nanoparticles and the protein-nanoparticle interactions were thoroughly investigated. Silica stabilized GST-PTEN displayed sound structure, function and stability. Therefore the subsequent judicious step was to study the effect of this nanoconjugate on cancer cell line.

U-87 MG cells were treated with varying concentration of GST-PTEN alone for 48 h, which displayed no significant reduction in the viability of the treated cells as discussed above. PTEN null U-87 MG cells were then treated with varying concentrations of silica nanoparticles (varying from 0.9 mg/ml to 5.4 mg/ml) and silica bound GST-PTEN (Protein concentration varying from 0.375 μg/ml to 2.25 μg/ml) for 48 h. Silica bound GST-PTEN exhibited dose dependent reduction of cell viability as indicated by the assay **(Figure 4.26B)**. The slight reduction in viability of cells treated with silica nanoparticles could be due to their high concentration and small size.

Silica nanoparticles have been reported to induce size and concentration dependent toxicity with small sized nanoparticles ranging from 25 nm to 75 nm being more toxic as compared to larger nanoparticles. However, comparative analysis between the silica nanoparticles and the recombinant protein bound nanoparticles showed protein bound nanoparticles were more effective in reducing the viability of the cells. Statistical analysis was performed by ANOVA using GraphPad Prism software with statistical significance denoted by * ($p<0.05$).

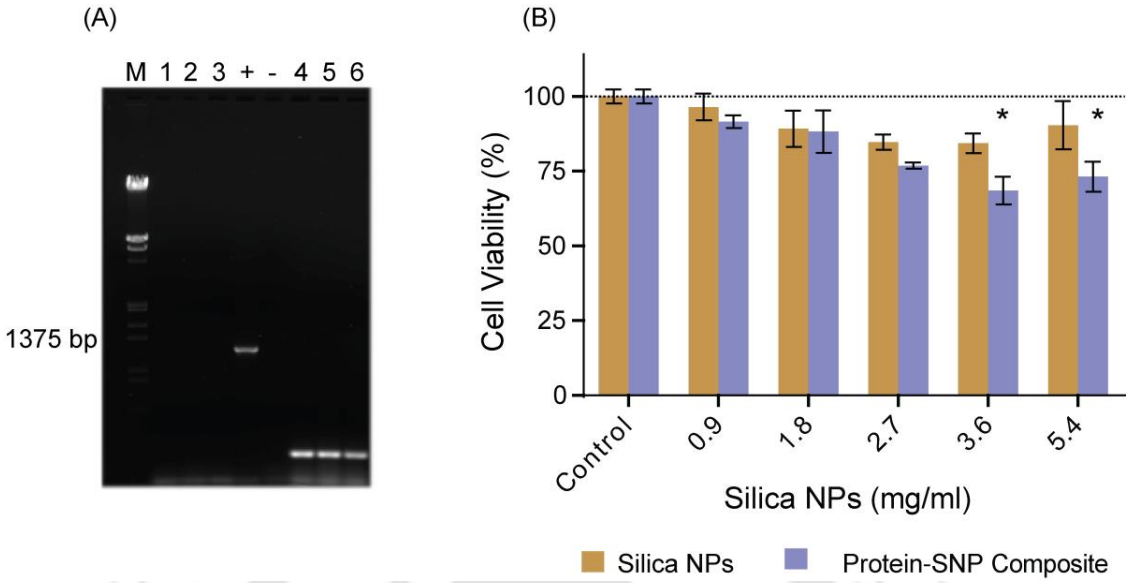

Figure 4.26 Assessment of cell viability (A) Expression study of PTEN in U-87 MG cells, where M is the DNA marker (Lambda DNA/ EcoRI + HindIII Marker), Lanes 1, 2 and 3 represent amplification of cDNA using PTEN gene specific primers at 50 °C, 55 °C and 60 °C annealing temperatures respectively, (+) Positive control showing 1.2 kbp PTEN band, (-) Negative Control, Lanes 4, 5 and 6 represent amplification of cDNA using β-actin primers as control at 50 °C, 55 °C and 60 °C annealing temperatures respectively (B) Evaluation of viability of U-87 MG cells upon treatment with free and protein bound silica nanoparticles for 48 h by MTT assay.

To understand the effect of GST-PTEN-SNP bioconjugate on the cell cycle progression of U-87 MG cells, the treated and untreated cells were incubated with propidium iodide (PI) DNA staining dye and analyzed using flow cytometry. The treated and untreated U-87 MG cells were fixed by 70% alcohol fixation. The fixed cells were then further processed and incubated with propidium iodide dye. PI, a fluorescent dye, is capable of binding and thereby labelling DNA stoichiometrically. Analysis of silica bound GST-PTEN treated U-87 MG cells displayed S phase arrest **(Figure 4.27)**, with a 1.47 fold increase compared to the untreated cells proposes silica bound GST-PTEN as a potential candidate for biomedical applications. Statistical analysis was performed by ANOVA using GraphPad Prism software with statistical significance denoted by * ($p<0.05$), ** ($p<0.01$).

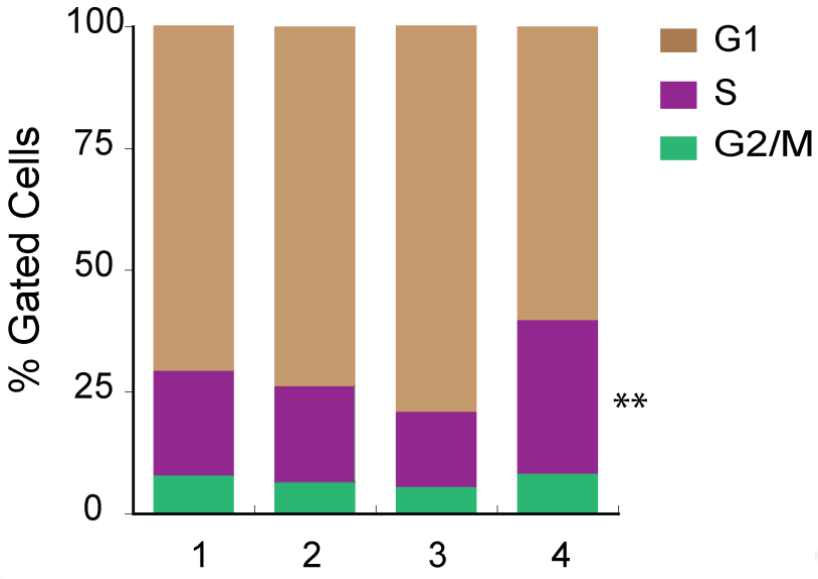

Figure 4.27 Cell cycle analysis of U-87 MG cells by flow cytometry upon treatment for 48 h where 1 is control cells, 2 is GST-PTEN protein treated cells, 3 is silica nanoparticles treated cells and 4 is GST-PTEN-SNP treated cells.

Existence of strong correlation between structure and function for all biological entities implies that both structure and function needs to be conserved to meet successful delivery formulation. Successful purification and characterization of the recombinant protein was followed by immobilization of GST-PTEN onto silica nanoparticles, which was validated by fluorescence spectroscopy, FTIR spectroscopy, ELISA and DLS. The nanosystem ensured efficient release of the protein from the surface of silica nanoparticles with intact structural integrity and preservation of dual phosphatase activity when compared to the free enzyme indicating that immobilization does not alter the enzymatic activity of GST-PTEN. Additionally, higher phosphatase activity of bound GST-PTEN in comparison to free GST-PTEN post incubation with a protease imply that the nanoparticles confer better stability to the protein upon adsorption onto the silica nanoparticles. Thus, the results attained addresses the major prerequisites and challenges in protein stabilization and serve as a model system to understand protein-nanoparticles interactions. Further to achieve encapsulation of the protein coupled with fluorescent tracking for theranostic implications of PTEN, silver nanoclusters were synthesized and characterized.

Theranostic Application of the Protein-Nanocarrier Composite

Advancement in fabrication of nanomaterials gave rise to a new class of nanomaterials known as metal nanoclusters that comes armed with attractive properties such as optical stability, efficient clearance from the body and low side effects, making them suitable for biomedical applications (Song *et al.,* 2016). Currently the focus application of the nanoclusters is as fluorescent probes or labels for bioimaging application (Li *et al.,* 2012, Das *et al.,* 2015, Yang *et al.,* 2015), additional promising avenue of nanoclusters applications involve combination of fluorescent imaging with delivery of drug or gene to combat disease conditions (Li *et al.,* 2013, Yahia-Ammar *et al.,* 2016). In this prospective, amalgamation of delivery and tracking of therapeutically relevant moieties on a single platform can be made possible by the application of metal nanoclusters, an innovative class of luminescent nanomaterials. To apprehend simultaneous delivery and tracking of GST-PTEN, the recombinant protein was stabilized onto lysozyme-template silver nanoclusters.

4.9 Synthesis and Characterization of PTEN-Nanocomposites

Lysozyme stabilized silver nanoclusters were synthesized by sodium borohydride mediated reduction of silver salt under alkaline condition, as developed by Zhou *et al.* with slight modifications. The synthesis of the silver nanoclusters was characterized by UV-Vis absorption, fluorescence spectra and TEM imaging. The absorbance profile **(Figure 4.28A)** of the nanoclusters display a peak around 480 nm with no characteristic surface plasmon resonance peak for larger Ag nanoparticles at around 425 nm (Zhou *et al.,* 2012). Upon excitation at 480 nm fluorescence spectra of the synthesized silver nanoclusters exhibited emission maxima at 650 nm **(Figure 4.28B)**. The inset shows orange-brown solution of silver nanoclusters under visible light, while a bright red emission was exhibited under UV excitation. Synthesis of silver nanoclusters was confirmed by TEM analysis which revealed the average diameter of 2±0.5 nm of the nanoclusters **(Figure 4.28C)**. The particle size distribution was determined by ImageJ software analysis **(Figure 4.28D)**. Zeta potential measurement of the synthesized clusters revealed positive charge of +7 mV at pH 7.4 and DLS measurement displayed hydrodynamic diameter of 7.5 nm **(Figure 4.29)**.

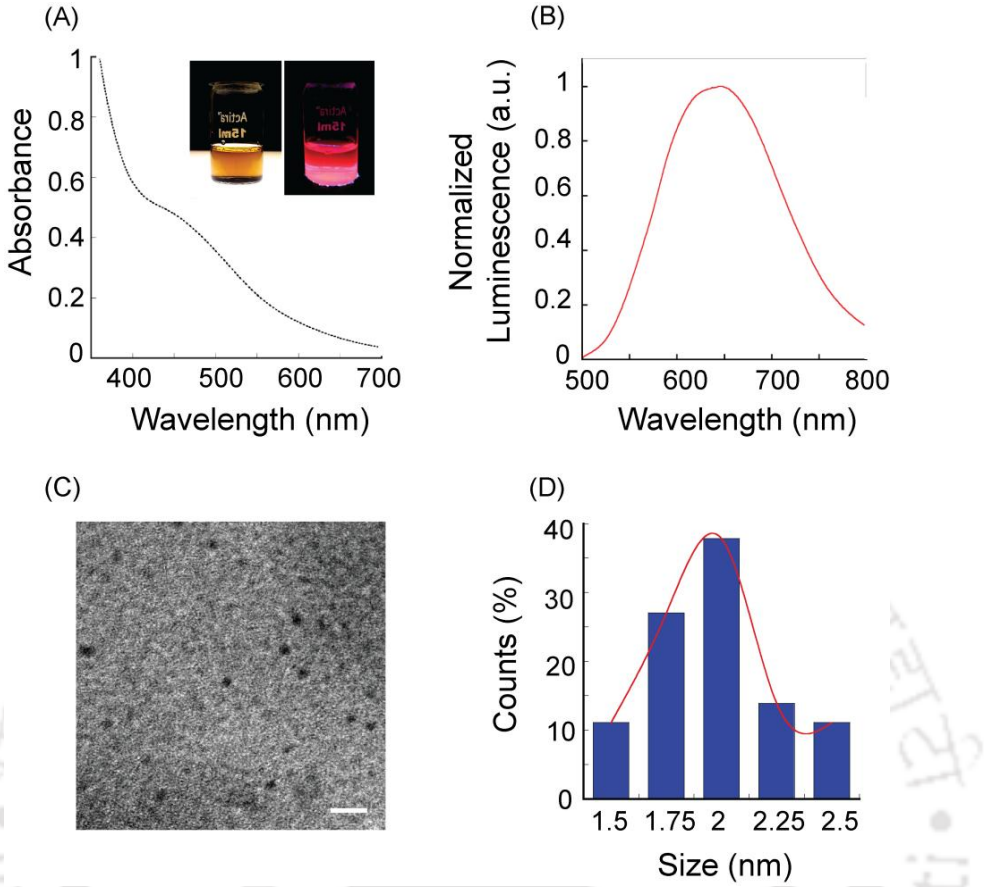

Figure 4.28 Characterization of lysozyme stabilized silver nanoclusters (A) Absorbance profile of synthesized silver nanoclusters (B) Fluorescence spectra of silver nanoclusters with emission maxima at 650 nm upon excitation at 480 nm (C) TEM image displaying synthesized nanoclusters with average diameter of 2 ± 0.5 nm (Scale Bar 10 nm) (D) Particle size distribution of silver nanoclusters calculated using ImageJ software.

Following synthesis of the nanoclusters, binding of GST-PTEN to the nanoclusters was performed. Interaction between protein and silver nanoclusters was determined by probing the luminescence of the silver nanoclusters using fluorescence spectroscopy. A decrease in the florescence of the nanoclusters was observed upon increase in protein binding, and the maximum binding was calculated to be 60 %, at 24 nM of protein concentration **(Figure 4.30A and 4.30B)**. The interaction between biological systems and nanomaterials is driven by the intrinsic properties of the nanomaterials, such as shape, size surface charge and hydrophobicity (Mu *et al.*, 2014, Zhao *et al.*, 2016). The surface charge of the nanomaterials is one of the critical factor in binding of the protein with the nanomaterials (Welsch *et al.*, 2013).

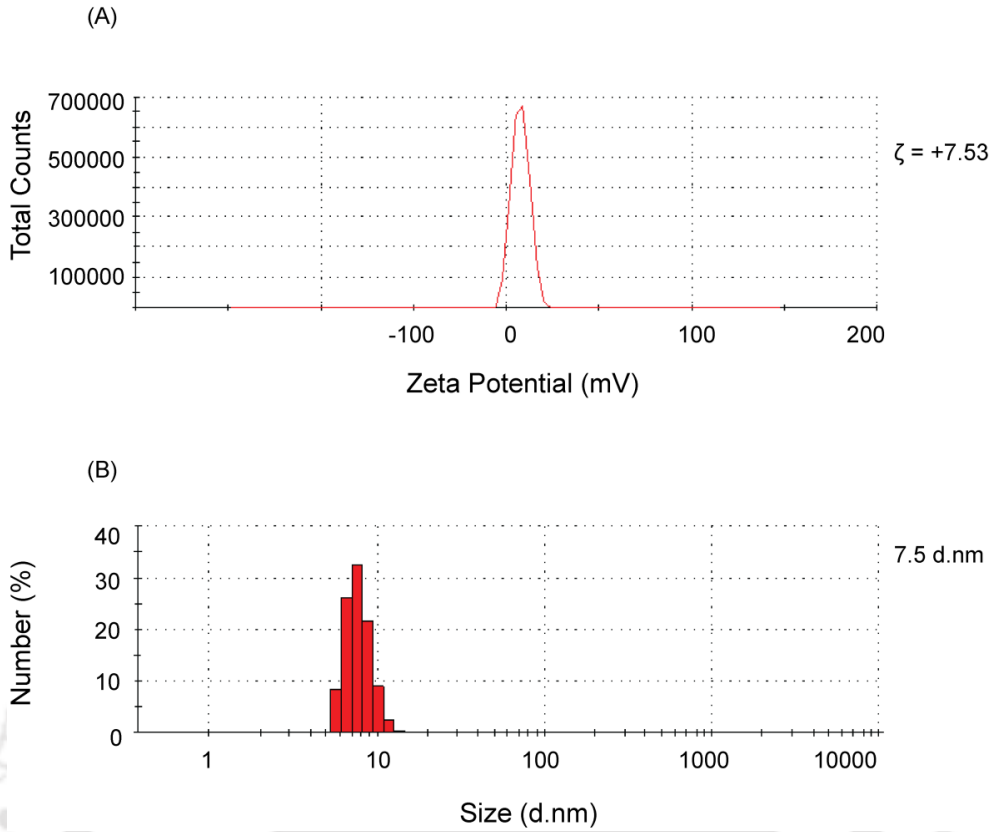

Figure 4.29 Characterization of silver nanoclusters (A) Zeta potential measurement of silver nanoclusters using Malvern Zeta sizer Nano ZS (ζ= -4.26 mV) (B) Hydrodynamic diameter of nanoclusters after dialysis against MilliQ for 12 h (Average diameter = 7.5 d.nm).

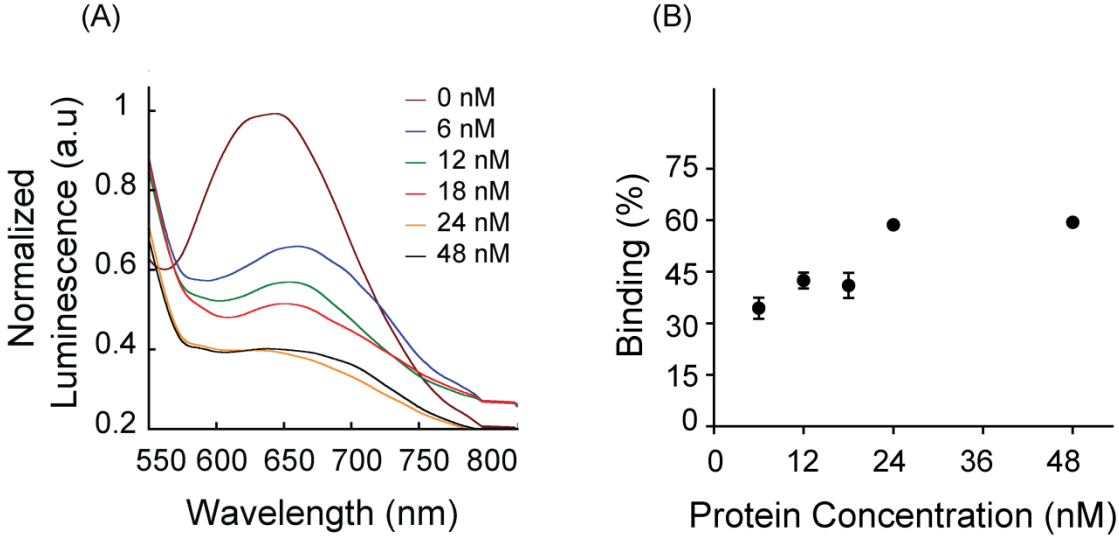

Figure 4.30 Characterization of GST-PTEN-Cluster binding (A) Binding of GST-PTEN to silver nanoclusters as determined by probing the luminescence of the nanoclusters (B) Determination of binding percentage of GST-PTEN and nanoclusters.

The pI (Isoelectric pH) of GST-PTEN, as determined by bioinformatic tool Expasy/pI, was 4.9 (Gasteiger *et al.,* 2003). Therefore, at pH of 7.4 the GST-PTEN protein is negatively charged. The synthesized silver nanoclusters are positively charged (+7.5 mV) at pH 7.4 as experimentally determined by zeta potential measurements. Therefore, the possible driving force between negatively charged GST-PTEN protein and positively charged silver nanoclusters binding is charged based electrostatic interactions.

A key feature of this study is the use of polyethylene glycol (PEG) coating that allows fabrication of the assembly into spherical nanocomposites. Along with fabrication of spherical morphology, PEG coating has been well investigated to provide additional advantages for biomedical applications. The non-fouling or 'sleath' behaviour of PEG reduces non-specific protein interactions reducing aggregation (Jokerst *et al.,* 2011). Therefore, after binding of PTEN to the silver nanoclusters, the protein bound silver nanoclusters were encapsulated within polyethylene glycol 4000 (PEG) coating by double emulsification technique. Only cluster and protein loaded clusters were coated with PEG and the synthesis of nanocomposites were determined by TEM study **(Figure 4.31A and Figure 4.31B)**. The TEM images revealed the fabrication of spherical nanocomposites of size 125±10 nm after polymeric coating of GST-PTEN bound silver nanoclusters (named as PTEN-nanocomposites). Similarly, synthesized silver nanoclusters were also coated with PEG to fabricate spherical nanoparticles of size 18±3 nm. These spherical nanoparticles are referred to as nanocomposites. Besides PTEN-nanocomposite, other nanocomposites (without PTEN) were synthesized as required for appropriate controls in the subsequent experiments. The particle size distribution of the nanocomposites and PTEN-nanocomposites determined by employing ImageJ software is illustrated in **Figure 4.31C and 4.31D**. The concentration of the nanocomposites is expressed as nM of protein (PTEN) and μg/ml of silver in the cluster. The loading percentage of the PTEN-nanocomposites was determined by protocol developed by Sah *et al*. The analysis of protein content revealed the encapsulation percentage to be 78±3 %. PTEN-nanocomposites were also characterized by zeta potential measurements (**Figure. 4.31E**). The overall negative surface potential of -4.26 mV is in consistence with the surface charge distribution of reported PEGylated nanoparticles (Pelaz *et al.,* 2015).

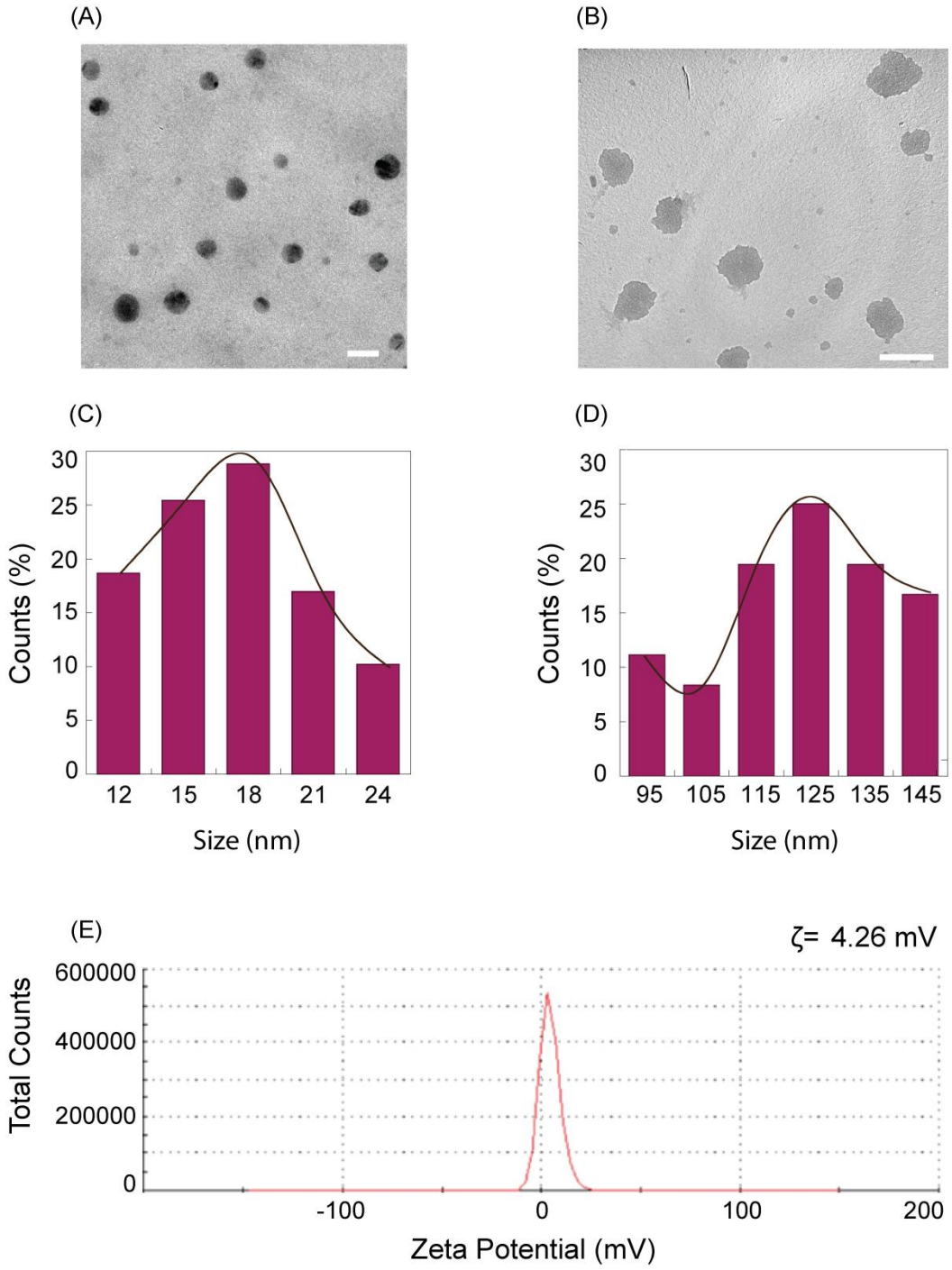

Figure 4.31 Characterization of PEG coated silver nanoclusters (referred as nanocomposites) (A) TEM image of nanocomposites (Scale bar 10 nm) (B) TEM image of distribution of PEG coated protein loaded silver nanoclusters (referred as PTEN-nanocomposites) (Scale bar 200 nm) (C) Particle size distribution of nanocomposite using ImajeJ (Average diameter 18±3 nm) (D) Particle size distribution of PTEN-nanocomposites using ImajeJ (Average diameter 125±10 nm) (E) Zeta potential measurement of PTEN-nanocomposites using Malvern Zeta sizer Nano ZS (ζ= -4.26 mV).

4.10 Evaluation of Kinetic parameters of PTEN in nanocomposite

Successful formulation of the macromolecules with intact functional integrity for intracellular delivery is a challenging task. In the perspective of protein therapy, determination of the function of the protein following interaction with the delivery vehicle is imperative. Therefore, to determine the effect of nanocluster interaction with GST-PTEN, a step by step analysis of phosphatase activity was performed. Initially, phosphatase activity of PTEN bound to silver nanoclusters was determined towards PNPP substrate. It was interesting to observe retention of enzymatic activity of PTEN after binding to silver nanoclusters (Referred to as GST-PTEN-AgNCs) **(Figure 4.32A)**. Once the activity was confirmed we embarked on the study of phosphatase activity of PTEN present in PTEN-nanocomposites. Both free and PEG encapsulated PTEN exhibited Michealis-Menten kinetics towards PNPP as illustrated in **Figure 4.32B**. Kinetic parameters Km and k_{cat}/K_m, evaluated using Graphpad Prism software, of free and PTEN-nanocomposites has been illustrated in **Table 4.3**. The kinetic parameters revealed that the kinetic efficiencies of free PTEN and PTEN-nanocomposites were comparable. Therefore, the retention of functionality of the PTEN protein upon interaction with silver nanoclusters followed by PEG encapsulation

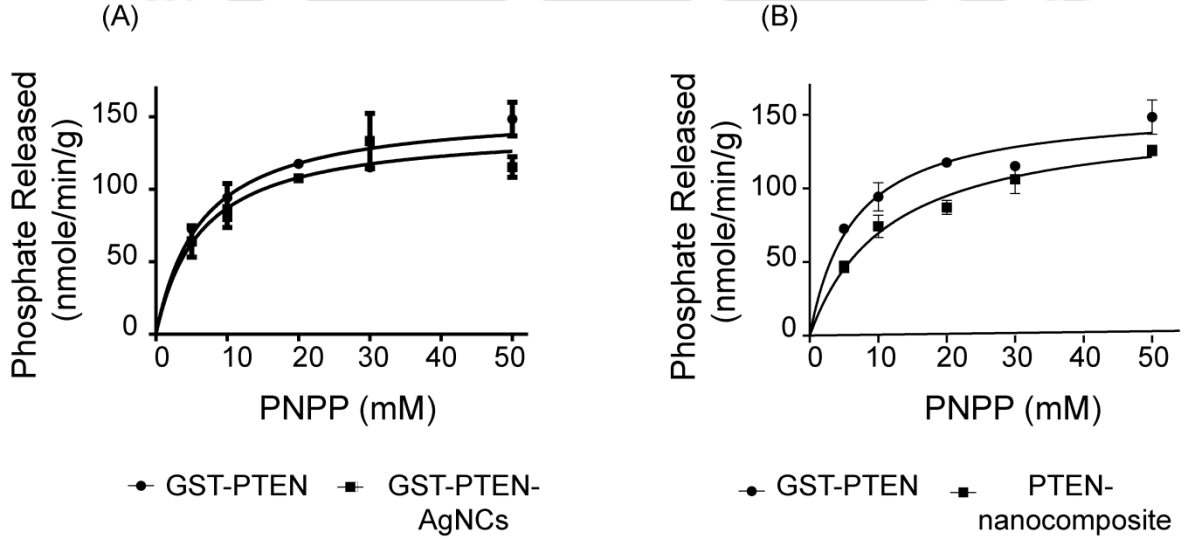

Figure 4.32 Kinetic profile towards PNPP (A) Free GST-PTEN and GST-PTEN bound to silver nanoclusters (GST-PTEN AgNCs) (B) Kinetic profile of free GST-PTEN and GST-PTEN present in PTEN-nanocomposites.

Sample	K_m (μM)	K_{cat}/ K_m (min^{-1} $μM^{-1}$)
GST-PTEN	6329	0.24×10^{-3}
GST-PTEN-AgNCs	6354	0.22×10^{-3}
PTEN-nanocomposite	10060	0.15×10^{-3}

Table 4.3 Kinetic parameters for catalysis by GST-PTEN, GST-PTEN-AgNCs and PTEN-Nanocomposites towards PNPP.

paved the way for further analysis of the PTEN-nanocomposites as a suitable therapeutic module.

4.11 Cellular Internalization Study of PTEN-Nanocomposites

Prior to cell based studies, the cellular uptake of the composite was confirmed. Cellular uptake studies were carried out using confocal microscopy, flow cytometry and fluorescence spectroscopy capitalizing on the luminescent property of the silver nanoclusters. Cellular uptake study analyzed at different time intervals of 2 h, 4 h and 8 h by flow cytometry and fluorescence spectroscopy suggested time-dependent uptake of the PTEN-nanocomposites in both U-87 MG and MCF7 cells **(Figure 4.33)**. Additionally, to confirm the internalization of the nanocomposites and PTEN-nanocomposites inside the cells confocal microscopy accompanied with z-stacking was performed in MCF7 and U-87 MG cells.

Confocal microscope images of MCF7 and U-87 MG cells upon incubation with PTEN-nanocomposites for 4 h displayed red fluorescence of the nanocomposites. The uptake of the cargo was further confirmed by performing z-stacking with layer interval of 0.4 μm. The green colour on the depth coding scale depicted that the PTEN-nanocomposites were internalized into the cells. There was no fluorescence observed in the control cells under same analysis parameters **(Figure 4.34)**.

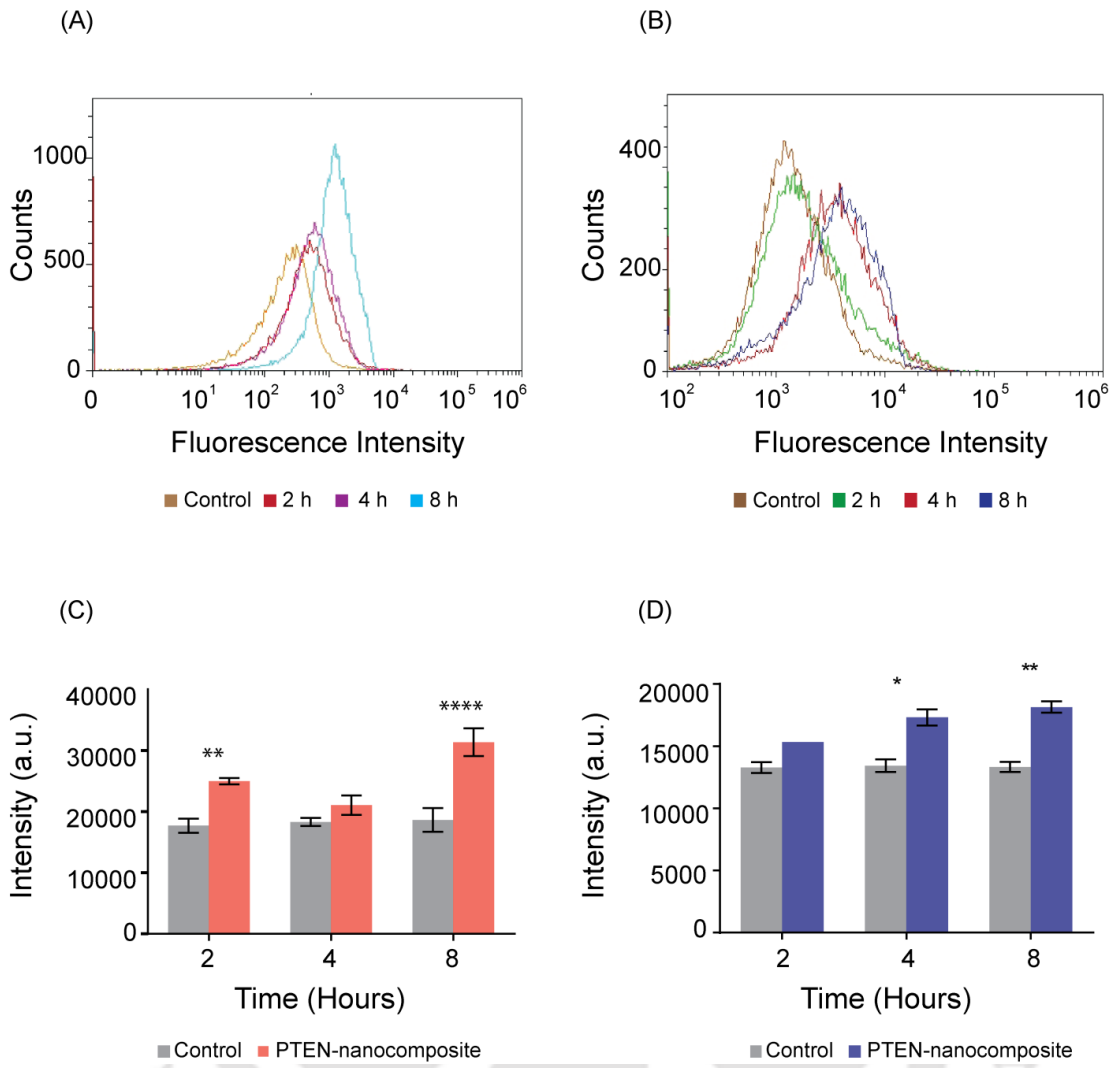

Figure 4.33 Time dependent cellular uptake study of PTEN-nanocomposite by flow cytometry in (A) U-87 MG cells (B) MCF7 cells. Time dependent cellular uptake study of PTEN-nanocomposite by fluorescence spectroscopy in (C) U-87 MG cells (D) MCF7 cells.

U-87 MG and MCF7 were incubated with only nanocomposites as well. Confocal study performed after 4 h incubation shows similar red fluorescence in the cytoplasm of the cells with z-stack image confirming the cellular internalization of the nanocomposites **(Figure 4.35)**. Further to investigate the uptake mechanism of the nanocomposites inside the cells, inhibitors for endocytosis were employed. Endocytosis is the established route for nanoparticles uptake in different cell types (Yameen *et al.*, 2014). Nonetheless, to confirm the same for PTEN-nanocomposites uptake by U-87 MG and MCF7, the cells were treated with broad spectrum inhibitors of endocytosis, that is, sodium azide and low temperature.

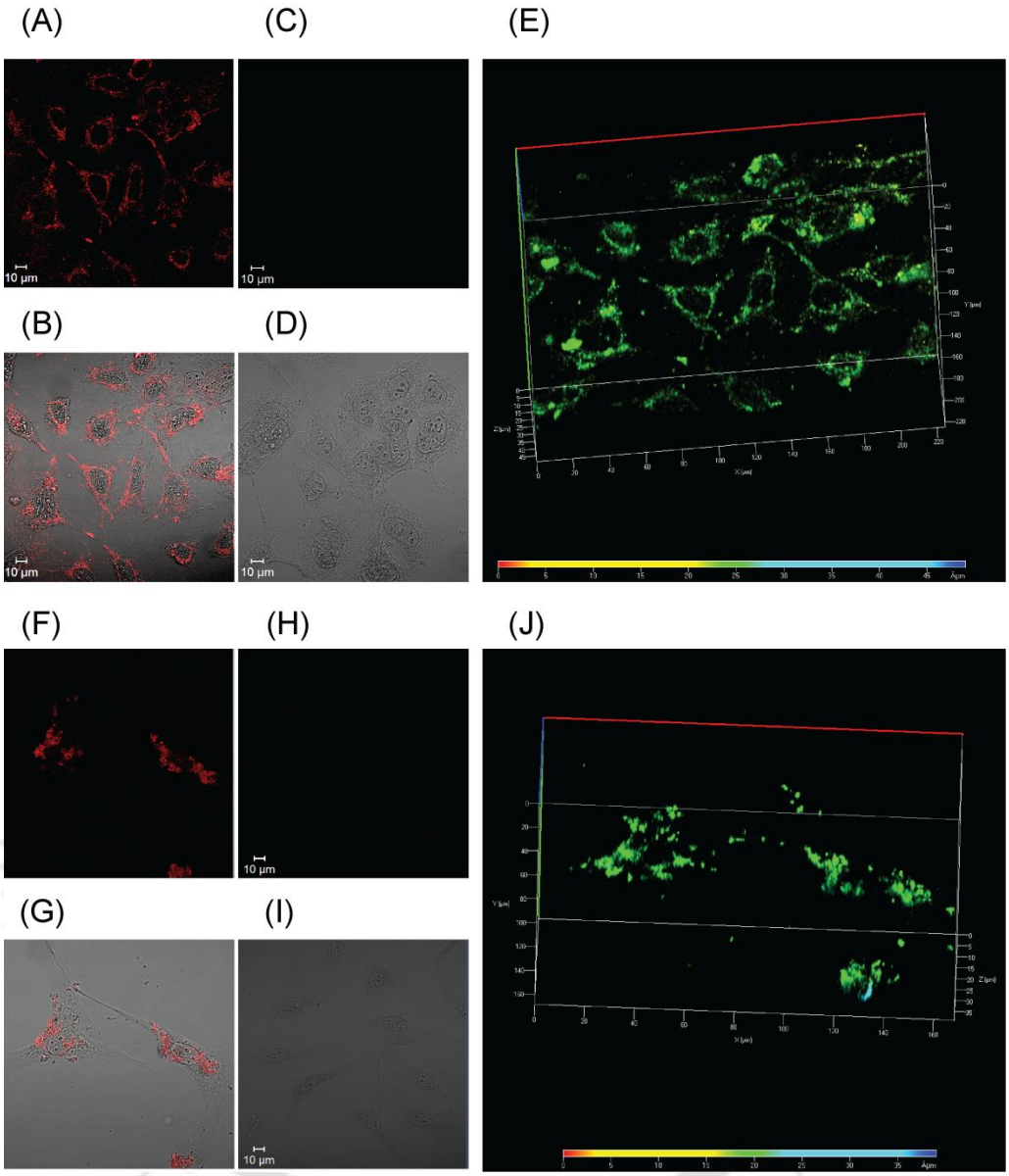

Figure 4.34 Confocal microscopy based cellular internalization study of PTEN-nanocomposites where (A) Fluorescence image of MCF7 cells incubated with PTEN-nanocomposites and (B) Merged image of the same cell, (C) Fluorescence image of control MCF7 cells and (D) Merged image of the same cell, (E) A z-stack projection of MCF7 cells incubated with PTEN-nanocomposites, (F) Fluorescence image of U-87 MG cells incubated with PTEN-nanocomposites and (G) Merged image of the same cell, (H) Fluorescence image of control U-87 MG cells and (I) Merged image of the same cell, (J) A z-stack projection of U-87 MG cells incubated with PTEN-nanocomposites. The coloured scale depicts the depth of the entities from the cover slip. (Scale bar 10 µm).

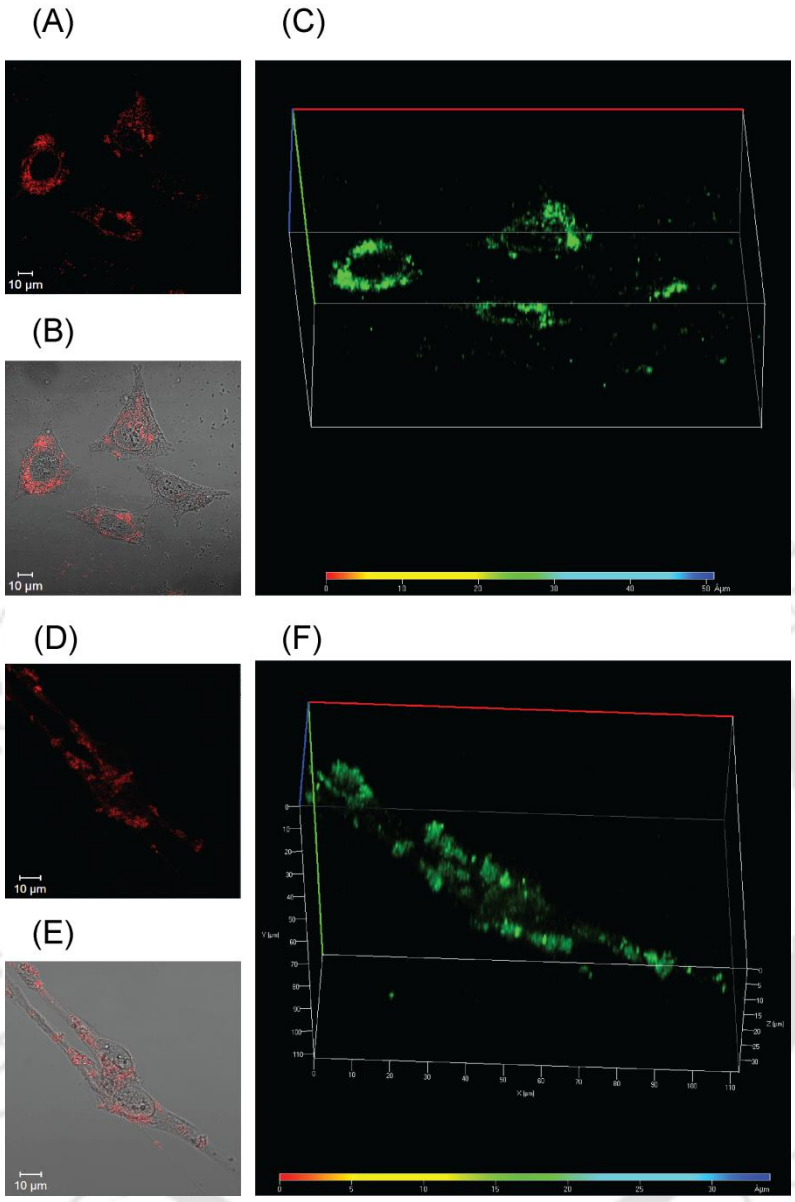

Figure 4.35 Confocal microscopy based cellular internalization study of nanocomposites where (A) Fluorescence image of MCF7 cells incubated with nanocomposites and (B) Merged image of the same cell, (C) A z-stack projection of MCF7 cells incubated with nanocomposites, (D) Fluorescence image of U-87 MG cells incubated with nanocomposites and (E) Merged image of the same cell, (F) A z-stack projection of U-87 MG cells incubated with nanocomposites. The coloured scale depicts the depth of the entities from the cover slip. (Scale bar 10 µm).

U-87 MG and MCF7 cells were either incubated with sodium azide or kept at 4 °C for 30 min or left untreated prior to incubation with the PTEN-nanocomposites. Since almost all the endocytic pathways are energy driven, the energy dependence can be blocked by lower temperature of 4 °C or ATPase inhibition by sodium azide (Kou *et al.*, 2013).

Inhibitor treated and untreated cells were then subjected to fluorescence spectroscopy based analysis. For both MCF7 and U-87 MG cells, studying the fluorescence at 650 nm upon excitation at 480 nm reveal reduced fluorescence in cells incubated with sodium azide and low temperature as compared to untreated cells. Thus, the study confirms endocytosis dependent uptake of the nanocomposites in MCF7 and U-87 MG cells. The results are consistent with endocytosis based uptake of PEGylated nanoparticles (Brandenberger *et al.*, 2010, Li *et al.*, 2014) **(Figure 4.36)**

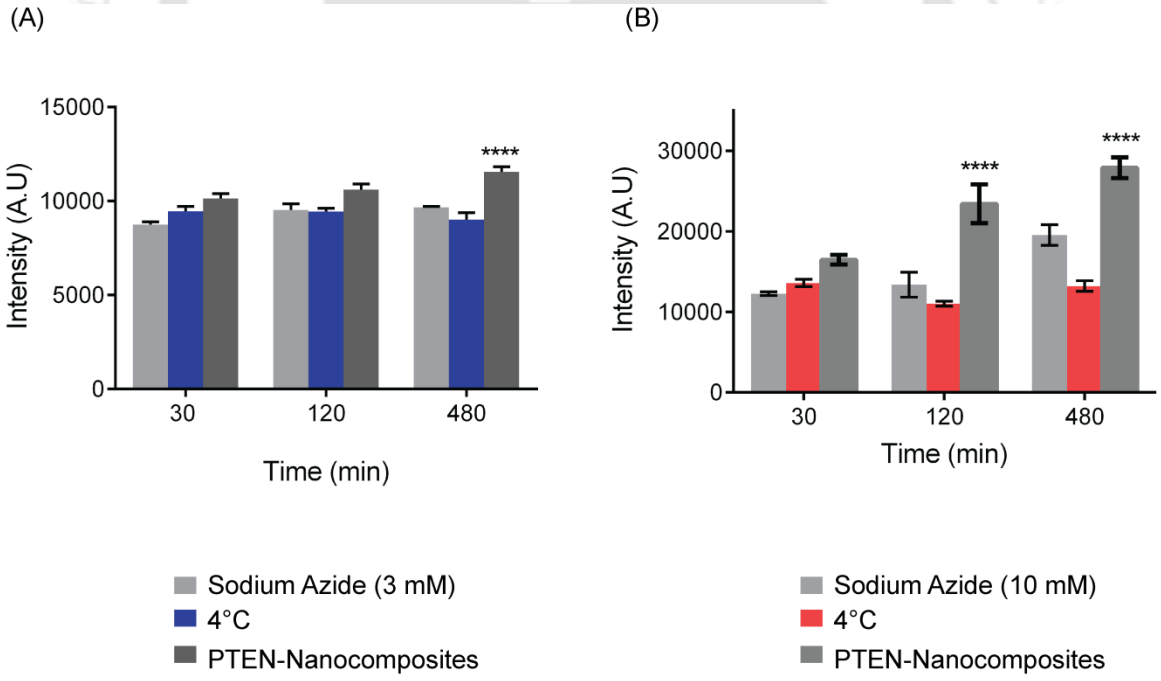

Figure 4.36 Mode of PTEN-nanocomposites internalization in (A) MCF7 cells (B) U-87MG cells.

4.12 Deciphering Effect of PTEN-Nanocomposites on Cellular Signalling

Tumour suppressor PTEN has been identified as a critical negative regulator of PI3K/Akt pathway by de-phosphorylation of phosphatidylinositol-(3,4,5)-tri phosphate (PIP_3) to phosphatidylinositol-(4,5)-di phosphate (PIP2) (Maehama and Dixon 1998, Song *et al.*, 2005). PIP_3 is known to activate Akt by assisting phosphorylation at two regulatory sites threonine308 and serine473. Phosphorylated Akt in turn activates a signalling cascade culminating into cell survival, growth and proliferation (Jiang and Liu 2008). This strengthens the rationale for targeting Akt to achieve therapeutic benefit.

The cellular uptake of PTEN-nanocomposites was determined by optical techniques. However, to further validate the intracellular delivery of GST-PTEN into U-87 MG and MCF7 cell lines, total protein was isolated and subjected to the Western blot analysis. Total protein was isolated from cells treated with nanocomposites and PTEN-nanocomposites along with untreated control. MCF7 cell line showed a legitimate band around 81 kDa for GST-PTEN along with band for endogenous PTEN when the cells were incubated with PTEN-nanocomposites confirming intracellular delivery of the protein. U-87 MG cells displayed a band corresponding to GST-PTEN expression only in case of cells treated with the PTEN-nanocomposites with no endogenous PTEN, thereby validating PTEN delivery **(Figure 4.37)**. Once the delivery of PTEN was confirmed, the consequent judicious step was to investigate the modulation of Akt expression level. The isolated protein was probed with anti-Akt (rabbit) antibody and anti-pAktS473 (rabbit) antibody. HRP conjugated anti-rabbit secondary antibody was applied to develop the blot by chemiluminescence technique. Expression analysis of phospho-Akt in MCF7 and U-87 MG cells revealed reduction in expression of the phosphorylated protein in cells treated with PTEN-nanocomposites as compared to the nanocomposites treated cells and untreated control cells. A 3.7-fold decrease in the expression of pAKT in treated MCF7 cells was observed as determined by imageJ software. For U-87 MG cells there was 2-fold decrease in expression of pAKT. There was no difference in the expression of total Akt in all the treated and untreated cells.

Alongside de-phosphorylation of lipid PIP_3, being a dual specificity phosphatase, PTEN is known to interact with focal adhesion kinase (FAK) by catalyzing its de-phosphorylation and

thereby regulating integrin mediated cell invasion and migration (Tamura *et al.,* 1998, Tamura *et al.,* 1999). Therefore, the expression of pFAKTyr397in treated and untreated MCF7 and U-87 MG cells was evaluated using anti-pFAKTyr397(rabbit) antibody and HRP-conjugated anti-rabbit secondary antibody. Western blot analysis of samples from both MCF7 and U-87 MG cells were in tandem with reduced expression of pFAK upon treatment with PTEN-nanocomposites. Meticulous analysis of the cellular signalling upon treatment with exogenously delivered GST tagged PTEN employing luminescent clusters suggested that PTEN protein was successfully delivered to MCF7 and U-87 MG cancer cell lines with retention of its functional integrity thereby successfully modulating the cellular signalling mechanism **(Figure 4.37)**. Since AKT and FAK are key node proteins in the PIP3/Akt and FAK/Integrin signal transduction pathways, respectively it was crucial to determine the subsequent implications of the altered signalling on MCF7 and U-87 MG cell lines.

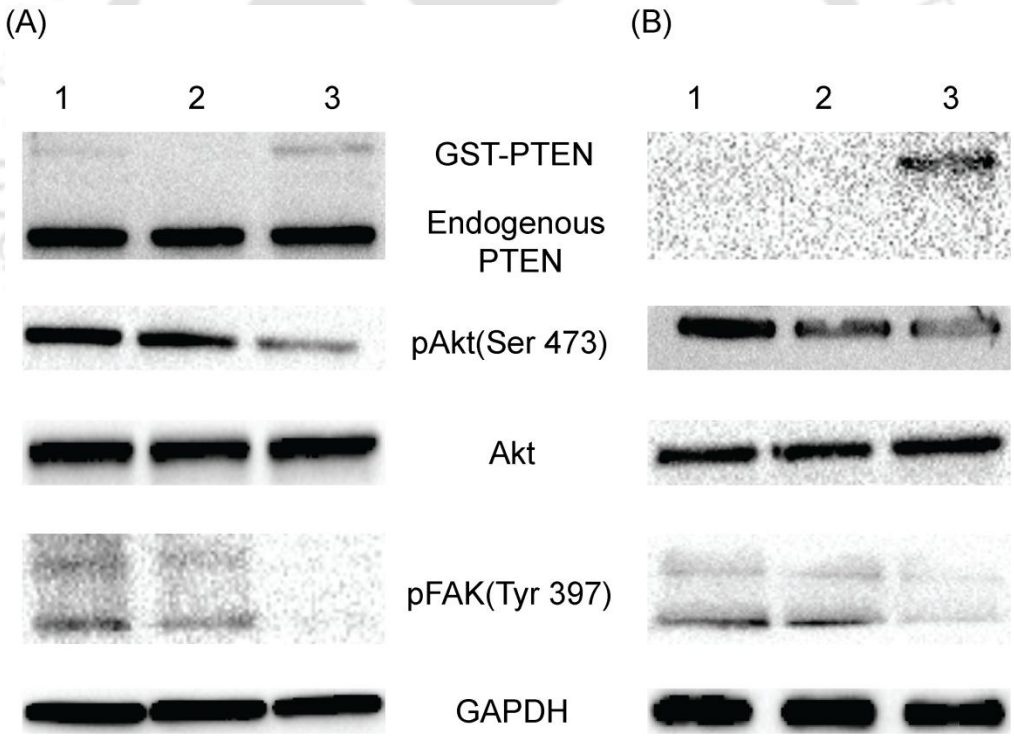

Figure 4.37 Western blot analysis of PTEN, pAKT, Akt, pFAK, GAPDH in (A) MCF7 cells (B) U-87 MG cells where, Lane 1 represents control untreated cells, Lane 2 represents nanocomposite treated cells and Lane 3 represents PTEN-nanocomposites treated cells.

The repertoire of PTEN functions includes inhibition of cell migration through its C2 domain (Raftopoulou *et al.,* 2004). This activity of PTEN is dependent on its protein phosphatase activity that catalyses de-phosphorylation of FAK at tyrosine397 residue. Integrin-FAK signalling promotes tumour progression and metastasis through phosphorylation of several regulatory proteins (Mitra, Hanson et al. 2005, Zhao and Guan 2011). To study the effect of exogenously delivered PTEN protein on the migration of U-87 MG and MCF7 cells, wound healing assay was performed. Scratch was made in the confluent monolayer of the cells using a sterile pipette tip and the wound was photographed using Nikon ECLIPSE Ti microscope. The recovery of the wound, depending on the migration of the cells, was then recorded after 24 h. U-87 MG and MCF7 cells incubated with PTEN-nanocomposites displayed slower healing as compared to untreated or only nanocomposite treated cells. The slow wound healing corroborated with the reduced expression of pFAK in cells treated with PTEN-nanocomposites. Thus, PTEN expression in glioblastoma cells that lack the protein resulted in inhibition of cell migration **(Figure 4.38)**. For MCF7 cells, the presence of exogenously delivered recombinant PTEN assisted in modulation of cellular signalling leading to reduced cell migration **(Figure 4.38)**.

To study the effect of GST-PTEN on the cell cycle progression of MCF7 and U-87 MG cells, flow cytometry analysis with propidium iodide was performed. Cells treated with PTEN-nanocomposites for 48 h were subjected to PI staining as per standard protocol. PI stained treated and untreated samples were subjected to cell cycle analysis using BD FACSCalibur. Treatment of MCF7 with PTEN-nanocomposites displayed accumulation of cells in S phase with a 1.4 fold increase in treated cells (60.01 %) as compared to untreated control cells (46.47 %) and nanocomposite treated cells (46.33 %). Treatment of U-87 MG cells with PTEN-nanocomposites displayed accumulation of cells in G2/M phase with a 5 fold increase in treated cells (14.54 %) as compared to untreated control cells (3.40 %) and nanocomposite treated cells (2 %). Cell cycle analysis was performed using FCS express flow cytometry software **(Figure 4.39A and 4.39B)**.

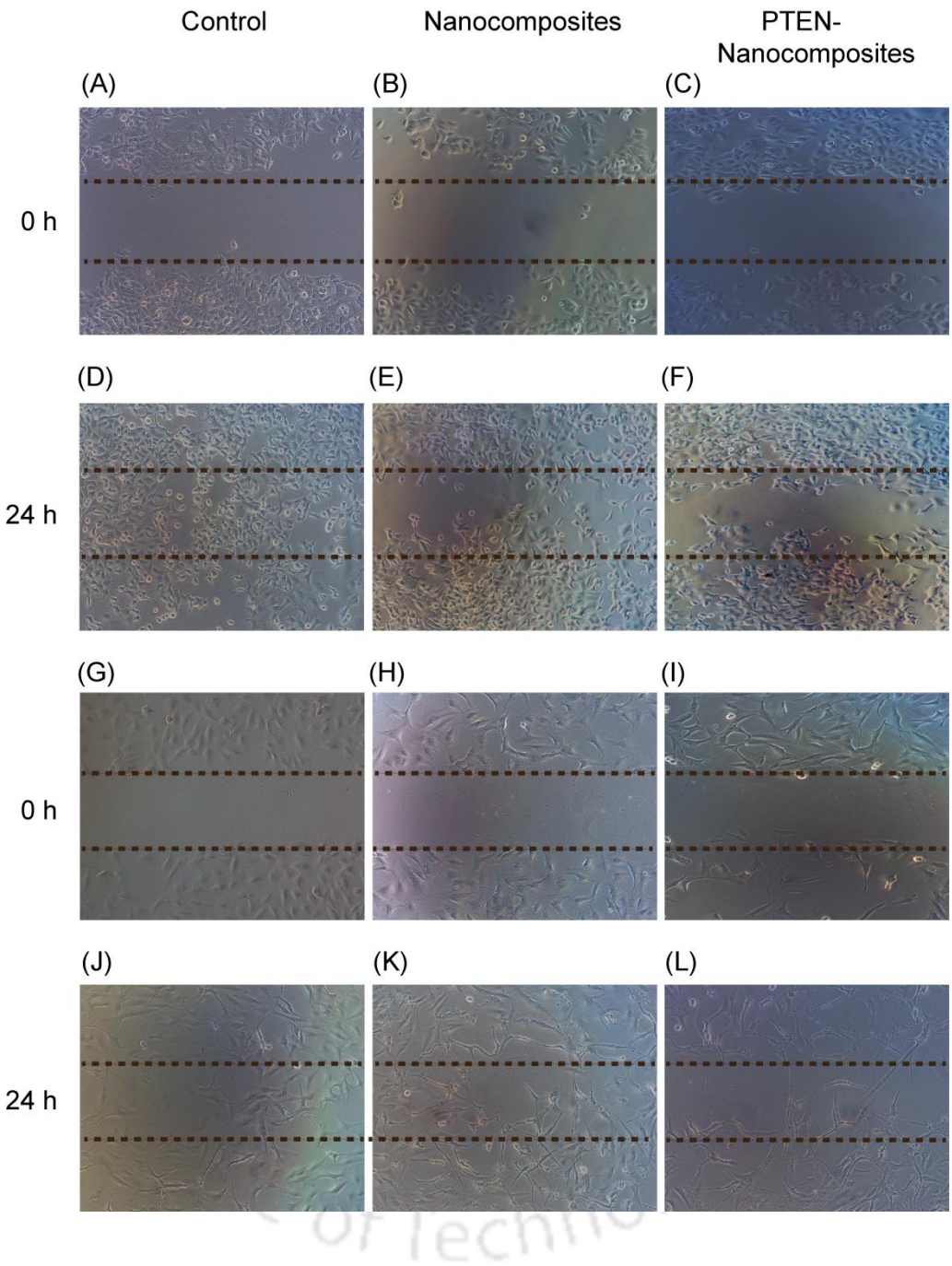

Figure 4.38 Scratch healing assays for MCF7 and U-87 MG Cells where A, B and C represents control, nanocomposite treated and PTEN-nanocomposites treated MCF7 cells at 0 h. D, E and F represents control, nanocomposite treated and PTEN-nanocomposites treated MCF7 cells at 24 h. G, H and I represents control, nanocomposite treated and PTEN-nanocomposite treated U-87 MG cells at 0 h. J, K and L represents control, nanocomposite treated and PTEN-nanocomposites treated U-87 MG cells at 24 h.

Cell cycle checkpoints principally control the progression through the cell cycle. These checkpoint control system comprises of the cyclin dependent kinases and cyclins. Cyclins positively regulate the cell cycle, thereby allowing passage from one phase to another. Akt is known to modulate the role of cyclins in the cell cycle progression (Chang *et al.*, 2003, Lee *et al.*, 2005). As a result, the subsequent down-regulation of Akt by exogenously delivered recombinant PTEN led to impaired transition of cell cycle phases effectuating in accumulation or arrest of cells in a particular phase for MCF7 and U-87 MG cells. To corroborate the regulation of Akt and progression of cell cycle, the expression level of cell cyclins were evaluated. Total RNA isolated from the treated and untreated cells were subjected to cDNA synthesis. The synthesized cDNA was applied as template in PCR reaction using cyclin specific primers. GAPDH was used as internal control.

In MCF7 cells, a decrease in the expression of cyclin B1 was observed upon treatment with PTEN-nanocomposites for a period of 48 h. Cyclin B1 is an important component of the cell cycle, which promotes S Phase and G2/M phase transitions (Moore, Kirk et al. 2003, Ou *et al.*, 2013) culminating into cell division. Inhibition of cyclin B1 resulted in accumulation of the PTEN-nanocomposites treated MCF7 cells in the S phase. Treatment of U-87 MG cells with PTEN-nanocomposites for 24 h, resulted in decreased expression of cyclin B2, a cyclin associated with G2/M transition (Wu *et al.*, 2010). The change in expression of cyclins in the control and PTEN-nanocomposite treated MCF7 and U-87 MG cells is represented in **Figure 4.39C and 4.39D**. Therefore, the regulation of AKT and the subsequent decrease in expression of cyclins resulted in S phase arrest in MCF7 cells and G2/M phase arrest in U-87 MG cells. The fold change of the cyclin expression in U-87 MG and MCF7 cell lines upon treatment with PTEN-Nanocomposites as compared to nanocomposite treated or untreated sample is presented in the annexure.

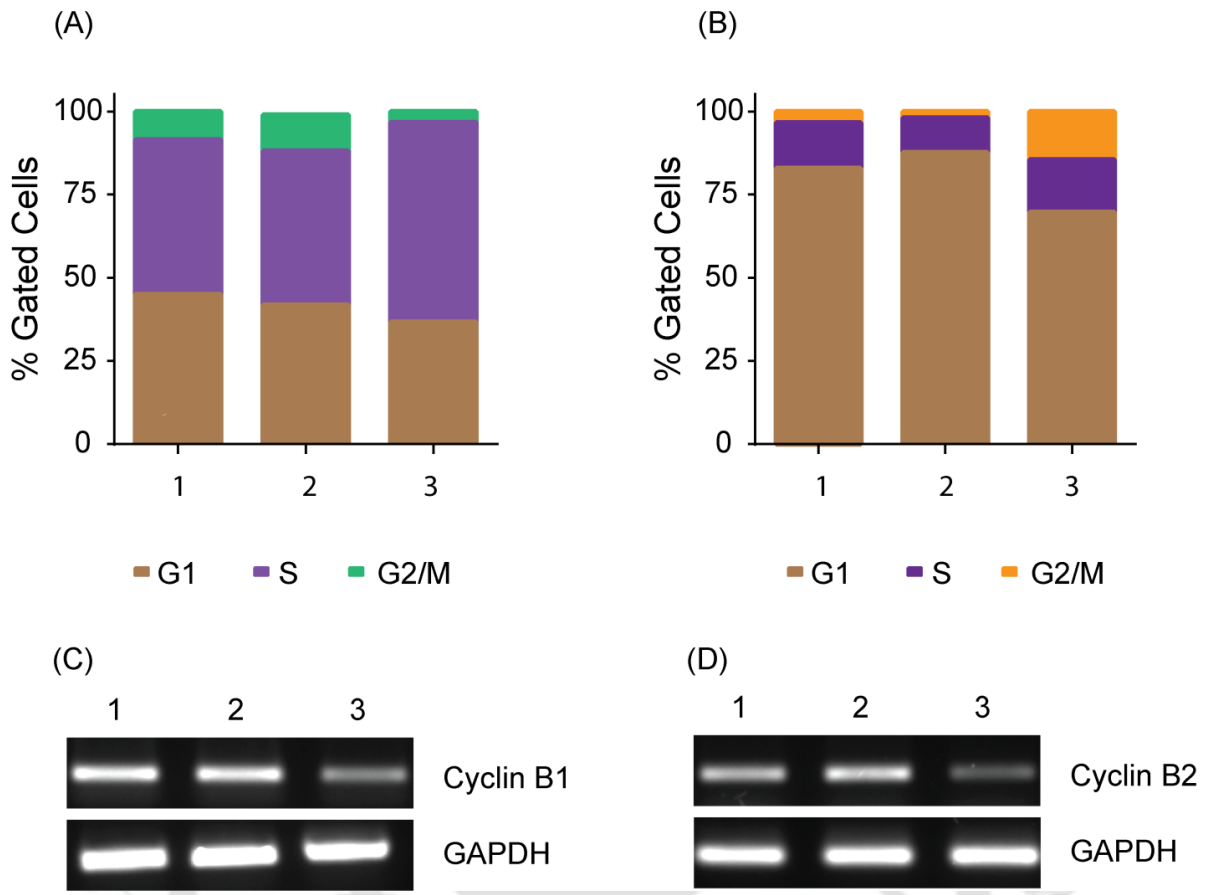

Figure 4.39 Evaluation of cell cycle profile (A) MCF7 cells, where 1, 2 and 3 are untreated control cells, nanocomposite treated cells and PTEN-nanocomposites treated cells, respectively (B) U-87 MG cells, where 1, 2 and 3 are untreated control cells, nanocomposite treated cells and PTEN-nanocomposites treated cells, respectively (C) Expression of cyclin B1 and GAPDH in MCF7 cells, where 1, 2 and 3 are control, nanocomposite treated and PTEN-nanocomposite treated cells, respectively (D) Expression of cyclin B2 and GAPDH in U-87 MG cells, where 1, 2 and 3 are control, nanocomposite treated and PTEN-nanocomposite treated cells, respectively.

4.13 Effect of PTEN-Nanocomposites on Cell Viability and Combination Therapy

To determine the effect of PTEN-nanocomposite on the proliferation of MCF7 and U-87 MG cells, calcein-AM/EtBr dual staining and MTT cell survival assay were performed. Dual staining with calcein-AM/EtBr assisted in visualization of the reduction in cell viability and presence of apoptotic cells upon treatment with the PTEN-nanocomposites for 24 h and 48 h as compared to only nanocomposites treated or untreated cells **(Figure 4.40)**

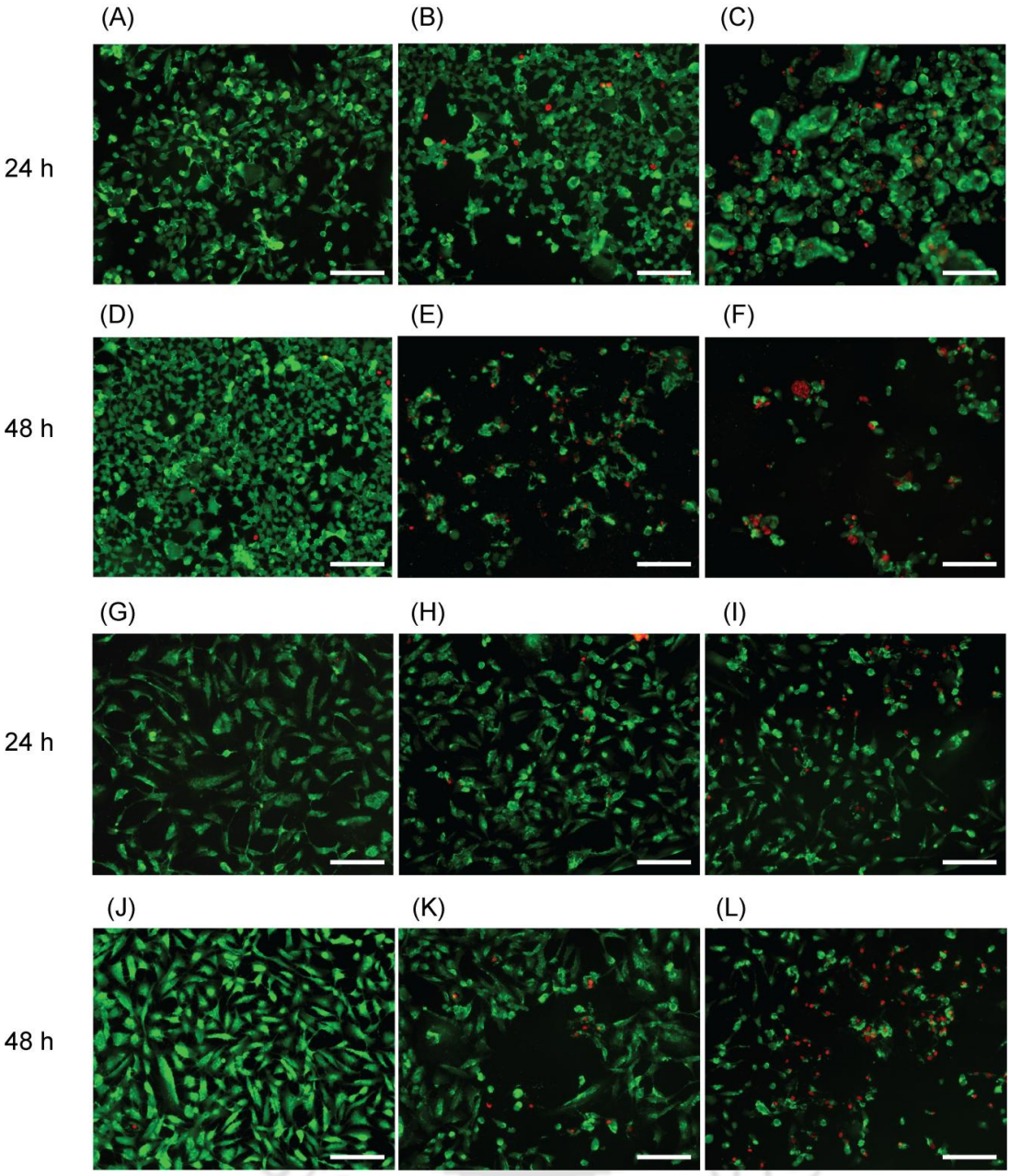

Figure 4.40 Calcein-AM/EtBr dual staining where A, B and C are merged images of control, nanocomposite, PTEN-nanocomposite treated MCF7 cells at 24 h, D, E and F are merged images of control, nanocomposite, PTEN-nanocomposite treated MCF7 cells at 48 h, G, H and I are merged images of control, nanocomposite, PTEN-nanocomposite treated U-87 MG cells at 24 h, J, K and L are merged images of control, nanocomposite, PTEN-nanocomposite treated U-87 MG cells at 48 h, respectively (Scale bar 25 μm).

The cells were incubated with varying concentrations of nanocomposites and PTEN-nanocomposites for 48 h. The results revealed dose dependent reduction in viability of the cells upon treatment with increasing concentrations of PTEN-nanocomposites for MCF7 **(Figure 4.41A)** and U-87 MG cells **(Figure 4.41B)**. The IC_{50} was achieved for MCF7 cells at concentration of the PTEN-nanocomposites of PTEN (36 nM)-Cluster (30 µg/ml) Composite. However, in case of glioblastoma U-87 MG cells IC_{50} was not achieved. This differential outcome in cell survival may be due to the multi-drug resistance characteristic of the glioblastoma U-87 MG cell line (Nagane *et al.*, 1998).

Direct role of EGFR over-expression in tumour aetiology and progression makes them an intensely pursued therapeutic target (Holbro and Hynes 2004). However, therapeutic strategies based on over-expression of EGFR have not met the expected results for glioblastoma therapy. Therefore, to sensitize U-87 MG cells, dual targeting of AKT and EGFR was attempted.

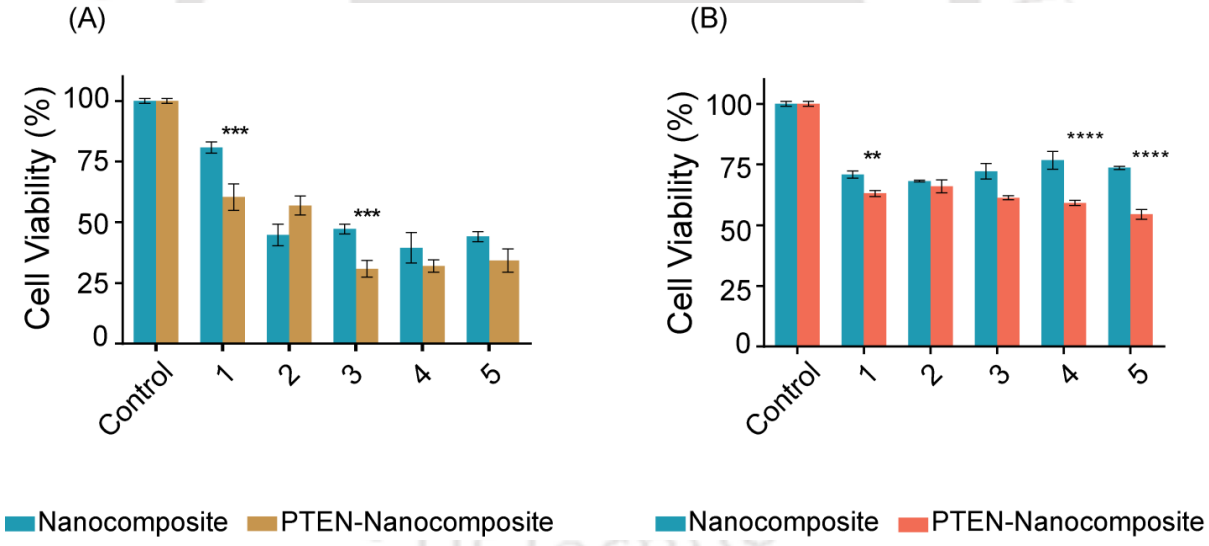

Figure 4.41 Assessment of cell viability in (A) MCF7 cells (B) U-87 MG cells. Evaluation of cell viability of MCF7 cells upon treatment with nanocomposite and PTEN-nanocomposites for 48 h by MTT assay, where 1, 2, 3, 4, and 5 are PTEN (12 nM)-Cluster (10 µg/ml) Composite, PTEN (24 nM)-Cluster (20 µg/ml) Composite, PTEN (36 nM)-Cluster (30 µg/ml) Composite, PTEN (48 nM)-Cluster (40 µg/ml) Composite and PTEN (72 nM)-Cluster (60 µg/ml) Composite, respectively.

In this regard, effect of PTEN-nanocomposites combined with anti-cancer drug erlotinib, a small molecule inhibitor of the EGFR tyrosine kinase, was determined. The EGFR gene expression in U-87 MG cells was confirmed using gene specific primers and is illustrated in **(Figure 4.42A)**. Once EGFR expression in U-87 MG cells was confirmed, the effect of the drug on the cell line was assessed by MTT based viability assay. Treatment with erlotinib resulted in dose dependent reduction with IC_{50} value of 25 μM **(Figure 4.42B)**. Determination of dose concentrations of erlotinib and PTEN-nanocomposite is a prerequisite for effective combination studies. The doses of erlotinib and PTEN-nanocomposite were determined based on the analysis of combination index of various doses employing compusyn software **(Figure 4.42C)**. It was observed that lower concentration of composite (12-36 nM PTEN protein) and drug (<20 μM) combinations resulted in synergistic effect on U-87 MG cells. However at higher concentrations of erlotinib and the PTEN-nanocomposites the effect was antagonistic **(Figure 4.42C)**. Concentration dependent synergism or antagonism is possibly linked to the mechanism of action of the drug (Meletiadis *et al.*, 2007). Erlotinib, an anti-cancer drug, binds and inhibits the tyrosine kinase activity of the epidermal growth factor receptor (EGFR). EGFR activates several proteins by phosphorylation and regulates signalling pathways, such as the Ras/Raf/MAPK pathway and the Akt pathway either directly or indirectly (Scaltriti and Baselga 2006). PTEN is a direct regulator of the Akt signalling pathway. It is to be noted that both erlotinib and PTEN at their higher concentrations may block the Akt signalling pathway. Therefore, the outcome of the combination was not profound at their higher concentrations as they both target the Akt signalling. However, erlotinib has multiple targets and PTEN blocks AKT at their lower concentrations and hence, the combinatorial effect was found to be synergistic. Based on this observation, the doses of erlotinib for treatment of the cells were determined. U-87 MG were treated with varying concentrations of erlotinib (2.5 to 10 μM) and fixed concentration of the PTEN-nanocomposites [PTEN (24 nM)-Cluster (20 μg/ml) composite]. There was a dose dependent reduction in the viability of the cells where IC_{50} was achieved in cells treated with erlotinib (10 μM) and PTEN (24 nM)-(20 μg/ml) composite combination module **(Figure 4.42D)**.Therefore, low concentration of both erlotinib and PTEN-nanocomposite sensitized U-87 MG cells ensuing reduced cell viability. Hence, the co-therapy protocol paves the way for application of this combination as a potential treatment option of drug resistant cancer.

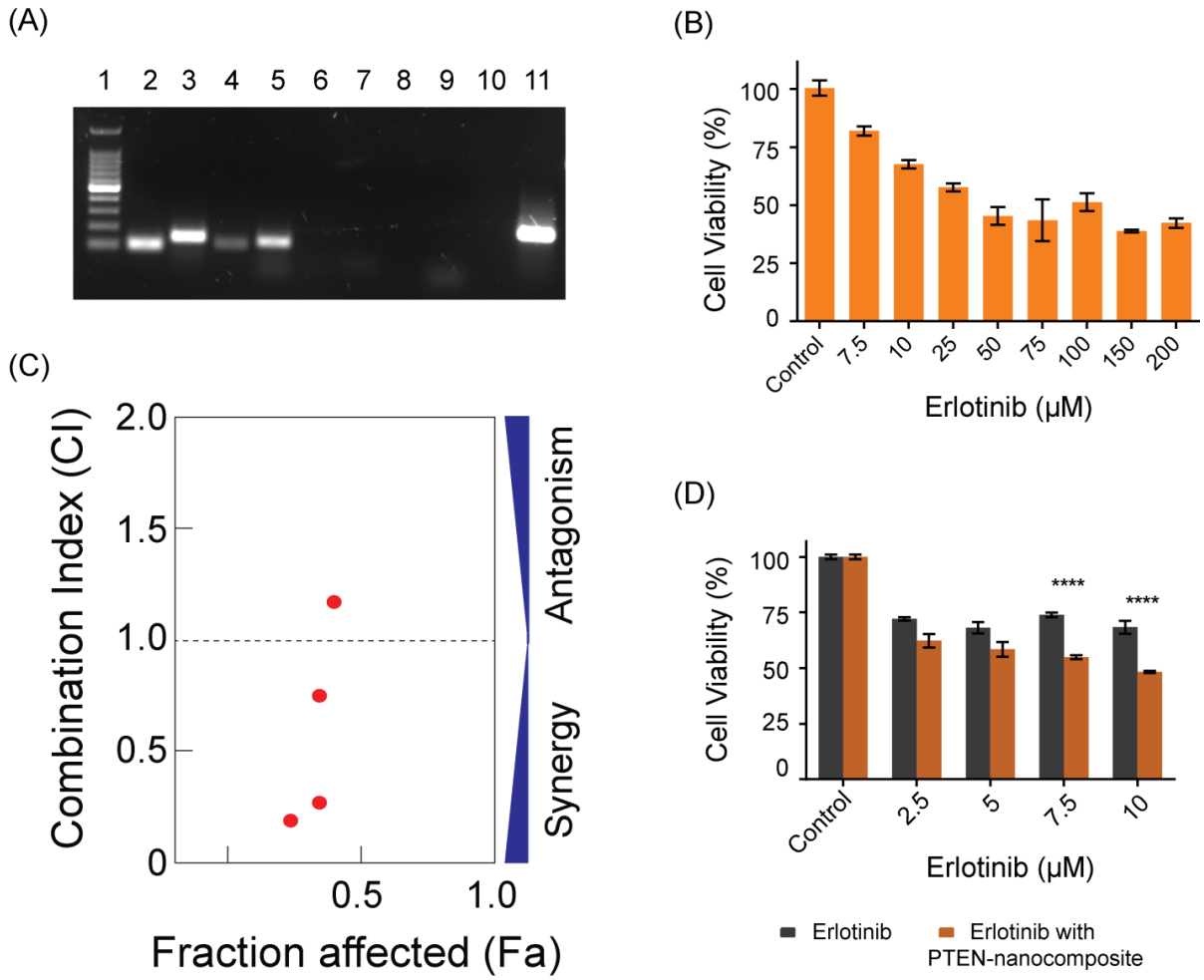

Figure 4.42 Evaluation of co-therapy module of PTEN-Nanocomposites and drug erlotinib (A) Expression study of EGFR in U-87 MG cell line where Lane 1 is 100bp DNA ladder. Lane 2 to 5 represents the expression of EGFR1, EGFR2, EGFR3 and EGFR4, respectively. Lane 6 to 9 represents template control for EGFR1, EGFR2, EGFR3 and EGFR4, respectively. Lane 10 is blank. Lane 11 represents expression of endogenous control β-actin (B) Evaluation of cell viability of U-87 MG cells upon treatment with erlotinib for 48 h (C) Combination index determination of erlotinib and PTEN-nanocomposite using compusyn software (D) Evaluation of cell viability of U-87 MG cells in combination therapy module with erlotinib and PTEN (24 nM)-Cluster (20 μg/ml) composite upon 48 h treatment by MTT based assay.

Thus, the results demonstrated successful formulation of a nanosystem based delivery cargo encapsulating tumour suppressor recombinant protein PTEN. Subsequent delivery and evaluation of therapeutic benefit of exogenous PTEN was attempted. Regulation of the

cellular signalling pathway and the associated consequences by PTEN ultimately resulted in dose dependent reduction of the cell viability of MCF7 cells. In case of drug resistant U-87 MG cells, the PTEN-nanocomposites helped in manoeuvring the cells into a state where it was susceptible to chemotherapeutic agent, erlotinib. Therefore, successful formulation of PTEN protein encapsulation for delivery and tracking was established which paved the foundation for potential PTEN based protein therapy.

Evaluation of PTEN-Nanocomposites on Spheroid Model

The comprehensive analysis of the PTEN-nanocomposites on the monolayer (2D) cultures of MCF7 and U-87 MG provided strong lead towards its potential biomedical applications. Although irrefutably the most convenient method for screening of therapeutically relevant products, there exists disparity between the complexity and heterogeneity of *in vivo* environment and monolayer cell culture. Three dimensional cell culture models serve as a bridge between the 2D cell culture and *in vivo* applications. Therefore, to comprehend the performance of the nanocomposite encapsulated PTEN protein (PTEN-Nanocomposite), three dimensional spheroid models were generated and the therapeutic efficacy of PTEN protein on three dimensional (3D) cultures was evaluated.

4.14 Generation of Spheroid Model

Tumour spheroid model of MCF7 and U-87 MG from their respective monolayer cultures was developed and the curative efficacy of PTEN-nanocomposites was tested. U-87 MG and MCF7 spheroids were developed in 96 well plates by facile forced flotation method as described in the materials and methods section. The formation and growth of spheroids were monitored every 24 h using Nikon Ti microscope.

Images captured under phase contrast revealed the formation of MCF7 spheroids of size around 600 μm and U-87 MG spheroids of size around 400 μm **(Figure 4.43)**. Spheroids formed after 96 h was tested for all subsequent experiments.

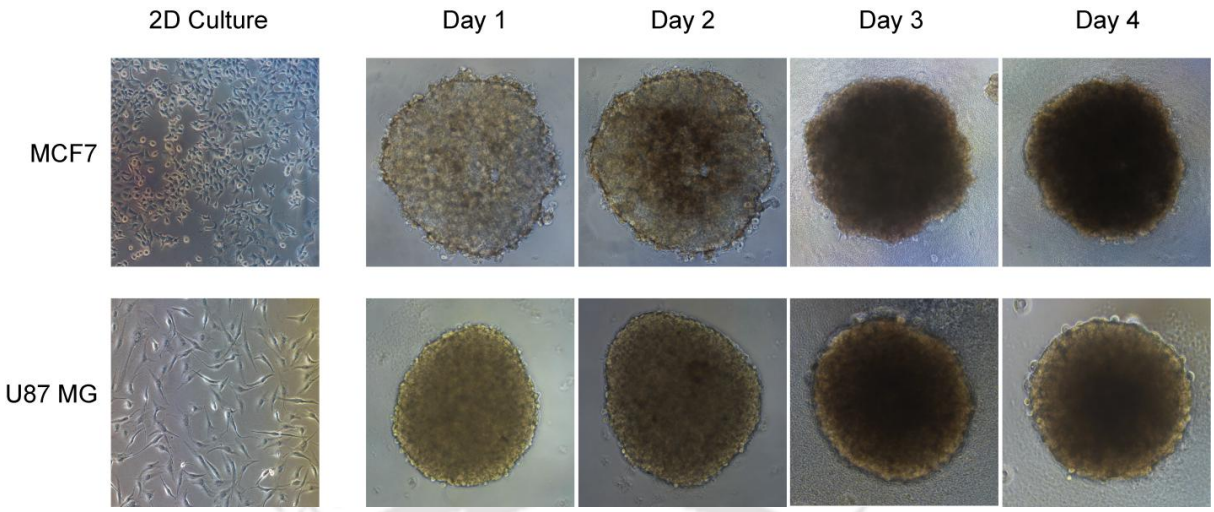

Figure 4.43 Monitoring the formation of MCF7 and U-87 MG spheroids.

4.15 Internalization and Effect of PTEN-Nanocomposites

The cellular internalization of the PTEN-nanocomposites in the spheroids was evaluated. The silver nanoclusters exhibited fluorescence maxima at 650 nm upon excitation at 480 nm, which was utilized to track the uptake of the protein loaded cargo in the spheroids. Following incubation with PTEN-nanocomposites and nanocomposites, the spheroids were washed with PBS and analyzed using Zeiss LSM 880 microscope. The microscope images exhibited red fluorescence in the cytoplasm of the treated cells indicating the internalization of the nanocomposites in the U-87 MG and MCF7 spheroids. However, no fluorescence was observed in the untreated control U-87 MG and MCF7 spheroids. To further corroborate the uptake, z-stacking of the spheroid was performed. Z-stacking allows the collection of images in the XZ focal planes, which provides three-dimensional data (Collazo *et al.*, 2005). The z-stack images confirmed the internalization of the nanocomposites into the spheroids. The green colour on the depth coding scale is indicative of the presence of the nanocomposites inside the spheroids. The cellular internalization of nanocomposites and PTEN-nanocomposites in MCF7 spheroids and U-87 MG spheroids is illustrated in **Figure 4.44 and Figure 4.45**.

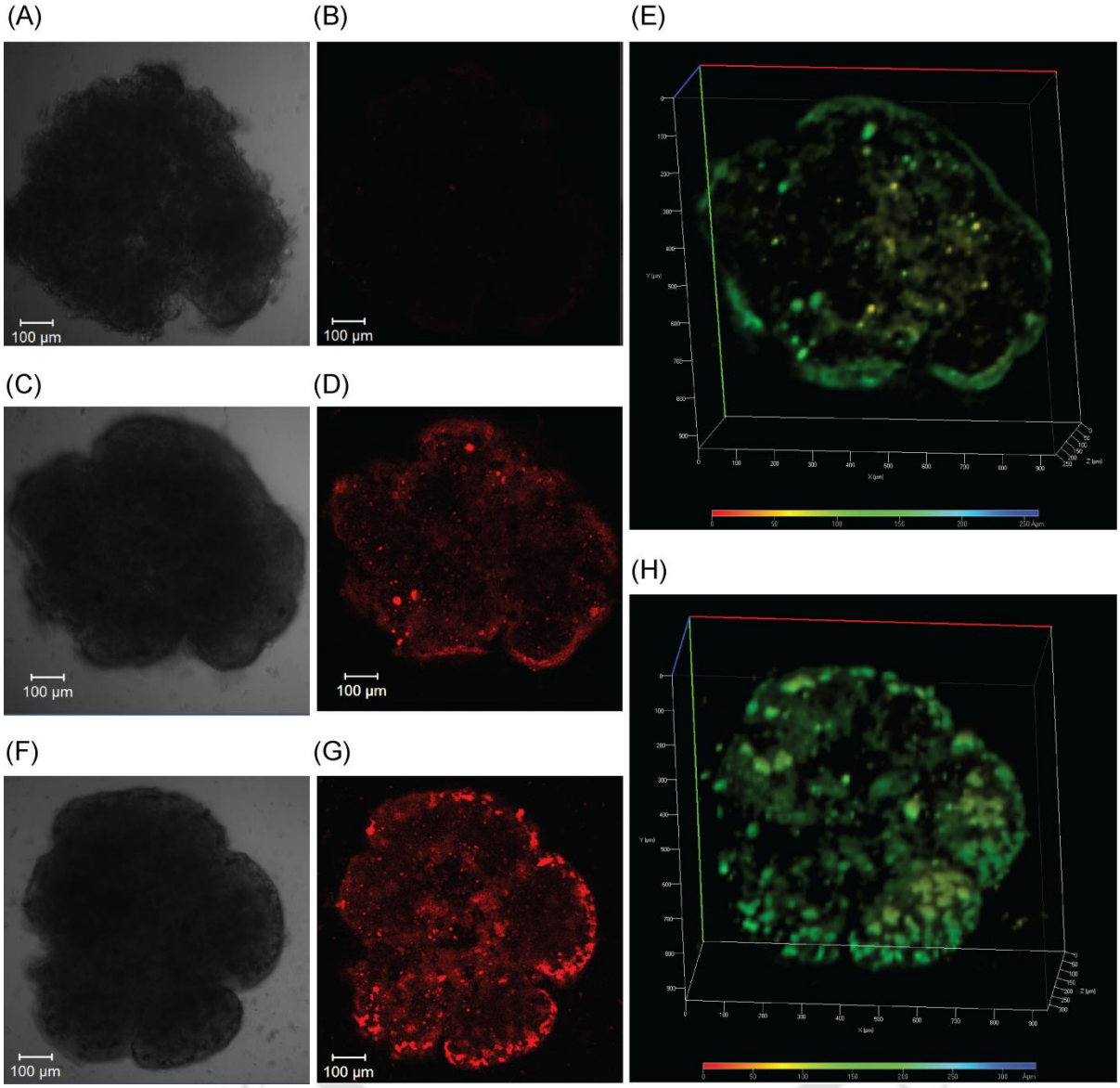

Figure 4.44 Confocal microscopy based cellular internalization study of PTEN-nanocomposites (A) Phase contrast of control MCF7 spheroids and (B) Fluorescence image of the same cell, (C) Phase contrast image of MCF7 spheroid incubated with nanocomposites and (D) Fluorescence image of the same cell, (E) A z-stack projection of MCF7 spheroids incubated with nanocomposites, (F) Phase contrast image of MCF7 spheroid incubated with PTEN-nanocomposites and (G) Fluorescence image of the same cell, (H) A z-stack projection of MCF7 spheroid incubated with PTEN-nanocomposites. The coloured scale depicts the depth of the entities from the cover slip. (Scale bar 100 µm).

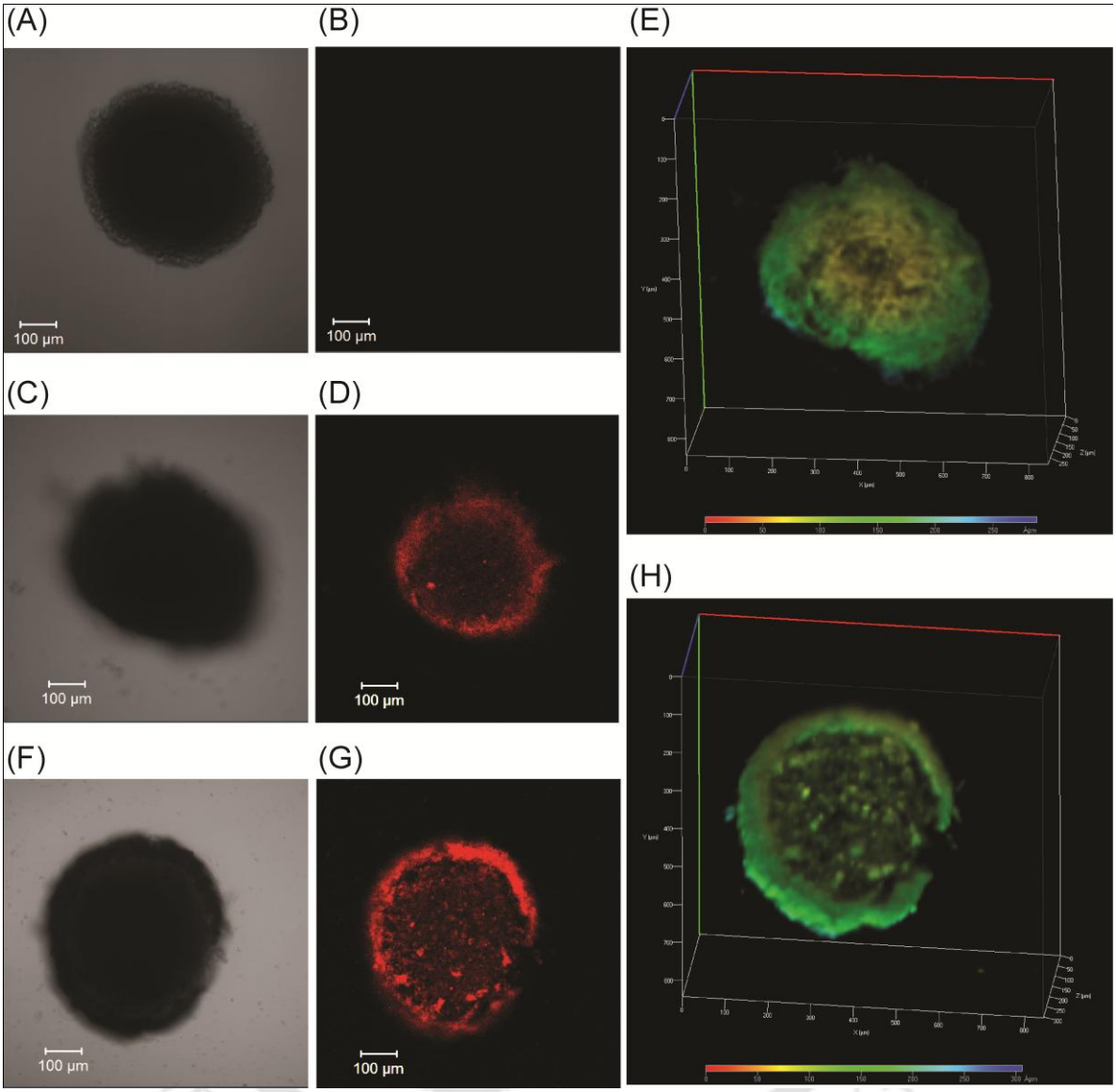

Figure 4.45 Confocal microscopy based cellular internalization study of PTEN-nanocomposites (A) Phase contrast of control U-87 MG spheroids and (B) Fluorescence image of the same cell, (C) Phase contrast image of U-87 MG spheroid incubated with nanocomposites and (D) Fluorescence image of the same cell, (E) A z-stack projection of U-87 MG spheroids incubated with nanocomposites, (F) Phase contrast image of U-87 MG spheroid incubated with PTEN-nanocomposites and (G) Fluorescence image of the same cell, (H) A z-stack projection of U-87 MG spheroid incubated with PTEN-nanocomposites. The coloured scale depicts the depth of the entities from the cover slip. (Scale bar 100 µm).

The effect of PTEN-nanocomposite on the spheroids was determined by assessing the viability using calcein-AM/PI dual staining procedure **(Figure 4.46 and 4.47)**. Fluorescent dyes have been routinely used for qualitative determination of cell viability (Chan *et al.*, 2012). Two-colour staining or dual staining with fluorescent dyes allows simultaneous detection of the viable and non-viable cells. The U-87 MG and MCF7 spheroids were stained with calcein-AM enzymatic dye, a non-fluorescent fluorescein derivative that passively crosses the cell membrane of intact viable cells and is converted by cytosolic esterase into green fluorescent calcein, to assess the live cells. In combination, propidium iodide (PI), DNA binding dye that is non-permeable to membrane intact live cells, was used to stain the dead cells. Dual stained spheroids were analyzed using Zeiss LSM 880 microscope, accompanied by z-stacking analysis. The confocal images and z-stacking data display lower calcein-AM stained live cells and higher PI stained dead cells in the spheroid treated with PTEN-nancomposites for 48 h as compared to only nanocomposite treated or untreated control spheroids.

4.16 Cell cycle analysis of Spheroids

To understand the retardation in cell proliferation, the cell cycle pattern of the treated and untreated MCF7 and U-87 MG spheroids was determined by PI based flow cytometry. Treatment of MCF7 with PTEN-nanocomposites displayed accumulation of cells in S phase with a 2.1 fold increase in treated cells (49.36%) as compared to untreated control cells (23.28%) and nanocomposite treated cells (18.92%). Treatment of U-87 MG cells with PTEN-nanocomposites displayed accumulation of cells in G2/M phase with a 1.78 fold increase in treated cells (20.74%) as compared to untreated control cells (11.59%) and nanocomposite treated cells (12.69 %). Cell cycle analysis was performed using FCS express flow cytometry software **(Figure 4.48A and 4.48B)**. Further to connect the cell cycle phase with the expression of the cell cycle regulators, total RNA was isolated from the spheroids by tri reagent based method. cDNA synthesized was used as template to study expression of the cyclins and apoptotic genes.

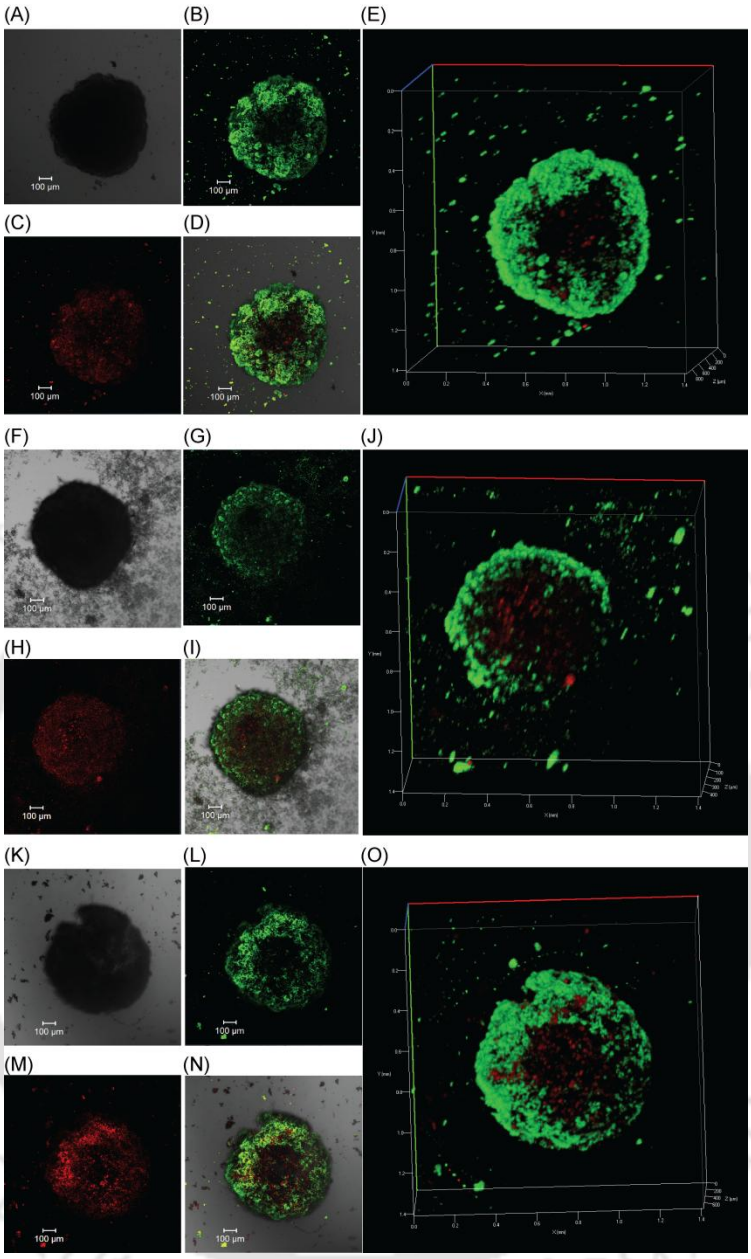

Figure 4.46 Dual staining study where A, B, C and D are phase contrast and fluorescence images of control MCF7 spheroids and (E) A z-stack projection of control MCF7 spheroids. F, G, H and I are phase contrast and fluorescence images of MCF7 spheroids incubated with nanocomposites (J) A z-stack projection of MCF7 spheroids incubated with nanocomposites. K, L, M and N are phase contrast and fluorescence images of MCF7 spheroid incubated with PTEN-nanocomposites and (O) A z-stack projection of MCF7 spheroid incubated with PTEN-nanocomposites.

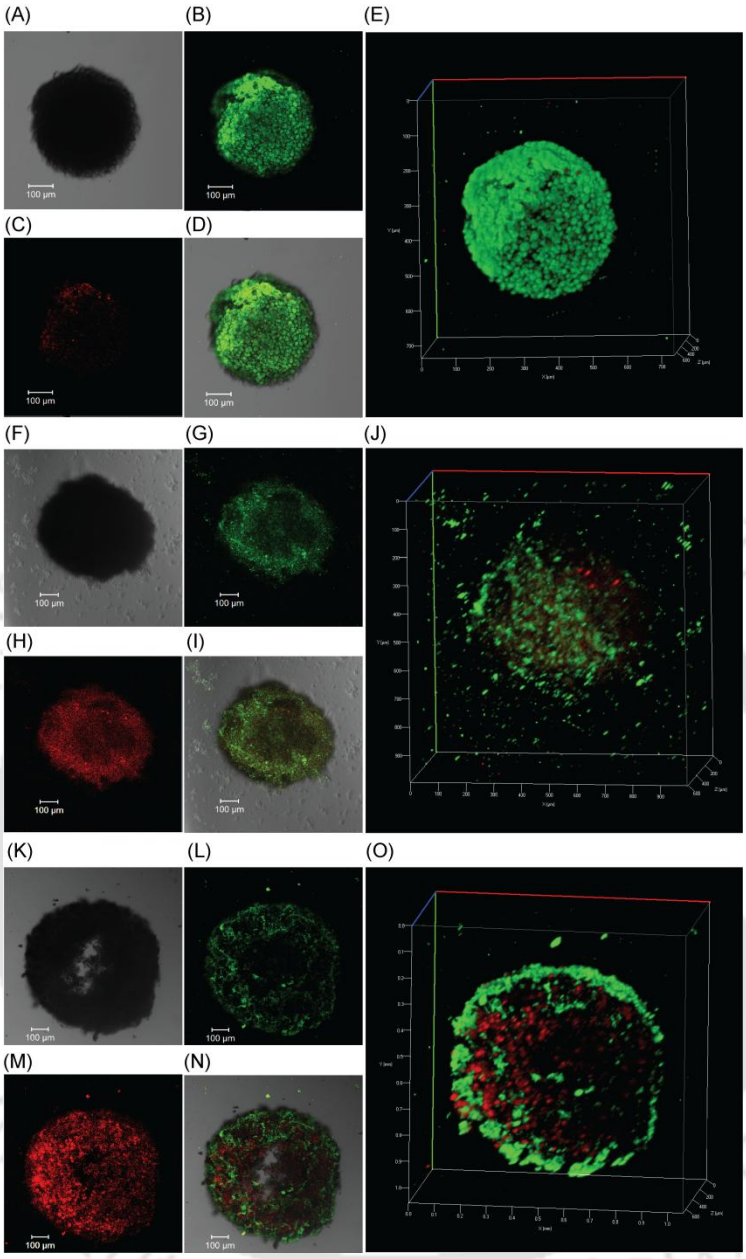

Figure 4.47 Dual staining study where A, B, C and D are phase contrast and fluorescence images of control U-87 MG spheroids and (E) A z-stack projection of control U-87 MG spheroids. F, G, H and I are phase contrast and fluorescence images of U-87 MG spheroids incubated with nanocomposites (J) A z-stack projection of control U-87 MG spheroids incubated with nanocomposites. K, L, M and N are phase contrast and fluorescence images of U-87 MG spheroid incubated with PTEN-nanocomposites and (O) A z-stack projection of MCF7 spheroid incubated with PTEN-nanocomposites.

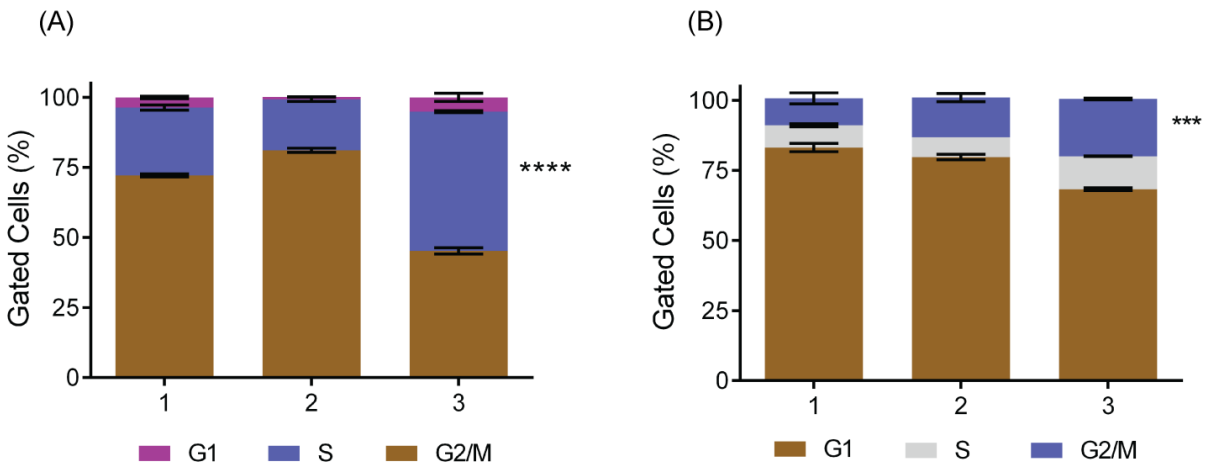

Figure 4.48 Evaluation of cell cycle profile (A) MCF7 spheroids, where 1, 2 and 3 are untreated control spheroids, nanocomposite treated spheroids and PTEN-nanocomposites treated spheroids, respectively (B) U-87 MG cells, where 1, 2 and 3 are untreated control spheroids, nanocomposite treated spheroids and PTEN-nanocomposites treated spheroids, respectively.

4.17 Gene Expression Profile of Spheroids

In MCF7, a decrease in the expression of cyclin A was observed upon treatment with PTEN (48 nM)-(30 μg/ml) Composites for a period of 48 h. Up-regulation of BAX, a gene involved in apoptosis, expression was also observed upon treatment with PTEN-nanocomposites for a period of 48 h. Calcein-AM/ Propidium iodide (PI) dual staining assay also depicted increase in the number of PI stained cells indicating augmented cell death upon treatment with PTEN-nanocomposites.

BAX is an important member of the BCL-2 family involved in promoting apoptosis. The translocation and localization of BAX in response to apoptotic stimuli has been well established (Westphal *et al.,* 2011). Research investigations have shown that the Akt pathway functions by inhibiting the apoptotic signalling cascade. In attempt to interrupt apoptosis, PI3K/Akt pathway plays a vital role in inhibiting BAX translocation to mitochondria (Tsuruta *et al.,* 2002). Additionally, treatment with PTEN-nanocomposites also demonstrated an increase in transcriptional regulator FoxO3a. Forkhead box O (FoxOs) transcription factors are ubiquitously expressed in all mammals and are known to maintain tissue homeostasis by regulating important cellular functions such as, apoptosis, metabolism and

tumour suppression (Dansen and Burgering 2008, Fu and Tindall 2008). FoxOs also control cell division by inhibition of cyclin–CDK complexes via transcription of p21 and p27 (Medema *et al.,* 2000, Zhang *et al.,* 2011), and interestingly Cyclin A is one of the various transcriptional targets of FoxO. On the other hand, FoxOs are the downstream target of Akt, and during tumorigenesis Akt is known to inhibit transcriptional functions of FoxOs by mediating its phosphorylation (Zhang, Tang et al. 2011). However treatment with PTEN-nanocomposites resulted in down-regulation of Cyclin A and up-regulation of BAX and FoxO3a as compared to nanocomposite or untreated spheroids. Thus, the modulation of gene expressions can be possibly linked to the down-regulation of Akt upon treatment with PTEN-nanocomposites **(Figure 4.49A)**. In U-87 MG spheroids, a decrease in the expression of cyclin B **(Figure 4.49B)** was observed upon treatment with PTEN (48 nM)-Cluster (30 µg/ml) composites for a period of 48 h, which is consistent with the results obtained in U-87 MG monolayer culture.Thus, based on this observation the PTEN-nanocomposite treated U-87 MG and MCF7 spheroids were further subjected to quantitative cell viability study.

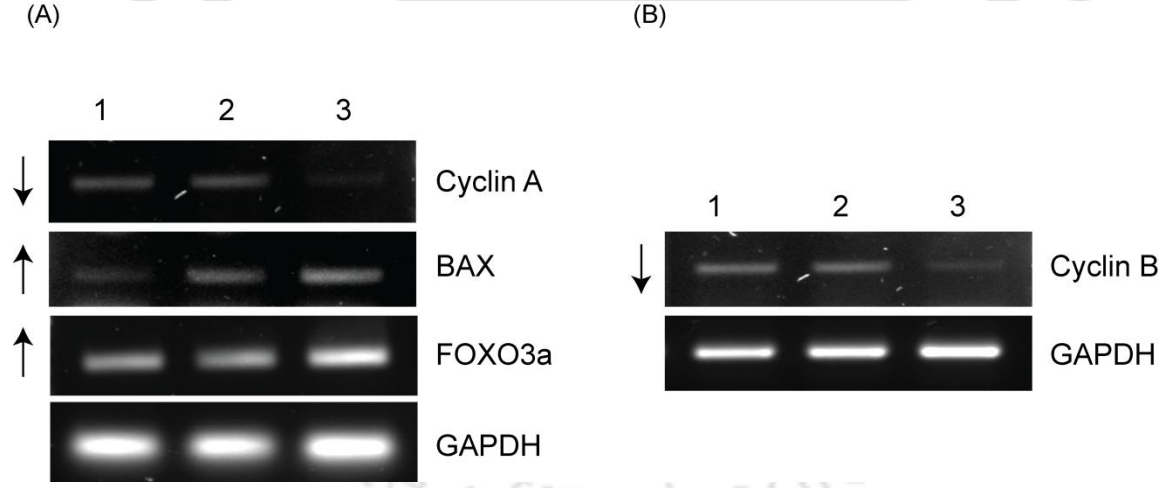

Figure 4.49 RNA profiling of spheroids (A) Expression of cyclin A, BAX, FOXO3a and GAPDH in MCF7 cells, where 1, 2 and 3 are control, nanocomposite treated and PTEN-nanocomposite treated spheroids, respectively (B) Expression of cyclin B and GAPDH in U-87 MG cells, where 1, 2 and 3 are control, nanocomposite treated and PTEN-nanocomposite treated spheroids, respectively.

4.18 Determination of Viability of Spheroids and Combination Therapy

Glioblastoma cell line U-87 MG and breast cancer cell line MCF7 were induced to form three dimensional spheroids. The spheroids were treated with varying concentrations of PTEN-nanocomposites and nanocomposites for 48 h. MCF7 spheroids upon treatment displayed dose dependent reduction with IC_{50} at PTEN (96 nM)-Cluster (60 µg/ml) composite as compared to IC_{50} at PTEN (36 nM)-Cluster (30 µg/ml) composite for monolayer MCF7 culture **(Figure 4.50)**.

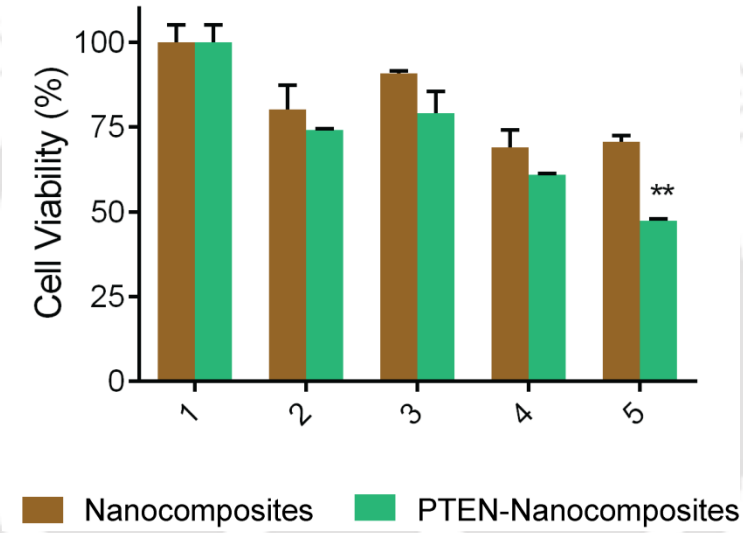

Figure 4.50 Determination of viability of MCF7 spheroids upon treatment with nanocomposites and PTEN-nanocomposites for 48 h by alamar blue assay where 1 is control spheroids, 2, 3, 4 and 5 are PTEN (24 nM)-Cluster (15 µg/ml) Composite, PTEN (36 nM)-Cluster (22 µg/ml) Composite, PTEN (48 nM)-Cluster (30 µg/ml) Composite and PTEN (96 nM)-Cluster (60 µg/ml) Composite, respectively.

Thus, this demonstrates the variation in two-dimensional culture results and three-dimensional culture results. Testing the effect on spheroids impart biological relevance to the data, as the spheroids closely resemble *in vivo* tumour organization. U-87 MG spheroids upon treatment displayed dose dependent reduction, however IC_{50} was not achieved even till concentration of PTEN (96 nM)-Cluster (60 µg/ml) composite **(Figure 4.51A)**. The reduction pattern was consistent with the PTEN-nanocomposite treated monolayer culture of U-87 MG cells. However, possibly due to the multi-drug resistance

nature of U-87 MG IC_{50} was not achieved. Therefore, co-therapy module was attempted. U-87 MG spheroids were treated with varying concentration of tamoxifen in combination with fixed concentration of the PTEN-Nanocomposite. There was a dose dependent reduction in the viability of the spheroid where IC_{50} was achieved in cells treated with 25 µM of tamoxifen (TMX) and PTEN-Nanocomposite [PTEN (36 nM)-Cluster (22 µg/ml) composite] combination module **(Figure 4.51B)**. Combination module resulted in 2 fold decrease in the concentration of tamoxifen with change in IC_{50} of TMX from 50 µM to 25 µM in presence of PTEN-nanocomposites. Therefore, low concentration of both tamoxifen and PTEN-nanocomposite sensitized U-87 MG spheroids ensuing reduced cell viability.

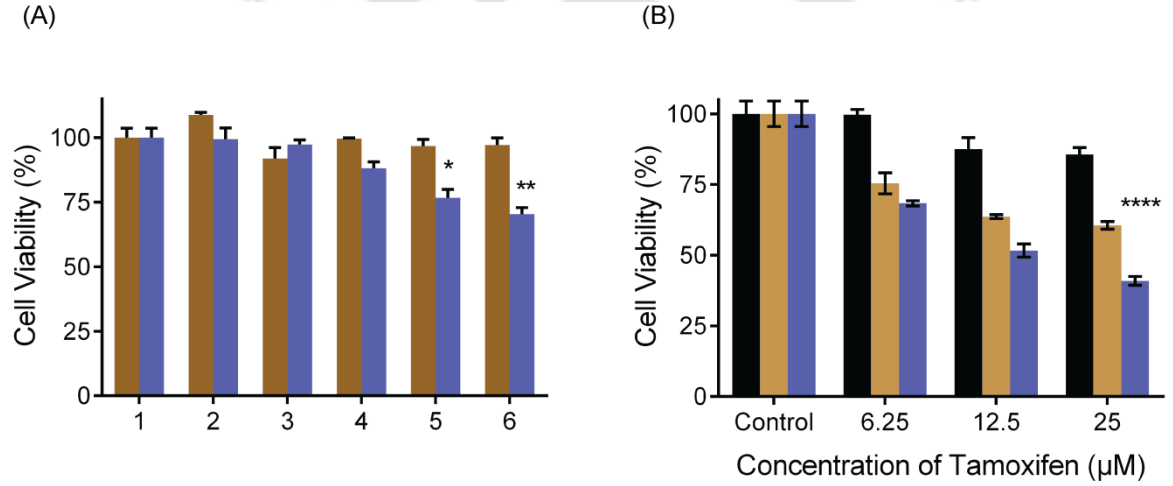

Figure 4.51 Determination of viability of U-87 MG spheroids (A) Alamar blue assay upon treatment with nanocomposites and PTEN-nanocomposites for 48 h where 1 is control spheroids, 2, 3, 4, 5 and 6 are PTEN (18 nM)-Cluster (10 µg/ml) Composite, PTEN (24 nM)-Cluster (15 µg/ml) Composite, PTEN (36 nM)-Cluster (22 µg/ml) Composite, PTEN (48 nM)-Cluster (30 µg/ml) Composite and PTEN (96 nM)-Cluster (60 µg/ml) Composite, respectively (B) Combination therapy with varying concentration of tamoxifen and PTEN-nanocomposites at a concentration of PTEN (36 nM)-Cluster (22 µg/ml) Composite.

Thus, the current experimental evidence demonstrates the role of exogenously delivered recombinant protein PTEN in modulation of cellular signaling leading to reduction in cell viability in monolayer cultures of U-87 MG and MCF7, which translated in three dimensional spheroid cultures as well imparting biological relevance and paving the way for PTEN based therapy in future.

4.19 References

(**2017**). Radiation plus Temozolomide in Patients with Glioblastoma. New England Journal of Medicine **376**(22), 2195-2197.

Barth, A. (**2007**). Infrared spectroscopy of proteins. Biochimica et Biophysica Acta (BBA) - Bioenergetics **1767**(9), 1073-1101.

Benezra, M., Penate-Medina, O., Zanzonico, P. B., Schaer, D., Ow, H., Burns, A., DeStanchina, E., Longo, V., Herz, E., Iyer, S., Wolchok, J., Larson, S. M., Wiesner, U. and Bradbury, M. S. (**2011**). Multimodal silica nanoparticles are effective cancer-targeted probes in a model of human melanoma. J Clin Invest **121**(7), 2768-2780.

Billsten, P., Wahlgren, M., Arnebrant, T., McGuire, J. and Elwing, H. (**1995**). Structural Changes of T4 Lysozyme upon Adsorption to Silica Nanoparticles Measured by Circular Dichroism. Journal of Colloid and Interface Science **175**(1), 77-82.

Bolduc, D., Rahdar, M., Tu-Sekine, B., Sivakumaren, S. C., Raben, D., Amzel, L. M., Devreotes, P., Gabelli, S. B. and Cole, P. (**2013**). Phosphorylation-mediated PTEN conformational closure and deactivation revealed with protein semisynthesis. eLife **2**, e00691.

Brandenberger, C., Mühlfeld, C., Ali, Z., Lenz, A.-G., Schmid, O., Parak, W. J., Gehr, P. and Rothen-Rutishauser, B. (**2010**). Quantitative Evaluation of Cellular Uptake and Trafficking of Plain and Polyethylene Glycol-Coated Gold Nanoparticles. Small **6**(15), 1669-1678.

Chan, L. L., Wilkinson, A. R., Paradis, B. D. and Lai, N. (**2012**). Rapid image-based cytometry for comparison of fluorescent viability staining methods. J Fluoresc **22**(5), 1301-1311.

Chang, F., Lee, J. T., Navolanic, P. M., Steelman, L. S., Shelton, J. G., Blalock, W. L., Franklin, R. A. and McCubrey, J. A. (**2003**). Involvement of PI3K/Akt pathway in cell cycle progression, apoptosis, and neoplastic transformation: a target for cancer chemotherapy. Leukemia **17**(3), 590-603.

Chen, Y.-H. and Yang, J. T. (**1971**). A new approach to the calculation of secondary structures of globular proteins by optical rotatory dispersion and circular dichroism. Biochemical and Biophysical Research Communications **44**(6), 1285-1291.

Clemments, A. M., Botella, P. and Landry, C. C. (**2015**). Protein Adsorption From Biofluids on Silica Nanoparticles: Corona Analysis as a Function of Particle Diameter and Porosity. ACS Applied Materials & Interfaces **7**(39), 21682-21689.

Collazo, A., Bricaud, O. and Desai, K. (2005). Use of Confocal Microscopy in Comparative Studies of Vertebrate Morphology. Methods in Enzymology, Academic Press. **395:** 521-543.

Dansen, T. B. and Burgering, B. M. T. (**2008**). Unravelling the tumor-suppressive functions of FOXO proteins. Trends in Cell Biology **18**(9), 421-429.

Das, N. K., Ghosh, S., Priya, A., Datta, S. and Mukherjee, S. (**2015**). Luminescent Copper Nanoclusters as a Specific Cell-Imaging Probe and a Selective Metal Ion Sensor. The Journal of Physical Chemistry C **119**(43), 24657-24664.

Fu, Z. and Tindall, D. J. (**2008**). FOXOs, cancer and regulation of apoptosis. Oncogene **27**, 2312.

Gagner, J. E., Lopez, M. D., Dordick, J. S. and Siegel, R. W. (**2011**). Effect of gold nanoparticle morphology on adsorbed protein structure and function. Biomaterials **32**(29), 7241-7252.

Gasteiger, E., Gattiker, A., Hoogland, C., Ivanyi, I., Appel, R. D. and Bairoch, A. (**2003**). ExPASy: the proteomics server for in-depth protein knowledge and analysis. Nucleic Acids Research **31**(13), 3784-3788.

Geng, Y., Yuan, W., Wu, F., Chen, J., He, M. and Jin, T. (**2008**). Formulating erythropoietin-loaded sustained-release PLGA microspheres without protein aggregation. J Control Release **130**(3), 259-265.

Hanada, S., Fujioka, K., Inoue, Y., Kanaya, F., Manome, Y. and Yamamoto, K. (**2014**). Cell-Based in Vitro Blood–Brain Barrier Model Can Rapidly Evaluate Nanoparticles' Brain Permeability in Association with Particle Size and Surface Modification. International Journal of Molecular Sciences **15**(2), 1812-1825.

Harper, S. and Speicher, D. W. (**2011**). Purification of proteins fused to glutathione S-transferase. Methods Mol Biol **681**, 259-280.

Holbro, T. and Hynes, N. E. (**2004**). ErbB receptors: directing key signaling networks throughout life. Annu Rev Pharmacol Toxicol **44**, 195-217.

Hopkins, B. D., Fine, B., Steinbach, N., Dendy, M., Rapp, Z., Shaw, J., Pappas, K., Yu, J. S., Hodakoski, C., Mense, S., Klein, J., Pegno, S., Sulis, M.-L., Goldstein, H., Amendolara, B., Lei, L., Maurer, M., Bruce, J., Canoll, P., Hibshoosh, H. and Parsons, R. (**2013**). A Secreted PTEN Phosphatase That Enters Cells to Alter Signaling and Survival. Science **341**(6144), 399.

Hopkins, B. D., Fine, B., Steinbach, N., Dendy, M., Rapp, Z., Shaw, J., Pappas, K., Yu, J. S., Hodakoski, C., Mense, S., Klein, J., Pegno, S., Sulis, M. L., Goldstein, H., Amendolara, B., Lei, L., Maurer, M., Bruce, J., Canoll, P., Hibshoosh, H. and Parsons, R. (**2013**). A secreted PTEN phosphatase that enters cells to alter signaling and survival. Science **341**(6144), 399-402.

Huang, X. and Brazel, C. S. (**2001**). On the importance and mechanisms of burst release in matrix-controlled drug delivery systems. Journal of Controlled Release **73**(2–3), 121-136.

Jiang, B. H. and Liu, L. Z. (**2008**). PI3K/PTEN signaling in tumorigenesis and angiogenesis. Biochim Biophys Acta **1784**(1), 150-158.

Jokerst, J. V., Lobovkina, T., Zare, R. N. and Gambhir, S. S. (**2011**). Nanoparticle PEGylation for imaging and therapy. Nanomedicine (London, England) **6**(4), 715-728.

Kong, J. and Yu, S. (**2007**). Fourier transform infrared spectroscopic analysis of protein secondary structures. Acta Biochim Biophys Sin (Shanghai) **39**(8), 549-559.

Kou, L., Sun, J., Zhai, Y. and He, Z. (**2013**). The endocytosis and intracellular fate of nanomedicines: Implication for rational design. Asian Journal of Pharmaceutical Sciences **8**(1), 1-10.

Lee, C. Y. (**2017**). Strategies of temozolomide in future glioblastoma treatment. OncoTargets and therapy **10**, 265-270.

Lee, S. R., Park, J. H., Park, E. K., Chung, C. H., Kang, S. S. and Bang, O. S. (**2005**). Akt-induced promotion of cell-cycle progression at G2/M phase involves upregulation of NF-Y binding activity in PC12 cells. J Cell Physiol **205**(2), 270-277.

Leslie, N. R. (**2012**). PTEN: An Intercellular Peacekeeper? Science Signaling **5**(250), pe50.

Li, J., Wang, W., Sun, D., Chen, J., Zhang, P.-H., Zhang, J.-R., Min, Q. and Zhu, J.-J. (**2013**). Aptamer-functionalized silver nanoclusters-mediated cell type-specific siRNA delivery and tracking. Chemical Science **4**(9), 3514-3521.

Li, J., Zhong, X., Cheng, F., Zhang, J.-R., Jiang, L.-P. and Zhu, J.-J. (**2012**). One-Pot Synthesis of Aptamer-Functionalized Silver Nanoclusters for Cell-Type-Specific Imaging. Analytical Chemistry **84**(9), 4140-4146.

Li, Y., Kröger, M. and Liu, W. K. (**2014**). Endocytosis of PEGylated nanoparticles accompanied by structural and free energy changes of the grafted polyethylene glycol. Biomaterials **35**(30), 8467-8478.

Maehama, T. and Dixon, J. E. (**1998**). The Tumor Suppressor, PTEN/MMAC1, Dephosphorylates the Lipid Second Messenger, Phosphatidylinositol 3,4,5-Trisphosphate. Journal of Biological Chemistry **273**(22), 13375-13378.

Maehama, T. and Dixon, J. E. (**1998**). The tumor suppressor, PTEN/MMAC1, dephosphorylates the lipid second messenger, phosphatidylinositol 3,4,5-trisphosphate. J Biol Chem **273**(22), 13375-13378.

Marino, M., Galluzzo, P. and Ascenzi, P. (**2006**). Estrogen signaling multiple pathways to impact gene transcription. Curr Genomics **7**(8), 497-508.

Marucco, A., Turci, F., O'Neill, L., Byrne, H. J., Fubini, B. and Fenoglio, I. (**2014**). Hydroxyl density affects the interaction of fibrinogen with silica nanoparticles at physiological concentration. Journal of Colloid and Interface Science **419**, 86-94.

Medema, R. H., Kops, G. J. P. L., Bos, J. L. and Burgering, B. M. T. (**2000**). AFX-like Forkhead transcription factors mediate cell-cycle regulation by Ras and PKB through p27kip1. Nature **404**, 782.

Meletiadis, J., Stergiopoulou, T., O'Shaughnessy, E. M., Peter, J. and Walsh, T. J. (**2007**). Concentration-Dependent Synergy and Antagonism within a Triple Antifungal Drug Combination against Aspergillus Species: Analysis by a New Response Surface Model. Antimicrobial Agents and Chemotherapy **51**(6), 2053-2064.

Mitra, S. K., Hanson, D. A. and Schlaepfer, D. D. (**2005**). Focal adhesion kinase: in command and control of cell motility. Nat Rev Mol Cell Biol **6**(1), 56-68.

Moncada, E., Quijada, R. and Retuert, J. (**2007**). Nanoparticles prepared by the sol–gel method and their use in the formation of nanocomposites with polypropylene. Nanotechnology **18**(33), 335606.

Moore, J. D., Kirk, J. A. and Hunt, T. (**2003**). Unmasking the S-Phase-Promoting Potential of Cyclin B1. Science **300**(5621), 987.

Mu, Q., Jiang, G., Chen, L., Zhou, H., Fourches, D., Tropsha, A. and Yan, B. (**2014**). Chemical Basis of Interactions Between Engineered Nanoparticles and Biological Systems. Chemical reviews **114**(15), 7740-7781.

Myers, M. P., Stolarov, J. P., Eng, C., Li, J., Wang, S. I., Wigler, M. H., Parsons, R. and Tonks, N. K. (**1997**). P-TEN, the tumor suppressor from human chromosome 10q23, is a dual-specificity phosphatase. Proceedings of the National Academy of Sciences **94**(17), 9052-9057.

Nagane, M., Levitzki, A., Gazit, A., Cavenee, W. K. and Huang, H. J. S. (**1998**). Drug resistance of human glioblastoma cells conferred by a tumor-specific mutant epidermal growth factor receptor through modulation of Bcl-X(L) and caspase-3-like proteases. Proceedings of the National Academy of Sciences of the United States of America **95**(10), 5724-5729.

Ou, Y., Ma, L., Ma, L., Huang, Z., Zhou, W., Zhao, C., Zhang, B., Song, Y., Yu, C. and Zhan, Q. (**2013**). Overexpression of cyclin B1 antagonizes chemotherapeutic-induced apoptosis through PTEN/Akt pathway in human esophageal squamous cell carcinoma cells. Cancer Biology & Therapy **14**(1), 45-55.

Pelaz, B., del Pino, P., Maffre, P., Hartmann, R., Gallego, M., Rivera-Fernández, S., de la Fuente, J. M., Nienhaus, G. U. and Parak, W. J. (**2015**). Surface Functionalization of Nanoparticles with Polyethylene Glycol: Effects on Protein Adsorption and Cellular Uptake. ACS Nano **9**(7), 6996-7008.

Raftopoulou, M., Etienne-Manneville, S., Self, A., Nicholls, S. and Hall, A. (**2004**). Regulation of Cell Migration by the C2 Domain of the Tumor Suppressor PTEN. Science **303**(5661), 1179.

Saptarshi, S. R., Duschl, A. and Lopata, A. L. (**2013**). Interaction of nanoparticles with proteins: relation to bio-reactivity of the nanoparticle. Journal of Nanobiotechnology **11**(1), 26.

Satzer, P., Svec, F., Sekot, G. and Jungbauer, A. (**2015**). Protein adsorption onto nanoparticles induces conformational changes: Particle size dependency, kinetics, and mechanisms. Engineering in Life Sciences, n/a-n/a.

Scaltriti, M. and Baselga, J. (**2006**). The Epidermal Growth Factor Receptor Pathway: A Model for Targeted Therapy. Clinical Cancer Research **12**(18), 5268.

Shang, L., Wang, Y., Jiang, J. and Dong, S. (**2007**). pH-Dependent Protein Conformational Changes in Albumin:Gold Nanoparticle Bioconjugates: A Spectroscopic Study. Langmuir **23**(5), 2714-2721.

Song, G., Ouyang, G. and Bao, S. (**2005**). The activation of Akt/PKB signaling pathway and cell survival. J Cell Mol Med **9**(1), 59-71.

Song, X.-R., Goswami, N., Yang, H.-H. and Xie, J. (**2016**). Functionalization of metal nanoclusters for biomedical applications. Analyst **141**(11), 3126-3140.

Spinelli, L. and Leslie, N. R. (**2015**). Assaying PTEN catalysis in vitro. Methods **77–78**, 51-57.

Tamura, M., Gu, J., Danen, E. H., Takino, T., Miyamoto, S. and Yamada, K. M. (**1999**). PTEN interactions with focal adhesion kinase and suppression of the extracellular matrix-dependent phosphatidylinositol 3-kinase/Akt cell survival pathway. J Biol Chem **274**(29), 20693-20703.

Tamura, M., Gu, J., Matsumoto, K., Aota, S., Parsons, R. and Yamada, K. M. (**1998**). Inhibition of cell migration, spreading, and focal adhesions by tumor suppressor PTEN. Science **280**(5369), 1614-1617.

Tanaka, M. and Grossman, H. B. (**2003**). In vivo gene therapy of human bladder cancer with PTEN suppresses tumor growth, downregulates phosphorylated Akt, and increases sensitivity to doxorubicin. Gene Ther **10**(19), 1636-1642.

Tang, L. and Cheng, J. (**2013**). Nonporous silica nanoparticles for nanomedicine application. Nano Today **8**(3), 290-312.

Terpe, K. (**2003**). Overview of tag protein fusions: from molecular and biochemical fundamentals to commercial systems. Appl Microbiol Biotechnol **60**(5), 523-533.

Tsuruta, F., Masuyama, N. and Gotoh, Y. (**2002**). The Phosphatidylinositol 3-Kinase (PI3K)-Akt Pathway Suppresses Bax Translocation to Mitochondria. Journal of Biological Chemistry **277**(16), 14040-14047.

Vertegel, A. A., Siegel, R. W. and Dordick, J. S. (**2004**). Silica Nanoparticle Size Influences the Structure and Enzymatic Activity of Adsorbed Lysozyme. Langmuir **20**(16), 6800-6807.

Welsch, N., Lu, Y., Dzubiella, J. and Ballauff, M. (**2013**). Adsorption of proteins to functional polymeric nanoparticles. Polymer **54**(12), 2835-2849.

Westphal, D., Dewson, G., Czabotar, P. E. and Kluck, R. M. (**2011**). Molecular biology of Bax and Bak activation and action. Biochimica et Biophysica Acta (BBA) - Molecular Cell Research **1813**(4), 521-531.

Wu, H., Wang, S., Weng, D., Xing, H., Song, X., Zhu, T., Xia, X., Weng, Y., Xu, G., Meng, L., Zhou, J. and Ma, D. (**2008**). Reversal of the malignant phenotype of ovarian cancer A2780 cells through transfection with wild-type PTEN gene. Cancer Lett **271**(2), 205-214.

Wu, T., Zhang, X., Huang, X., Yang, Y. and Hua, X. (**2010**). Regulation of cyclin B2 expression and cell cycle G2/m transition by menin. J Biol Chem **285**(24), 18291-18300.

Yahia-Ammar, A., Sierra, D., Mérola, F., Hildebrandt, N. and Le Guével, X. (**2016**). Self-Assembled Gold Nanoclusters for Bright Fluorescence Imaging and Enhanced Drug Delivery. ACS Nano **10**(2), 2591-2599.

Yameen, B., Choi, W. I., Vilos, C., Swami, A., Shi, J. and Farokhzad, O. C. (**2014**). Insight into nanoparticle cellular uptake and intracellular targeting. Journal of Controlled Release **190**, 485-499.

Yang, J., Xia, N., Wang, X., Liu, X., Xu, A., Wu, Z. and Luo, Z. (**2015**). One-pot one-cluster synthesis of fluorescent and bio-compatible Ag14 nanoclusters for cancer cell imaging. Nanoscale **7**(44), 18464-18470.

Yuan, W., Geng, Y., Wu, F., Liu, Y., Guo, M., Zhao, H. and Jin, T. (**2009**). Preparation of polysaccharide glassy microparticles with stabilization of proteins. Int J Pharm **366**(1-2), 154-159.

Zhang, X., Tang, N., Hadden, T. J. and Rishi, A. K. (**2011**). Akt, FoxO and regulation of apoptosis. Biochimica et Biophysica Acta (BBA) - Molecular Cell Research **1813**(11), 1978-1986.

Zhao, H., Lin, Z. Y., Yildirimer, L., Dhinakar, A., Zhao, X. and Wu, J. (**2016**). Polymer-based nanoparticles for protein delivery: design, strategies and applications. Journal of Materials Chemistry B **4**(23), 4060-4071.

Zhao, X. and Guan, J.-L. (**2011**). Focal adhesion kinase and its signaling pathways in cell migration and angiogenesis. Advanced drug delivery reviews **63**(8), 610-615.

Zhou, T., Huang, Y., Li, W., Cai, Z., Luo, F., Yang, C. J. and Chen, X. (**2012**). Facile synthesis of red-emitting lysozyme-stabilized Ag nanoclusters. Nanoscale **4**(17), 5312-5315.

Conclusion and Future Prospects

Section 5

5.1 Conclusions

The drug industry is undergoing a paradigm shift towards protein as therapeutics, owing to their functional advantages. This necessitates the formulation of a suitable delivery strategy to achieve the therapeutic benefit of intracellular signaling proteins. The present investigation focuses on harnessing the therapeutic potential of tumor suppressor proteins PTEN-Long and PTEN by comprehensive analysis of the regulatory roles of the recombinant proteins in cancer cell lines and three dimensional spheroid models. The salient findings of the work are summarized below under the following important categories.

5.1.1 Cloning expression and Purification

- The signaling proteins PTEN-Long and PTEN were sub-cloned into bacterial expression vector PGEX-4T-2 and purified by affinity chromatography based purification method

5.1.2 Functional Characterizations

- The purified PTEN-Long and PTEN proteins were confirmed by the Western blot and MALDI TOF-TOF analysis
- The structural analysis by circular dichroism revealed intact secondary structure of the proteins following bacterial purification
- Enzymatic analysis using para-nitrophenylphosphate (PNPP) substrate confirmed the protein phosphatase activity of both PTEN-Long and PTEN. Protein phosphatase activity of PTEN-Long can be useful in understanding the dual phosphatase role *in vivo*. Comparable kinetic efficiencies of GST tagged and untagged proteins confirmed that GST tag does not hinder the enzyme activity of the proteins
- Assessment of GST-PTEN-Long on cancer cell line U-87 MG ad MCF7 revealed that although GST tag did not alter *in vitro* phosphatase activity, it may be responsible for posing hindrance to cellular uptake of the otherwise membrane-permeable PTEN-Long. This necessitated the thrombin cleavage of the tag and assessment of the untagged protein on the cell lines

- Treatment of U-87 MG with PTEN-Long revealed that along with regulation of canonical Akt activity, PTEN-Long also regulated the expression of focal adhesion kinase (FAK), confirming its anti-invasive role in the U-87 MG cell line
- Further the combination therapy module with temozolomide, used for treatment of gliomas, displayed enhanced anti-proliferative activity as compared to mono-therapy.
- Following evaluation of anti-proliferative activity of PTEN-Long, the cellular study of PTEN protein was performed

5.1.3 Intracellular Delivery of PTEN

- Intracellular delivery of PTEN was mediated by binding of the recombinant protein onto silica nanoparticles. PTEN protein-silica nanoparticles interaction was confirmed by spectroscopy based techniques and ELISA
- Once the binding was confirmed, it was imperative to determine the functional and structural alterations upon interaction with the nanoparticles
- Structural changes of the protein after interacting with nanoparticles is inevitable, however circular dichroism study of the GST-PTEN released from nanoparticles displayed minimal structural re-organization, which is the prerequisite of any protein based therapy
- Structural integrity was further corroborated by analysis of the functional integrity of the recombinant enzyme. Functional analysis of the protein-nanoparticles composite illustrated retention of dual phosphatase activity towards PIP_3 diC8 and PNPP substrates, with kinetic efficiency comparable to free recombinant protein
- Treatment of U-87 MG with PTEN-silica composite resulted in concentration dependent reduction in proliferation of the cells accompanied with amended cell cycle pattern, highlighting successful stabilization of the PTEN protein onto the silica nanoparticles

5.1.4 Intracellular Tracking

- To achieve amalgamation of delivery, tracking and improved binding of the protein, lysozyme-template silver nanoclusters (AgNCs) were synthesized and subsequently characterized

- The favorable optical property of the nanoclusters was capitalized to study the interaction with the recombinant protein and the cellular internalization of the cargo
- The formulation of the protein delivery vehicle is very crucial to preserve the protein function in complex environment. In this context, the GST-PTEN-AgNCs were encapsulated within polyethylene glycol (PEG) to aid fabrication of spherical nanoparticles to mediate intracellular delivery accompanied with additional advantages of polymeric coating such as 'sleath' behavior that prevents nanoparticles aggregation
- TEM DLS zeta potential measurements of PEG coated composite (named as PTEN-Nanocomposites) confirmed the formation of spherical nanocomposites of average diameter of 125 nm with neutral surface charge
- An imperative emphasis of the study was demonstration of functional aspect of the encapsulated recombinant protein. Proteins are delicate biomacromolecules, prone to degradation and disintegration. As a result each step of the formulation demands meticulous inspection of the function of the protein. The functional integrity of the recombinant protein was analyzed after binding to the nanoclusters and also after PEG encapsulation. The enzyme kinetic assay elucidated retention of the phosphatase activity of PTEN

5.1.5 Modulation of Cellular Signaling

- Endocytosis mediated cellular uptake of the PTEN-Nanocomposites in cell lines expressing endogenous PTEN differentially (PTEN null U-87 MG and PTEN expressing MCF7) effectuated in modulation of the cellular signaling
- PTEN-Nanocomposites regulated the expression of two central signaling proteins Akt and FAK along with modulation of cell cycle regulators
- The implications of altered cellular signaling was perceptible as reduced wound healing capacity, cell cycle arrest and reduced proliferation in both U-87 MG and MCF7 cell lines
- Further the capacity of PTEN-Nanocomposites to function as co-therapy agent was evaluated in presence of drug erlotinib. Treatment of U-87 MG cells with the combined therapy resulted in chemo-sensitization towards erlotinib, thereby reducing

the concentration of the small molecule drug to bring about the same effect in the multi-drug resistant cell line

- The monolayer culture results provided strong lead towards the potential therapeutic application of the nanocomposite, which provided the motivation to translate the results to three dimensional cultures

5.1.6 Effect on Spheroids

- Three dimensional cultures have gained enormous importance as a drug testing platforms due to their close resemblance to the complex and heterogeneous *in vivo* tumor microenvironment
- PTEN-Nanocomposite uptake in the spheroid model was confirmed by z-stacking analysis using confocal microscopy
- Cellular uptake of PTEN-Nanocomposites resulted in modulation of expression of genes involved in apoptosis and cell cycle regulation, which effectuated in successfully reduction in the proliferation of the spheroids
- In case of MCF7 spheroids, IC_{50} was achieved at a considerably higher concentration of PTEN-Nanocomposites as compared to monolayer MCF7 cultures. This confirms the incongruity in monolayer cultures and *in vivo* tumor environment, making three dimensional cultures a vital screening step to augment the biological relevance of the therapeutic agent
- Successful co-therapy module was executed in U-87 MG spheroids, where tamoxifen and PTEN-nanocomposites in combination displayed dose dependent inhibition of the spheroids proliferation. Thus, the present investigations strengthen the foundation for application of recombinant signaling protein as a therapeutic agent. It further paves the way for generating novel composites to accomplish the stabilization and delivery of intracellular recombinant protein PTEN. The recombinant proteins were successful as a therapeutic agent in both mono-therapy therapy and combination therapy modules. Successful co-therapy with anti-cancer drugs assisted in reducing the required dosage of the small molecule drug, which can be applied to reduce the drug associated side effects. The essence of the work is illustrated in **Scheme 5.1**.

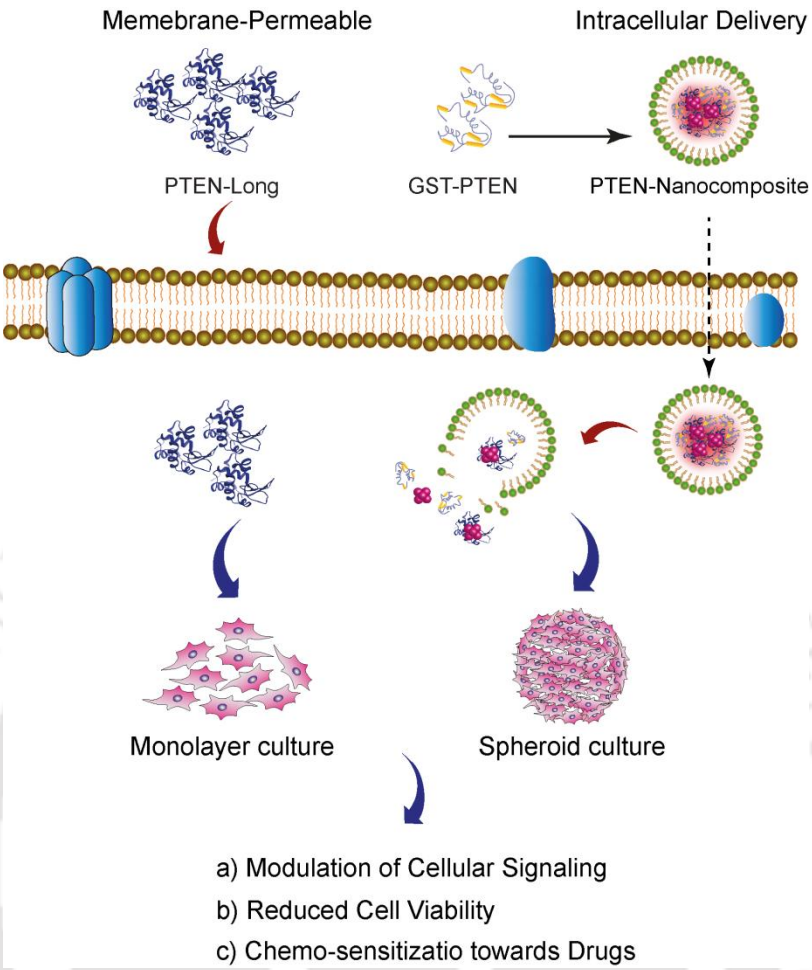

Scheme 5.1 The essence of the current investigation.

5.2 Future Prospects

The future scope of the work based on current investigations include

- Appropriate functionalization of the nanocomposites will furnish scope for development of targeted cancer therapy
- Understanding signaling pathways in presence of the drugs will provide a better insight in developing successful combination therapy modules to combat drug resistant cancer
- Since PTEN-nanocomposite demonstrated successful activity on spheroid model, the efficacy of the nanocomposite system can be further evaluated on *in vivo* studies

ANNEXURE

- **Fold change**

Recombinant proteins PTEN-Long and PTEN treatment of U-87 MG and MCF7 cell lines resulted in modulation of expression of signaling proteins and genes. The fold change of the treated and untreated samples is presented in the table below, where U-87 MG and MCF7 refers to the control cells, U-87 MG-PTEN-Long (2h) refers to cells treated with PTEN-Long for 2 h, U-87 MG-PTEN-Long (4h) refers to cells treated with PTEN-Long for 4 h, U-78 MG-Nancomposites refers to cells treated with only nanocomposites, U-78 MG-PTEN-Nancomposites refers to cells treated with PTEN encapsulated within the nanocomposites. MCF7-Nancomposites refers to cells treated with only nanocomposites, MCF7-PTEN-Nancomposites refers to cells treated with PTEN encapsulated within the nanocomposites. The fold change was calculated using ImajeJ software and normalized against endogenous control GAPDH.

Western Blot Study	
Treatment with PTEN-Long	
Expression Analysis of pAKTS473	
U-78 MG	1
U-78 MG-PTEN-Long (2h)	0.53
U-78 MG-PTEN-Long (4h)	0.23
Expression Analysis of pFAKTyr397	
U-78 MG	1
U-78 MG-PTEN-Long (2h)	0.51
U-78 MG-PTEN-Long (4h)	0.35

Treatment with PTEN-Nanocomposite on Cell lines (Monolayer Culture)	
Expression Analysis of pAKTS473	
U-78 MG	1
U-78 MG-Nancomposites	0.84
U-78 MG-PTEN-Nancomposites	0.52
MCF7	1
MCF7-Nancomposites	0.84
MCF7-PTEN-Nancomposites	0.26
Expression Analysis of pFAKTyr397	
U-78 MG	1
U-78 MG-Nancomposites	0.77
U-78 MG-PTEN-Nancomposites	0.12
MCF7	1
MCF7-Nancomposites	0.59
MCF7-PTEN-Nancomposites	0.06
RNA Expression Study	
Treatment with PTEN-Long	
Expression Analysis of Cyclin B	
U-78 MG	1

U-78 MG-Buffer	1.21
U-78 MG-PTEN-Long	0.64
Expression Analysis of Cyclin D	
U-78 MG	1
U-78 MG-Buffer	1.15
U-78 MG-PTEN-Long	0.37
Treatment with PTEN-Nanocomposites on Cell Lines (Monolayer Culture)	
Expression Analysis of Cyclin B2	
U-78 MG	1
U-78 MG-Nanocomposites	1.1
U-78 MG-PTEN-Nanocomposites	0.44
Expression Analysis of Cyclin B1	
MCF7	1
MCF7-Nanocomposites	1.04
MCF7-PTEN-Nanocomposites	0.52
Treatment with PTEN-Nanocomposites on Spheroid Culture	
Expression analysis of Cyclin A	
U-78 MG	1
U-78 MG-Nanocomposites	0.89

U-78 MG-PTEN-Nanocomposites	0.2
Expression analysis of Bax	
U-78 MG	1
U-78 MG-Nanocomposites	1.5
U-78 MG-PTEN-Nanocomposites	1.6
Expression Analysis of FOXO3a	
U-78 MG	1
U-78 MG-Nanocomposites	1.1
U-78 MG-PTEN-Nanocomposites	1.61
Expression analysis of Cyclin B1	
MCF7	1
MCF7-Nanocomposites	0,88
MCF7-PTEN-Nanocomposites	0.27

- **Buffers and their composition**

Alkaline lysis solution for plasmid isolation I	50 mM glucose, 25 mM Tris-Cl (pH-8.0), EDTA (10 mM)
Alkaline lysis solution II	0.2 N NaOH, (freshly diluted from 10 N stock), 1% (w/v) SDS
Alkaline lysis solution III	5 M potassium acetate (60 mL), glacial acetic acid (11.5 mL), water (28.5 mL)
Blocking buffer for western blot	3% (w/v) BSA in PBST/TBST
Cleaning buffer 1 for column regeneration (pH-8.5)	0.1 M boric acid, 0.5 M NaCl, adjust the pH 8.5 with sodium hydroxide
Cleaning buffer 2 for column regeneration (pH-4.5)	0.1 M sodium acetate, 0.5 M NaCl, adjust the pH 4.5 with acetic acid
Hepes Buffer Saline	50 mM Hepes and 150 mM NaCl, pH adjusted to 7.4 with NaOH
Lysis buffer for PTEN-Long protein purification	50 mM Tris pH 7.4, 1 mM EDTA, 1 mM PMSF and 150 mM NaCl
Lysis buffer for PTEN protein purification	20 mM Tris pH 7.4, 1 mM EDTA, 1 mM PMSF and 150 mM NaCl
Phosphate buffered saline	137 mM NaCl, 2.68 mM KCl, 7.98 mM Na2HPO4, 1.4 mM KH2PO4, pH 7.4
Polyacrylamide solution (30%)	29.2% (w/w) acrylamide, 0.8% (w/w) N,N'-methylenebisacrylamide
Protein elution buffer	25 mM Hepes, pH 8.0 and 15 mM L-reduced glutathione
Tris-acetate EDTA (TAE) 50X (100 mL)	24.2 g Tris base, 5.71 mL of glacial acetic acid, 10 mL of 0.5 M EDTA (pH-8.0)
Tris Buffered Saline Tween-20	Tris-HCl (50 mM), NaCl (150 mM), Tween-20 (0.1% v/v) pH-7.5
TSS buffer for competent cells	10% (w/v) PEG 8000, 0.6% (w/v) MgCl2.6H2O, 5% (v/v) DMSO in LB media
4X protein loading dye (for 10 mL)	2.0 ml 1 M Tris-HCl (pH 6.8), 0.8 g SDS, 4.0 ml 100% glycerol, 0.4 ml 14.7 M β-mercaptoethanol, 8 mg bromophenol blue in water
6X DNA loading dye	0.25 (%)(w/v) bromophenol blue, 0.25% (w/v) xylene cyanol FF, 30% (v/v) glycerol in water

PUBLICATIONS AND CONFERENCES

- **Journal Publications From Thesis Work**

1. **Neha Arora** and Siddhartha Sankar Ghosh **(2016),** Functional Characterizations of Interactive Recombinant PTEN Silica Nanoparticles for Potential Biomedical Applications, ***RSC Advances*****,** 6, 114944-114954, DOI: 10.1039/C6RA23036A [**RSC publishing group**]

2. **Neha Arora,** Lalitha Gavya S, Siddhartha Sankar Ghosh **(2018),** Multi-facet Implications of PEGylated Lysozyme Stabilized-Silver Nanoclusters Loaded Recombinant PTEN Cargo in Cancer Theranostics, ***Biotechnology and Bioengineering*****,** 115(5), 1116-1127, DOI: 10.1002/bit.26553 [**Wiley publishing group**]

3. **Neha Arora**, Rajib Shome, Siddhartha Sankar Ghosh **(2018),** Effect of PEGylated Lysozyme Stabilized-Silver Nanoclusters Loaded Recombinant PTEN Cargo on 3D spheroids (Manuscript Under Preparation)

- **Journal Publications From Collaborative Work**

1. Sharmila Narayana, Deepanjalee Dutta, **Neha Arora**, Lingaraj Sahoo, Siddhartha Sankar Ghosh (**2017**) Phytaspase-loaded, Mn-doped ZnS quantum dots when embedded into chitosan nanoparticles leads to improved chemotherapy of HeLa cells using in cisplatin, ***Biotechnology Letters***, 39, 1591–1598, DOI: 10.1007/s10529-017-2395-1 **[Springer publishing group]**

2. Lalitha Gavya S, **Neha Arora,** Siddhartha Sankar Ghosh **(2017)** Retention of Functional characteristics of Gulathione-S-Transferase and Lactate Dehydrogenase-A in Fusion Protein, ***Preparative Biochemistry and Biotechnology*****,** DOI: 10.1080/10826068.2017 **[Taylor and Francis publishing group]**

3. Karuna Mahato, **Neha Arora**, Prasanta Ray Bagdi, Radhakrishna Gattu, Siddhartha Sankar Ghosh and Abu T. Khan **(2018)** An oxidative cross-couping reaction of 4-hydroxydithiocoumarin and amines/thiols using a combination of I_2 and THBP: access to lead molecules for biomedical applications, ***Chem Comm,*** DOI: 10.1039/c7cc08502h [**RSC publishing group**]

4. Debananda Gogoi, **Neha Arora**, Bhargab Kalita, Rahul Sarma, Taufkul Islam, Sidhhartha S. Ghosh, Rajlakshmi Devi & Ashis K. Mukherjee **(2018)** Anticoagulant mechanism, pharmacological activity and assessment of preclinical safety of a novel fbrin(ogen)olytic serine protease frm leaves of *Leucas indica*, ***Scientific Reports***, DOI: 10.1038/s41598-018-24422-y **[Nature publishing group]**

5. Karuna Mahato, Prasanta Ray Bagdi**, Neha Arora**, Siddhartha Sankar Ghosh and Abu T. Khan **(2018)** Unconventional sulfur transfer from 4-hydroxydithiocoumarin: Synthesis of 3-alkyl-[1,2]dithiolo[3,4-*b*]thiochromen-4(3H)-ones formation from the reaction of 4-hydroxydithiocoumarin and aldehydes in aqueous media catalyzed by copperoxide nanoparticles (Manuscript Under Preparation)

- **Conference Presentations**

1. **Poster Presentation, Neha Arora,** Anil Bidkar, N.Sharmila, Siddhartha Sankar Ghosh, Emergence of Protein Therapeutics in Cancer Medicine, **Research Conclave 2016, IIT Guwahati**, March 17th to March 20th organized by Indian Institute of Technology Guwahati, Assam, India

2. **Poster Presentation, Neha Arora** and Siddhartha Sankar Ghosh, Functional Stabilization of Recombinant PTEN onto Silica Nanoparticles for Potential Biomedical Applications, 7th International Conference on Stem Cells and Cancer **(ICSCC) 2016**: Proliferation, Differentiation and Apoptosis, **Ravindra Bhavan, Goa**, October 21st to 23rd 2016 organized by International Center for Stem Cells, Cancer and Biotechnology (ICSCCB), Pune, India **[Received Best Poster Award]**

3. **Oral Presentation, Neha Arora** and Siddhartha Sankar Ghosh, Stabilization of Recombinant PTEN onto Silica Nanoparticles; Characterization of Protein-nanoparticles interaction for Biomedical Applications, International Conference on Sophisticated Instruments in Modern Research (**ICSIMR**) **2017**, **IIT Guwahati**, June 30th to July 1st 2017 organized by Central Instrumentation Facility, Indian Institute of Technology Guwahati, Assam, India

4. **Poster Presentation, Neha Arora** and Siddhartha Sankar Ghosh, PEGylated Silver Nanoclusters Mediated Cytosolic Delivery of Tumor Suppressor Protein PTEN to Modulate *in vitro* Cellular Signaling, **Nano Today Conference 2017, Hawaii USA**, December 6th to December 10th organized by Elsevier publishing group and the Institute of Bioengineering and Nanotechnology (IBN) Singapore **[Received Student Travel Award from organizing committee (Elsevier) and Full Travel Grant from Department of Biotechnology (DBT), India]**

5. **Poster Presentation, Neha Arora** and Siddhartha Sankar Ghosh, Understanding Therapeutic Potential of PEGylated Silver Nanoclusters Loaded Recombinant PTEN, 5th International Conference on Advanced Materials and Nanotechnology (**ICANN) 2017, IIT Guwahati**, December 18th to December 21st 2017 organized by Centre for Nanotechnology, Indian Institute of Technology Guwahati, Assam, India **[Received ACS Best Poster Award]**

Functional characterizations of interactive recombinant PTEN–silica nanoparticles for potential biomedical applications

N. Arora and S. S. Ghosh, *RSC Adv.*, 2016, **6**, 114944
DOI: 10.1039/C6RA23036A

- For reproduction of material from PPS:
  [Original citation] - Reproduced by permission of The Royal Society of Chemistry (RSC) on behalf of the European Society for Photobiology, the European Photochemistry Association, and RSC
- For reproduction of material from all other RSC journals:
  [Original citation] - Reproduced by permission of The Royal Society of Chemistry

If you are the author of this article you still need to obtain permission to reproduce the whole article in a third party publication with the exception of reproduction of the whole article in a thesis or dissertation.

Information about reproducing material from RSC articles with different licences is available on our Permission Requests page.

JOHN WILEY AND SONS LICENSE TERMS AND CONDITIONS

Oct 09, 2018

This Agreement between Miss. Neha Arora ("You") and John Wiley and Sons ("John Wiley and Sons") consists of your license details and the terms and conditions provided by John Wiley and Sons and Copyright Clearance Center.

License Number	4445111410455
License date	Oct 09, 2018
Licensed Content Publisher	John Wiley and Sons
Licensed Content Publication	Biotechnology & Bioengineering
Licensed Content Title	Multi-facet implications of PEGylated lysozyme stabilized-silver nanoclusters loaded recombinant PTEN cargo in cancer theranostics
Licensed Content Author	Neha Arora, Lalitha Gavya S, Siddhartha S. Ghosh
Licensed Content Date	Feb 21, 2018
Licensed Content Volume	115
Licensed Content Issue	5
Licensed Content Pages	12
Type of use	Dissertation/Thesis
Requestor type	Author of this Wiley article
Format	Print and electronic
Portion	Full article
Will you be translating?	No
Order reference number	permissionWiley
Title of your thesis / dissertation	Understanding the Potential of Recombinant PTEN in Cancer Therapeutics
Expected completion date	Oct 2018
Expected size (number of pages)	175
Requestor Location	Miss. Neha Arora Dept of BSBE, IIT Guwahati Guwahati, Assam 781039 India Attn: Miss. Neha Arora
Publisher Tax ID	EU826007151
Total	0.00 USD
Terms and Conditions	

TERMS AND CONDITIONS

This copyrighted material is owned by or exclusively licensed to John Wiley & Sons, Inc. or one of its group companies (each a"Wiley Company") or handled on behalf of a society with which a Wiley Company has exclusive publishing rights in relation to a particular work

TH-1979_136106013

(collectively "WILEY"). By clicking "accept" in connection with completing this licensing transaction, you agree that the following terms and conditions apply to this transaction (along with the billing and payment terms and conditions established by the Copyright Clearance Center Inc., ("CCC's Billing and Payment terms and conditions"), at the time that you opened your RightsLink account (these are available at any time at http://myaccount.copyright.com).

Terms and Conditions

- The materials you have requested permission to reproduce or reuse (the "Wiley Materials") are protected by copyright.

- You are hereby granted a personal, non-exclusive, non-sub licensable (on a stand-alone basis), non-transferable, worldwide, limited license to reproduce the Wiley Materials for the purpose specified in the licensing process. This license, **and any CONTENT (PDF or image file) purchased as part of your order,** is for a one-time use only and limited to any maximum distribution number specified in the license. The first instance of republication or reuse granted by this license must be completed within two years of the date of the grant of this license (although copies prepared before the end date may be distributed thereafter). The Wiley Materials shall not be used in any other manner or for any other purpose, beyond what is granted in the license. Permission is granted subject to an appropriate acknowledgement given to the author, title of the material/book/journal and the publisher. You shall also duplicate the copyright notice that appears in the Wiley publication in your use of the Wiley Material. Permission is also granted on the understanding that nowhere in the text is a previously published source acknowledged for all or part of this Wiley Material. Any third party content is expressly excluded from this permission.

- With respect to the Wiley Materials, all rights are reserved. Except as expressly granted by the terms of the license, no part of the Wiley Materials may be copied, modified, adapted (except for minor reformatting required by the new Publication), translated, reproduced, transferred or distributed, in any form or by any means, and no derivative works may be made based on the Wiley Materials without the prior permission of the respective copyright owner.**For STM Signatory Publishers clearing permission under the terms of the STM Permissions Guidelines only, the terms of the license are extended to include subsequent editions and for editions in other languages, provided such editions are for the work as a whole in situ and does not involve the separate exploitation of the permitted figures or extracts,** You may not alter, remove or suppress in any manner any copyright, trademark or other notices displayed by the Wiley Materials. You may not license, rent, sell, loan, lease, pledge, offer as security, transfer or assign the Wiley Materials on a stand-alone basis, or any of the rights granted to you hereunder to any other person.

- The Wiley Materials and all of the intellectual property rights therein shall at all times remain the exclusive property of John Wiley & Sons Inc, the Wiley Companies, or their respective licensors, and your interest therein is only that of having possession of and the right to reproduce the Wiley Materials pursuant to Section 2 herein during the continuance of this Agreement. You agree that you own no right, title or interest in or to the Wiley Materials or any of the intellectual property rights therein. You shall have no rights hereunder other than the license as provided for above in Section 2. No right, license or interest to any trademark, trade name, service mark or other branding

TH-1979_136106013

("Marks") of WILEY or its licensors is granted hereunder, and you agree that you shall not assert any such right, license or interest with respect thereto

- NEITHER WILEY NOR ITS LICENSORS MAKES ANY WARRANTY OR REPRESENTATION OF ANY KIND TO YOU OR ANY THIRD PARTY, EXPRESS, IMPLIED OR STATUTORY, WITH RESPECT TO THE MATERIALS OR THE ACCURACY OF ANY INFORMATION CONTAINED IN THE MATERIALS, INCLUDING, WITHOUT LIMITATION, ANY IMPLIED WARRANTY OF MERCHANTABILITY, ACCURACY, SATISFACTORY QUALITY, FITNESS FOR A PARTICULAR PURPOSE, USABILITY, INTEGRATION OR NON-INFRINGEMENT AND ALL SUCH WARRANTIES ARE HEREBY EXCLUDED BY WILEY AND ITS LICENSORS AND WAIVED BY YOU.

- WILEY shall have the right to terminate this Agreement immediately upon breach of this Agreement by you.

- You shall indemnify, defend and hold harmless WILEY, its Licensors and their respective directors, officers, agents and employees, from and against any actual or threatened claims, demands, causes of action or proceedings arising from any breach of this Agreement by you.

- IN NO EVENT SHALL WILEY OR ITS LICENSORS BE LIABLE TO YOU OR ANY OTHER PARTY OR ANY OTHER PERSON OR ENTITY FOR ANY SPECIAL, CONSEQUENTIAL, INCIDENTAL, INDIRECT, EXEMPLARY OR PUNITIVE DAMAGES, HOWEVER CAUSED, ARISING OUT OF OR IN CONNECTION WITH THE DOWNLOADING, PROVISIONING, VIEWING OR USE OF THE MATERIALS REGARDLESS OF THE FORM OF ACTION, WHETHER FOR BREACH OF CONTRACT, BREACH OF WARRANTY, TORT, NEGLIGENCE, INFRINGEMENT OR OTHERWISE (INCLUDING, WITHOUT LIMITATION, DAMAGES BASED ON LOSS OF PROFITS, DATA, FILES, USE, BUSINESS OPPORTUNITY OR CLAIMS OF THIRD PARTIES), AND WHETHER OR NOT THE PARTY HAS BEEN ADVISED OF THE POSSIBILITY OF SUCH DAMAGES. THIS LIMITATION SHALL APPLY NOTWITHSTANDING ANY FAILURE OF ESSENTIAL PURPOSE OF ANY LIMITED REMEDY PROVIDED HEREIN.

- Should any provision of this Agreement be held by a court of competent jurisdiction to be illegal, invalid, or unenforceable, that provision shall be deemed amended to achieve as nearly as possible the same economic effect as the original provision, and the legality, validity and enforceability of the remaining provisions of this Agreement shall not be affected or impaired thereby.

- The failure of either party to enforce any term or condition of this Agreement shall not constitute a waiver of either party's right to enforce each and every term and condition of this Agreement. No breach under this agreement shall be deemed waived or excused by either party unless such waiver or consent is in writing signed by the party granting such waiver or consent. The waiver by or consent of a party to a breach of any provision of this Agreement shall not operate or be construed as a waiver of or consent to any other or subsequent breach by such other party.

TH-1979_136106013

- This Agreement may not be assigned (including by operation of law or otherwise) by you without WILEY's prior written consent.
- Any fee required for this permission shall be non-refundable after thirty (30) days from receipt by the CCC.
- These terms and conditions together with CCC's Billing and Payment terms and conditions (which are incorporated herein) form the entire agreement between you and WILEY concerning this licensing transaction and (in the absence of fraud) supersedes all prior agreements and representations of the parties, oral or written. This Agreement may not be amended except in writing signed by both parties. This Agreement shall be binding upon and inure to the benefit of the parties' successors, legal representatives, and authorized assigns.
- In the event of any conflict between your obligations established by these terms and conditions and those established by CCC's Billing and Payment terms and conditions, these terms and conditions shall prevail.
- WILEY expressly reserves all rights not specifically granted in the combination of (i) the license details provided by you and accepted in the course of this licensing transaction, (ii) these terms and conditions and (iii) CCC's Billing and Payment terms and conditions.
- This Agreement will be void if the Type of Use, Format, Circulation, or Requestor Type was misrepresented during the licensing process.
- This Agreement shall be governed by and construed in accordance with the laws of the State of New York, USA, without regards to such state's conflict of law rules. Any legal action, suit or proceeding arising out of or relating to these Terms and Conditions or the breach thereof shall be instituted in a court of competent jurisdiction in New York County in the State of New York in the United States of America and each party hereby consents and submits to the personal jurisdiction of such court, waives any objection to venue in such court and consents to service of process by registered or certified mail, return receipt requested, at the last known address of such party.

WILEY OPEN ACCESS TERMS AND CONDITIONS

Wiley Publishes Open Access Articles in fully Open Access Journals and in Subscription journals offering Online Open. Although most of the fully Open Access journals publish open access articles under the terms of the Creative Commons Attribution (CC BY) License only, the subscription journals and a few of the Open Access Journals offer a choice of Creative Commons Licenses. The license type is clearly identified on the article.

The Creative Commons Attribution License

The Creative Commons Attribution License (CC-BY) allows users to copy, distribute and transmit an article, adapt the article and make commercial use of the article. The CC-BY license permits commercial and non-

Creative Commons Attribution Non-Commercial License

The Creative Commons Attribution Non-Commercial (CC-BY-NC)License permits use, distribution and reproduction in any medium, provided the original work is properly cited and is not used for commercial purposes.(see below)

TH-1979_136106013

Creative Commons Attribution-Non-Commercial-NoDerivs License
The Creative Commons Attribution Non-Commercial-NoDerivs License (CC-BY-NC-ND) permits use, distribution and reproduction in any medium, provided the original work is properly cited, is not used for commercial purposes and no modifications or adaptations are made. (see below)
Use by commercial "for-profit" organizations
Use of Wiley Open Access articles for commercial, promotional, or marketing purposes requires further explicit permission from Wiley and will be subject to a fee.
Further details can be found on Wiley Online Library http://olabout.wiley.com/WileyCDA/Section/id-410895.html

Other Terms and Conditions:

v1.10 Last updated September 2015

Questions? customercare@copyright.com or +1-855-239-3415 (toll free in the US) or +1-978-646-2777.

TH-1979_136106013